The influences of phosphorus cycling on the tropical ecosystem carbon cycle-A process-based modeling study

by

Zhuonan Wang

A dissertation submitted to the Graduate Faculty of
Auburn University
in partial fulfillment of the
requirements for the Degree of
Doctor of Philosophy

Auburn, Alabama
August 7, 2021

Keywords: Phosphorus cycle, Global changes, Carbon cycle,
CO_2 fertilization effect, Phosphorus limitation, Process-based model

Approved by

Hanqin Tian, Chair, Solon Dixon Professor of School of Forestry and Wildlife Sciences
Shufen Pan, Co-chair, Associate Professor of School of Forestry and Wildlife Sciences
B. Graeme Lockaby, Clinton McClure Professor of School of Forestry and Wildlife Sciences
Latif Kalin, Alumni Professor of School of Forestry and Wildlife Sciences
Christopher J. Anderson, Professor of School of Forestry and Wildlife Sciences

Abstract

The biogeochemical processes of phosphorous (P), carbon (C), and nitrogen (N) in the Earth system are fully coupled, which shapes the structure, functioning, and dynamics of terrestrial ecosystems. However, incorporating P-related processes into terrestrial biosphere models (TBMs) is still in an early stage. Tropical forests store more than half of the world's terrestrial carbon (C) pool and account for one-third of global net primary productivity (NPP). With their significant contribution to the global C cycle, tropical forests maintain critical negative feedback to climate warming through absorbing atmospheric CO_2. A few TBMs-based estimates indicate increasing productivity in tropical ecosystems throughout the 21st century due to the CO_2 fertilization effect. However, phosphorus (P) limitation on vegetation photosynthesis and productivity have not been considered by most current TBMs. In this dissertation, P impacts on C fluxes and the C-N-P interactions were investigated at both site and tropical scales. We examined how P limitation has affected C fluxes of tropical rainforests during 1860-2018. Our model results showed that consideration of the P cycle reduced the CO_2 fertilization effect on tropical rainforests gross primary production (GPP) by 25% and 45%, NPP by 25% and 46%, and net ecosystem production (NEP) by 28% and 41% relative to CN-only and C-only models. During the period from the 1860s to the 2010s, the DLEM-CNP estimated that for per unit area, the tropical rainforest GPP increased by 17 %, plant respiration (Ra) increased by 18%, NPP increased by 16%, heterotrophic respiration (Rh) increased by 13%, and NEP increased by 121%, respectively. Additionally, factorial experiments with DLEM-CNP showed that the enhanced GPP and NPP benefiting from the CO_2 fertilization effect had been offset by 147% and 135% due to deforestation from the 1860s to the 2010s. Using future environmental factors, we examined pan-tropic GPP, NPP, and carbon use efficiency (CUE) changes during 2020-2100. Results showed that the P limitation on the CO_2

fertilization effect would reduce future tropical GPP and NPP. Under the SSP585 scenario, the CO_2 fertilization effect would reach plateaus and the tropical ecosystem's capability to respond to CO_2 increase would weaken after 2060. Under future environmental conditions during 2020-2100, DLEM-CNP estimated that under the SSP126 scenario, the tropical GPP, NPP, and CUE would slightly increase, with a substantially interannual variation. Under the SSP585 scenario, the tropical GPP and NPP would increase by 44% and 21% from 2020 to 2100, respectively; the CUE shows a decrease of 15% under the SSP585 scenario. The CO_2 fertilization effect is the dominant factor that would likely increase the future GPP and NPP in the tropics. The climate effect is found to be the most significant factor that would decrease the CUE under both SSP126 and SSP585 scenarios. Our study revealed strong interactions among C, N, P processes, indicating that the inclusion of the P cycle in the current TBMs is essential to better understand the impacts of global change on terrestrial ecosystems.

Acknowledgments

My sincere gratitude goes to my advisor, Dr. Hanqin Tian. I am grateful to have him as my advisor during these past six years. His insightful comments and constructive suggestions were thought-provoking at different stages of my study. I would like to thank co-advisor Dr. Susan Pan for her continuous help in daily life and research. Without their support, great patience, and constant encouragement, I cannot complete this dissertation. I am deeply thankful for my research committees: Dr. Latif Kalin, Dr. B. Graeme Lockaby, and Dr. Christopher Anderson for their invaluable comments and suggestions, continuous assistance, and generous encouragement. I would like to thank my university reader of my dissertation, Dr. Di Tian.

I am also grateful to the former EDGE members for their pioneering contributions to the development of the Dynamic Land Ecosystem Model (DLEM). Special thanks go to Dr. Shree Dangal, Dr. Jia Yang, Dr. Bowen Zhang, Dr. Hao Shi, Dr. Yuanzhi Yao, Dr. Naiqing Pan, Mr. Zihao Bian, Mr. Yongfa You, Mr. Zhao Jin, Dr. Chengcheng Gang, Dr. Nan Lv for their valuable discussions and technical supports. I would like to express my appreciation to Ms. Audrey Grindle, Mr. James Fukai, and all the faculty and staff members in the School of Forestry and Wildlife Sciences.

Most importantly, I would express my deepest appreciation and gratitude to my friends and parents Zheng Wang, Haiyan Wang and my parents-in-law Zhanguo Jiang, Yanqiao Qu, my best friend and wife Xiaofei Jiang to whom I dedicate this work, and our family members Groot and Shumiao, Bradley Kirkland, Allison Kirkland, Connor Kirkland and Piper Kirkland. None of this would have been possible without their endless love and unconditional support.

Last, I would acknowledge funding supports from China Scholarship Council, National Science Foundation, and Auburn University's GIS and Remote Sensing Laboratory.

Table of Contents

List of Tables

List of Figures

Chapter 1. Introduction

Phosphorus (P) is fundamental to all living organisms: as an essential element, it is closely related to biochemical energy, genetic materials (DNA and RNA), and structural material of membranes and bone (Ruttenberg, 2003). Phosphorus, as one of three nutrients (nitrogen, potassium, and phosphorus) used in commercial fertilizer, is particularly important for crop yields (Cordell et al., 2009). For example, widely applying phosphate as fertilizer has promoted the "Green Revolution" in the 20th century, which relieves the severe food demand due to rapid population growth by boosting the crop yields dramatically (Elser & Bennett, 2011). However, P is a non-renewable resource and the global P cycle has been strongly enhanced by human activities, such as mining, since the industrial revolution and will be continued in the future. Given the importance of P in controlling vegetation growth and agriculture production, there are increasing concerns and attentions on the P cycle and its influence on the carbon (C) cycle (Cordell & White, 2014; Elser, 2012; Withers et al., 2015). An in-depth understanding of the P cycle and its influence on the C cycle will be important for decision-makers to develop feasible policies for managing P nutrient sustainability and C emission mitigation in the context of climate changing. However, our understanding of the P cycle in terrestrial ecosystems, including some P-specific processes and drivers, is far from fully understood (Achat et al., 2016; Reed et al., 2015).

In terrestrial ecosystems, P mainly resides in three pools: bedrock, soil, and living organisms (biomass). The terrestrial P cycle is the biogeochemical exchanges by which P is transported and converted among the soil, plants, animals and microbes. Phosphorus comes primarily from parent material weathering and is lost through leaching, soil erosion (Filippelli, 2008; Newman, 1995; Wang et al., 2015). Ecosystems with very old soils can become depleted in P. Walker and Syers demonstrated a pattern of lower total P and an increased fraction of

recalcitrant P in older substrates; they suggested old sites reach a “terminal steady state” of P depletion and biological limitation. Tropical areas have no glaciers existed for hundreds of millions of years, and so a larger fraction of tropical sites could approach Walker and Syers' terminal steady state of P depletion and limitation (Davidson et al., 2004; Turner et al., 2018; Vitousek et al., 2010).

The nutrient limitation lies at the heart of ecosystem ecology (Vitousek, 2004). Phosphorus is vitally important for plant photosynthesis. It is required for many transformations of phosphorus-rich molecules (ATP, NADP and sugar-phosphates from the Calvin cycle) and the regeneration of RuBP (ribulose-1, 5-bisphosphate) (Farquhar et al., 1980). Thus, P limitation is expected to reduce photosynthetic capacity by decreasing light-use efficiency, electron transport rates, regeneration of ribulose bisphosphate (RuBP) (Wang et al., 2018). Phosphorus limitation on plant growth and biome productivity has been widely acknowledged, and it is well recognized that there is more P limitation in the highly weathered tropical regions than high latitude areas (Vitousek et al., 2010). Tropical ecosystems account for 60% terrestrial gross primary production (GPP) (Beer et al., 2010) and store about 72% of global forest biomass carbon (C) (Pan et al., 2011), which thereby are considered as the most productive and vital component in the global carbon (C) cycle (Melillo et al., 1993). Therefore, P limitation on plant productivity in the tropics plays a key role in the global C cycle (Elser et al., 2007; Mackenzie et al., 2002; Vitousek et al., 2010).

The CO_2 fertilization effect that increases CO_2 concentrations in leaves enhances plants' capacity in fixing carbon through photosynthesis has been considered as a primary mechanism that maintains a critical negative feedback to climate warming by slowing the rate of increasing CO_2 concentration in the atmosphere (Schimel et al., 2015). Multiple lines of evidence suggest that the CO_2 fertilization effect is highest in tropical ecosystems (Liu et al., 2019; Lloyd, 1999; Schimel et al., 2015). However, studies from field, remote sensing, and process model indicate that tropical

forest response to CO_2 fertilization effect is heavily dependent on plant P acquisition (Ellsworth et al., 2017; Fleischer et al., 2019; Wang et al., 2020). In other words, tropical ecosystem future productivity and C storage are limited by P availability.

Although P limitation (or N/P co-limitation) is widespread throughout the terrestrial biosphere and is expected to increase in the future, our understanding of how P controls the tropical C cycle remains far from certain (Norby et al., 2016; Townsend et al., 2011). As studies show, failing to account for nutrient–C interactions can lead to substantial errors in predicting how ecosystems will respond to climate and other environmental changes (Terrer et al., 2019; Thornton et al., 2007). Thus, although resolving the complex nature of tropical forest nutrient limitation – and then incorporating such knowledge into predictive models – will be difficult, it is a challenge that the global change researchers must address. (Reed et al., 2015; Townsend et al., 2011).

Terrestrial Biosphere Models (TBMs) are an important tool to study terrestrial ecosystem activities under climate change and better understanding and simulating C, N, and P interactions. Within the past decades, TBMs have evolved from the first-generation C only models (Houghton et al., 2001; Lieth, 1975) to CN interactions models (Gerber et al., 2010; Thornton et al., 2007; Tian et al., 2010; Yang et al., 2009; Zaehle & Dalmonech, 2011; Zaehle et al., 2010). In recent years, the P cycle has been incorporated into several TBMs, such as Community Land Model (CLM -CNP) (Yang et al., 2014), CABLE-CNP (Wang et al., 2007), CASA-CNP (Wang et al., 2010), and Organizing Carbon and Hydrology In Dynamic Ecosystems (ORCHIDEE) (Goll et al., 2017), etc. There is mounting evidence that the representation of P in TBMs is important for our understanding and prediction of ecosystem dynamics, particularly for tropical forests with strong P limitation (Fleischer et al., 2019; Goll et al., 2018; Goll et al., 2012). Wang et al. (2010), Goll et al. (2012), and Yang et al. (2014) highlighted the importance of incorporating the P cycle in TBMs,

particularly in tropical ecosystems. Several studies also demonstrated that coupling P dynamics into TBMs could reduce the simulated terrestrial C sink due to increasing atmospheric CO_2 concentrations in the Amazon basin and other areas (Fleischer et al., 2019; Yang et al., 2019; Yang et al., 2016; Zhang et al., 2011). However, there are divergences in model structures and the simulated ecosystem dynamics. For example, TBMs differ in their assumptions on how nutrient limitation controls productivity and C allocation and their representation of soil P acquisition mechanisms (Fleischer et al., 2019).

As projected by IPCC, global atmospheric CO_2 concentration and N deposition are expected to continue to increase in the future (Pachauri & Reisinger, 2007), which could exacerbate P limitation in many regions of the world (Jiang et al., 2019). Many TBMs projected a large increase in tropical ecosystem productivity due to CO_2 concentration and N deposition increase in the 21st century (Hickler et al., 2008; Schimel et al., 2015). However, these model results may lead to an overestimation of carbon uptake by the tropical terrestrial biosphere due to the missed P cycle representation (Cox et al., 2013; Goll et al., 2012; Huntingford et al., 2013; Zhang et al., 2014).

In order to investigate the P cycling impacts on the C cycling in tropical terrestrial ecosystems and the future response of the tropical terrestrial ecosystem to climate change, we developed a process-based P module on the platform of the Dynamic Land Ecosystem Model (DLEM) by considering P impacts on vegetation and soil biogeochemical processes, which upgraded the coupled CN model (DLEM-CN) into the coupled CNP model (DLEM-CNP). The DLEM-CNP are then applied on sites, regions, and pan-tropical scales to estimate the P limitation induced C fluxes and storage changes.

2. Dissertation Structure

This Dissertation is organized according to the structure as below (Figure 1-1),

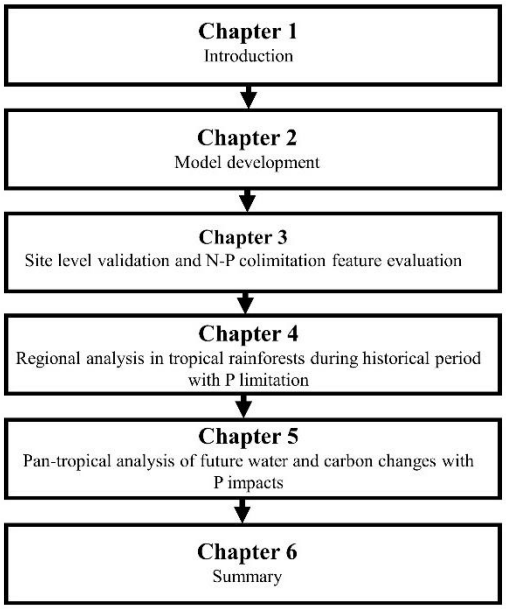

Figure1- 1 The structure of this dissertation.

Chapter 1 presents a brief introduction of background, previous P model works, research questions, and approaches to solve these questions.

Chapter 2 describes the detailed processes regarding the DLEM P module, including the processes of photosynthesis, allocation, turnover, nutrient uptake, decomposition, and P and N co-limitation on various processes.

Chapter 3 evaluate and validate the DLEM-CNP nutrients coupling feature. Simulated GPP, biomass, leaf N: P ratio and plant response to fertilizer addition are validated according to benchmark datasets at the site level.

Chapter 4 describes the simulation of tropical rainforests C cycle during 1860-2018. P limitation on the CO_2 fertilization effect in tropical rainforests is examined.

Chapter 5 investigates the pan tropical GPP, NPP, and CUE trends and changes in future "Shared Socioeconomic Pathways" (SSPs) climate scenarios from 2020 to 2100.

Chapter 6 summarizes the major findings of this study and discusses the possible improvement needs for future work.

References

Achat, D. L., Augusto, L., Gallet-Budynek, A., & Loustau, D. (2016). Future challenges in coupled C–N–P cycle models for terrestrial ecosystems under global change: a review. *Biogeochemistry, 131*(1), 173-202. https://doi.org/10.1007/s10533-016-0274-9

Beer, C., Reichstein, M., Tomelleri, E., Ciais, P., Jung, M., Carvalhais, N., et al. (2010). Terrestrial Gross Carbon Dioxide Uptake: Global Distribution and Covariation with Climate. *Science, 329*(5993), 834-838. https://doi.org/10.1126/science.1184984

Cordell, D., Drangert, J.-O., & White, S. (2009). The story of phosphorus: Global food security and food for thought. *Global Environmental Change, 19*(2), 292-305. https://doi.org/https://doi.org/10.1016/j.gloenvcha.2008.10.009

Cordell, D., & White, S. (2014). Life's Bottleneck: Sustaining the World's Phosphorus for a Food Secure Future. *Annual Review of Environment and Resources, 39*(1), 161-188. https://doi.org/10.1146/annurev-environ-010213-113300

Cox, P. M., Pearson, D., Booth, B. B., Friedlingstein, P., Huntingford, C., Jones, C. D., & Luke, C. M. (2013). Sensitivity of tropical carbon to climate change constrained by carbon dioxide variability. *Nature, 494*, 341. https://doi.org/10.1038/nature11882

Davidson, E. A., Reis de Carvalho, C. J., Vieira, I. C. G., Figueiredo, R. d. O., Moutinho, P., Yoko Ishida, F., et al. (2004). NITROGEN AND PHOSPHORUS LIMITATION OF BIOMASS GROWTH IN A TROPICAL SECONDARY FOREST. *Ecological applications, 14*(sp4), 150-163. https://doi.org/10.1890/01-6006

Ellsworth, D. S., Anderson, I. C., Crous, K. Y., Cooke, J., Drake, J. E., Gherlenda, A. N., et al. (2017). Elevated CO 2 does not increase eucalypt forest productivity on a low-phosphorus soil. *Nature Climate Change, 7*(4), 279.

Elser, J., & Bennett, E. (2011). Phosphorus cycle: A broken biogeochemical cycle. *Nature, 478*(7367), 29-31. https://doi.org/10.1038/478029a

Elser, J. J. (2012). Phosphorus: a limiting nutrient for humanity? *Curr Opin Biotechnol, 23*(6), 833-838. https://doi.org/10.1016/j.copbio.2012.03.001

Elser, J. J., Bracken, M. E., Cleland, E. E., Gruner, D. S., Harpole, W. S., Hillebrand, H., et al. (2007). Global analysis of nitrogen and phosphorus limitation of primary producers in freshwater, marine and terrestrial ecosystems. *Ecology letters, 10*(12), 1135-1142.

Farquhar, G. D., von Caemmerer, S. v., & Berry, J. A. J. P. (1980). A biochemical model of photosynthetic CO 2 assimilation in leaves of C 3 species. *149*(1), 78-90.

Filippelli, G. M. (2008). The global phosphorus cycle: past, present, and future. *Elements, 4*(2), 89-95.

Fleischer, K., Rammig, A., De Kauwe, M. G., Walker, A. P., Domingues, T. F., Fuchslueger, L., et al. (2019). Amazon forest response to CO2 fertilization dependent on plant phosphorus acquisition. *Nature Geoscience*. https://doi.org/10.1038/s41561-019-0404-9

Gerber, S., Hedin, L. O., Oppenheimer, M., Pacala, S. W., & Shevliakova, E. (2010). Nitrogen cycling and feedbacks in a global dynamic land model. *Global Biogeochemical Cycles, 24*(1). https://doi.org/10.1029/2008GB003336

Goll, D., Joetzjer, E., Huang, M., & Ciais, P. (2018). Low Phosphorus Availability Decreases Susceptibility of Tropical Primary Productivity to Droughts. *Geophysical Research Letters, 45*(16), 8231-8240.

Goll, D., Vuichard, N., Maignan, F., Jornet-Puig, A., Sardans, J., Violette, A., et al. (2017). A representation of the phosphorus cycle for ORCHIDEE (revision 4520). *Geoscientific Model Development Discussions, 10*(10), 3745-3770.

Goll, D. S., Brovkin, V., Parida, B. R., Reick, C. H., Kattge, J., Reich, P. B., et al. (2012). Nutrient limitation reduces land carbon uptake in simulations with a model of combined carbon, nitrogen and phosphorus cycling. *Biogeosciences, 9*(9), 3547-3569. https://doi.org/10.5194/bg-9-3547-2012

Hickler, T., Smith, B., Prentice, I. C., Mjöfors, K., Miller, P., Arneth, A., & Sykes, M. T. (2008). CO2 fertilization in temperate FACE experiments not representative of boreal and tropical forests. *Global Change Biology, 14*(7), 1531-1542.

Houghton, J. T., Ding, Y., Griggs, D., Noguer, M., van der Linden, P., Dai, X., et al. (2001). Climate Change 2001: The Scientific Basis, Cambridge Uni. In: Press.

Huntingford, C., Zelazowski, P., Galbraith, D., Mercado, L. M., Sitch, S., Fisher, R., et al. (2013). Simulated resilience of tropical rainforests to CO2-induced climate change. *Nature Geoscience, 6*(4), 268-273. https://doi.org/10.1038/ngeo1741

Jiang, M., Caldararu, S., Zaehle, S., Ellsworth, D. S., & Medlyn, B. E. (2019). Towards a more physiological representation of vegetation phosphorus processes in land surface models. *New Phytologist*.

Lieth, H. (1975). Modeling the Primary Productivity of the World. In H. Lieth & R. H. Whittaker (Eds.), *Primary Productivity of the Biosphere* (pp. 237-263). Berlin, Heidelberg: Springer Berlin Heidelberg.

Liu, Y., Piao, S., Gasser, T., Ciais, P., Yang, H., Wang, H., et al. (2019). Field-experiment constraints on the enhancement of the terrestrial carbon sink by CO2 fertilization. *Nature Geoscience*. https://doi.org/10.1038/s41561-019-0436-1

Lloyd, J. (1999). The CO2 dependence of photosynthesis, plant growth responses to elevated CO2 concentrations and their interaction with soil nutrient status, II. Temperate and boreal forest productivity and the combined effects of increasing CO2 concentrations and increased nitrogen deposition at a global scale. *Functional Ecology, 13*(4), 439-459. https://doi.org/10.1046/j.1365-2435.1999.00350.x

Mackenzie, F. T., Ver, L. M., & Lerman, A. (2002). Century-scale nitrogen and phosphorus controls of the carbon cycle. *Chemical Geology, 190*(1), 13-32.

Melillo, J. M., McGuire, A. D., Kicklighter, D. W., Moore, B., Vorosmarty, C. J., & Schloss, A. L. (1993). Global climate change and terrestrial net primary production. *Nature, 363*(6426), 234.

Newman, E. I. (1995). Phosphorus Inputs to Terrestrial Ecosystems. *Journal of Ecology, 83*(4), 713-726. https://doi.org/10.2307/2261638

Norby, R. J., Gu, L., Haworth, I. C., Jensen, A. M., Turner, B. L., Walker, A. P., et al. (2016). Informing models through empirical relationships between foliar phosphorus, nitrogen and photosynthesis across diverse woody species in tropical forests of Panama. *New Phytologist*.

Pachauri, R. K., & Reisinger, A. (2007). IPCC fourth assessment report. *IPCC, Geneva, 2007*.

Pan, Y., Birdsey, R. A., Fang, J., Houghton, R., Kauppi, P. E., Kurz, W. A., et al. (2011). A Large and Persistent Carbon Sink in the World's Forests. *Science, 333*(6045), 988. https://doi.org/10.1126/science.1201609

Reed, S. C., Yang, X., & Thornton, P. E. (2015). Incorporating phosphorus cycling into global modeling efforts: a worthwhile, tractable endeavor. *New Phytologist, 208*(2), 324-329.

Ruttenberg, K. (2003). The global phosphorus cycle. *Treatise on geochemistry, 8*, 682.

Schimel, D., Stephens, B. B., & Fisher, J. B. (2015). Effect of increasing CO2 on the terrestrial carbon cycle. *Proceedings of the National Academy of Sciences, 112*(2), 436-441.

Tanner, E. V. J., Vitousek, P. M., & Cuevas, E. (1998). EXPERIMENTAL INVESTIGATION OF NUTRIENT LIMITATION OF FOREST GROWTH ON WET TROPICAL MOUNTAINS. *Ecology, 79*(1), 10-22. https://doi.org/10.1890/0012-9658(1998)079[0010:EIONLO]2.0.CO;2

Terrer, C., Jackson, R. B., Prentice, I. C., Keenan, T. F., Kaiser, C., Vicca, S., et al. (2019). Nitrogen and phosphorus constrain the CO2 fertilization of global plant biomass. *Nature Climate Change, 9*(9), 684-689. https://doi.org/10.1038/s41558-019-0545-2

Thornton, P. E., Lamarque, J.-F., Rosenbloom, N. A., & Mahowald, N. M. (2007). Influence of carbon-nitrogen cycle coupling on land model response to CO2 fertilization and climate variability. *Global Biogeochemical Cycles, 21*(4). https://doi.org/10.1029/2006GB002868

Tian, H., Liu, M., Zhang, C., Ren, W., Xu, X., Chen, G., et al. (2010). The dynamic land ecosystem model (DLEM) for simulating terrestrial processes and interactions in the context of multifactor global change. *Acta Geographica Sinica, 65*(9), 1027-1047.

Townsend, A. R., Cleveland, C. C., Houlton, B. Z., Alden, C. B., & White, J. W. C. (2011). Multi-element regulation of the tropical forest carbon cycle. *Frontiers in Ecology and the Environment, 9*(1), 9-17. https://doi.org/https://doi.org/10.1890/100047

Turner, B. L., Brenes-Arguedas, T., & Condit, R. (2018). Pervasive phosphorus limitation of tree species but not communities in tropical forests. *Nature, 555*, 367. https://doi.org/10.1038/nature25789

Vitousek, P. M., Porder, S., Houlton, B. Z., & Chadwick, O. A. (2010). Terrestrial phosphorus limitation: mechanisms, implications, and nitrogen–phosphorus interactions. *Ecological applications, 20*(1), 5-15.

Walker, T. W., & Syers, J. K. (1976). The fate of phosphorus during pedogenesis. *Geoderma, 15*(1), 1-19. https://doi.org/https://doi.org/10.1016/0016-7061(76)90066-5

Wang, J., Wen, X., Zhang, X., Li, S., & Zhang, D.-Y. (2018). Co-regulation of photosynthetic capacity by nitrogen, phosphorus and magnesium in a subtropical Karst forest in China. *Scientific Reports, 8*(1), 7406. https://doi.org/10.1038/s41598-018-25839-1

Wang, R., Balkanski, Y., Boucher, O., Ciais, P., Peñuelas, J., & Tao, S. (2015). Significant contribution of combustion-related emissions to the atmospheric phosphorus budget. *Nature Geoscience, 8*(1), 48-54. https://doi.org/10.1038/ngeo2324

Wang, S., Zhang, Y., Ju, W., Chen, J. M., Ciais, P., Cescatti, A., et al. (2020). Recent global decline of CO_2 fertilization effects on vegetation photosynthesis. *Science, 370*(6522), 1295-1300. https://doi.org/10.1126/science.abb7772

Wang, Y. P., Houlton, B. Z., & Field, C. B. (2007). A model of biogeochemical cycles of carbon, nitrogen, and phosphorus including symbiotic nitrogen fixation and phosphatase production. *Global Biogeochemical Cycles, 21*(1). https://doi.org/10.1029/2006GB002797

Wang, Y. P., Law, R., & Pak, B. (2010). A global model of carbon, nitrogen and phosphorus cycles for the terrestrial biosphere. *Biogeosciences, 7*(7), 2261-2282.

Withers, P. J. A., Elser, J. J., Hilton, J., Ohtake, H., Schipper, W. J., & van Dijk, K. C. (2015). Greening the global phosphorus cycle: how green chemistry can help achieve planetary P sustainability. *Green Chem., 17*(4), 2087-2099. https://doi.org/10.1039/c4gc02445a

Yang, X., Ricciuto, D. M., Thornton, P. E., Shi, X., Xu, M., Hoffman, F., & Norby, R. J. (2019). The effects of phosphorus cycle dynamics on carbon sources and sinks in the Amazon region: a modeling study using ELM v1. *Journal of Geophysical Research: Biogeosciences, 0*(ja). https://doi.org/10.1029/2019JG005082

Yang, X., Thornton, P., Ricciuto, D., & Post, W. (2014). The role of phosphorus dynamics in tropical forests–a modeling study using CLM-CNP. *Biogeosciences, 11*(6), 1667-1681.

Yang, X., Thornton, P. E., Ricciuto, D. M., & Hoffman, F. M. (2016). Phosphorus feedbacks constraining tropical ecosystem responses to changes in atmospheric CO2 and climate. *Geophysical Research Letters, 43*(13), 7205-7214. https://doi.org/10.1002/2016GL069241

Yang, X., Wittig, V., Jain, A. K., & Post, W. (2009). Integration of nitrogen cycle dynamics into the Integrated Science Assessment Model for the study of terrestrial ecosystem responses to global change. *Global Biogeochemical Cycles, 23*(4). https://doi.org/10.1029/2009GB003474

Zaehle, S., & Dalmonech, D. (2011). Carbon–nitrogen interactions on land at global scales: current understanding in modelling climate biosphere feedbacks. *Current Opinion in Environmental Sustainability, 3*(5), 311-320. https://doi.org/https://doi.org/10.1016/j.cosust.2011.08.008

Zaehle, S., Friend, A. D., Friedlingstein, P., Dentener, F., Peylin, P., & Schulz, M. (2010). Carbon and nitrogen cycle dynamics in the O-CN land surface model: 2. Role of the nitrogen cycle in the historical terrestrial carbon balance. *Global Biogeochemical Cycles, 24*(1). https://doi.org/10.1029/2009gb003522

Zhang, Q., Wang, Y.-P., Matear, R., Pitman, A., & Dai, Y. (2014). Nitrogen and phosphorous limitations significantly reduce future allowable CO2 emissions. *Geophysical Research Letters, 41*(2), 632-637.

Zhang, Q., Wang, Y. P., Pitman, A. J., & Dai, Y. J. (2011). Limitations of nitrogen and phosphorous on the terrestrial carbon uptake in the 20th century. *Geophysical Research Letters, 38*(22). https://doi.org/10.1029/2011GL049244

Chapter 2. The description of the DLEM phosphorus module

1. The Dynamic Land Ecosystem Model (DLEM)

The Dynamic Land Ecosystem Model (DLEM) is a highly integrated process-based TBM aiming to provide an integrated modeling framework for predictive understanding of how multi-factor global changes have affected and will affect the structure and functioning of terrestrial ecosystems across multiple spatial and temporal scales. DLEM simulates the consequences of natural and anthropogenic disturbances on the structure and functions of terrestrial ecosystems and their feedbacks to human and natural systems on Earth's land surface and terrestrial-aquatic continuum. More specifically, the model has integrated biophysical, hydrological, and biogeochemical processes (C, N cycling), vegetation dynamics, disturbances including natural and anthropogenic stresses (e.g., changes in climate, atmospheric composition, and land use land cover patterns, intensive management on crops and forests, wildfire, etc.), and the synergy effects with the human system (Figure 2-1).

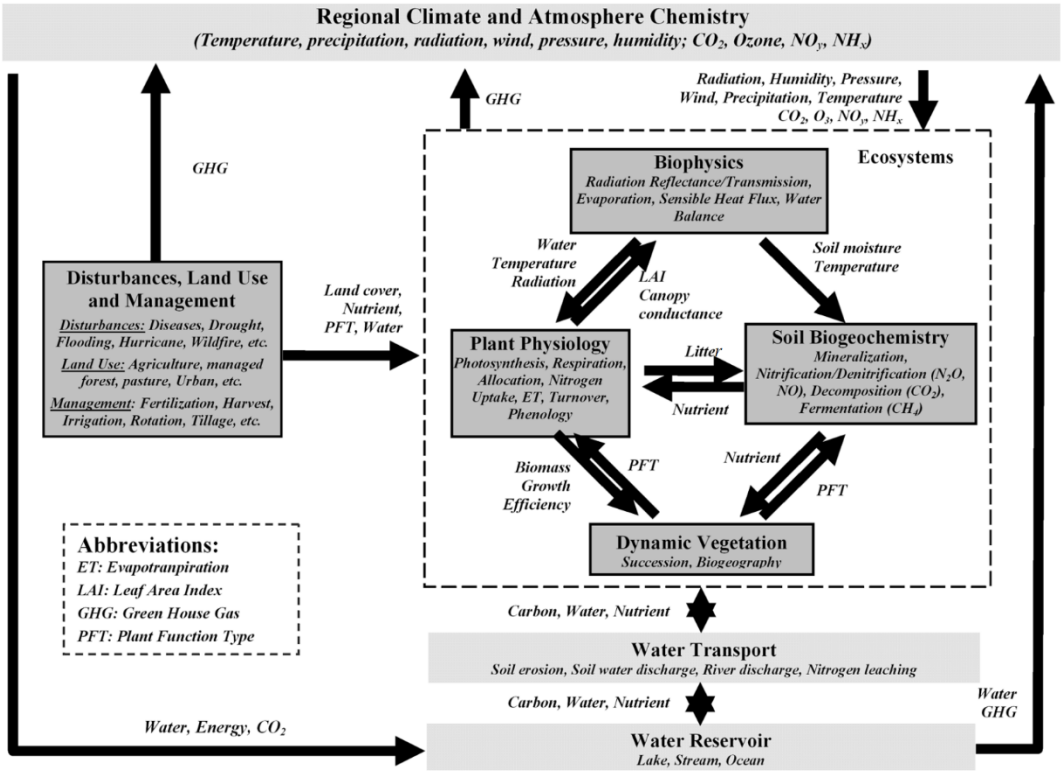

Figure2- 1 Framework of the Dynamic Land Ecosystem Model, version of DLEM-CN (Tian et al., 2010c).

In the DLEM, the simulation time step for soil thermal and hydrological processes (e.g., evapotranspiration, water interceptions, and water movement between grids) is 30-minute, while physiological and biogeochemical processes (such as photosynthesis, plant respiration, organic matter decomposition, nitrogen mineralization and immobilization, etc.) is daily. Land-use/land cover change and the associated carbon emissions are simulated annually. Spatial resolution for the DLEM is flexible and dependent on the input data. DLEM is driven by various input datasets mainly in four major types: (1) time invariant data (such as topography, soil properties, river network, and plant biophysical characteristics), (2) climate (including daily average/minimum/ maximum temperature, precipitation, and shortwave radiation), (3) atmospheric chemistry (e.g., atmospheric CO_2, and nitrogen deposition), and (4) land use history (including land use transitions

and land management). Currently, part of the time-series datasets, such as climate, is required as daily time step, while the other driving datasets, e.g., atmospheric CO_2 concentration, nitrogen deposition, land-use history, and land management (irrigation, N fertilizer application) are applied with monthly or annual time step.

As a spatially explicit ecosystem model, the basic simulation unit of DLEM is a single grid with a corresponding coverage area. In the DLEM, we use a cohort structure to represent multiple plant functional types (PFTs) and land covers in each grid. Totally seven types of land cover and water bodies can be specified in each grid, including vegetation cover, impervious surface, lake, stream, sea, bare ground, and glacier. DLEM builds on the concept of plant functional types to describe vegetation distributions. Many different PFTs who adapt to local climate can coexist in the same grid, competing for light, water, and nutrient resources. The vegetation area consists of up to five PFTs, among which four types are reserved for natural PFTs and one for crops. All land cover types in each grid share a common soil water column, while physiological and soil biogeochemical processes for each PFT are simulated independently. In the DLEM, C enters the ecosystems mainly through vegetation CO_2 uptake during photosynthesis and leaves the ecosystems via ecosystem respiration, various land disturbances and harvest, and lateral transport to a water body. N enters natural ecosystems through biological N fixation and atmospheric N deposition. N leaves ecosystem through different pathways, including NH_3 volatilization, emissions of N_2O, NO, and N_2 during nitrification and denitrification, N leaching from root zone to groundwater, and lateral N transport with surface runoff. The DLEM model is capable of making daily and spatially explicit estimates on fluxes of water, greenhouse gases (including CO_2, CH_4, and N_2O), dynamics of soil C, N, and water pools in terrestrial ecosystems, and the associated river discharge, riverine export of C and N from land to the ocean (Liu et al., 2013; Lu & Tian, 2013;

Lu et al., 2012; Pan et al., 2020; Ren et al., 2007; Tian et al., 2010a; Tian et al., 2011; Tian et al., 2015). The DLEM simulates the linkage between C, N, and water cycles across the plant-soil-atmosphere continuum, in which C and N processes had been included. However, P processes have not been incorporated.

2. The development of the DLEM-CNP

I added the P processes in the DLEM, and the cycles of C, N, and P are fully coupled in DLEM-CNP during photosynthesis, allocation, turnover, nutrient uptake, and decomposition (Figure 2-2). In DLEM-CNP, organic P transfers into inorganic forms through mineralization in the soil, while inorganic P converts to organic form through immobilization and vegetation uptake.

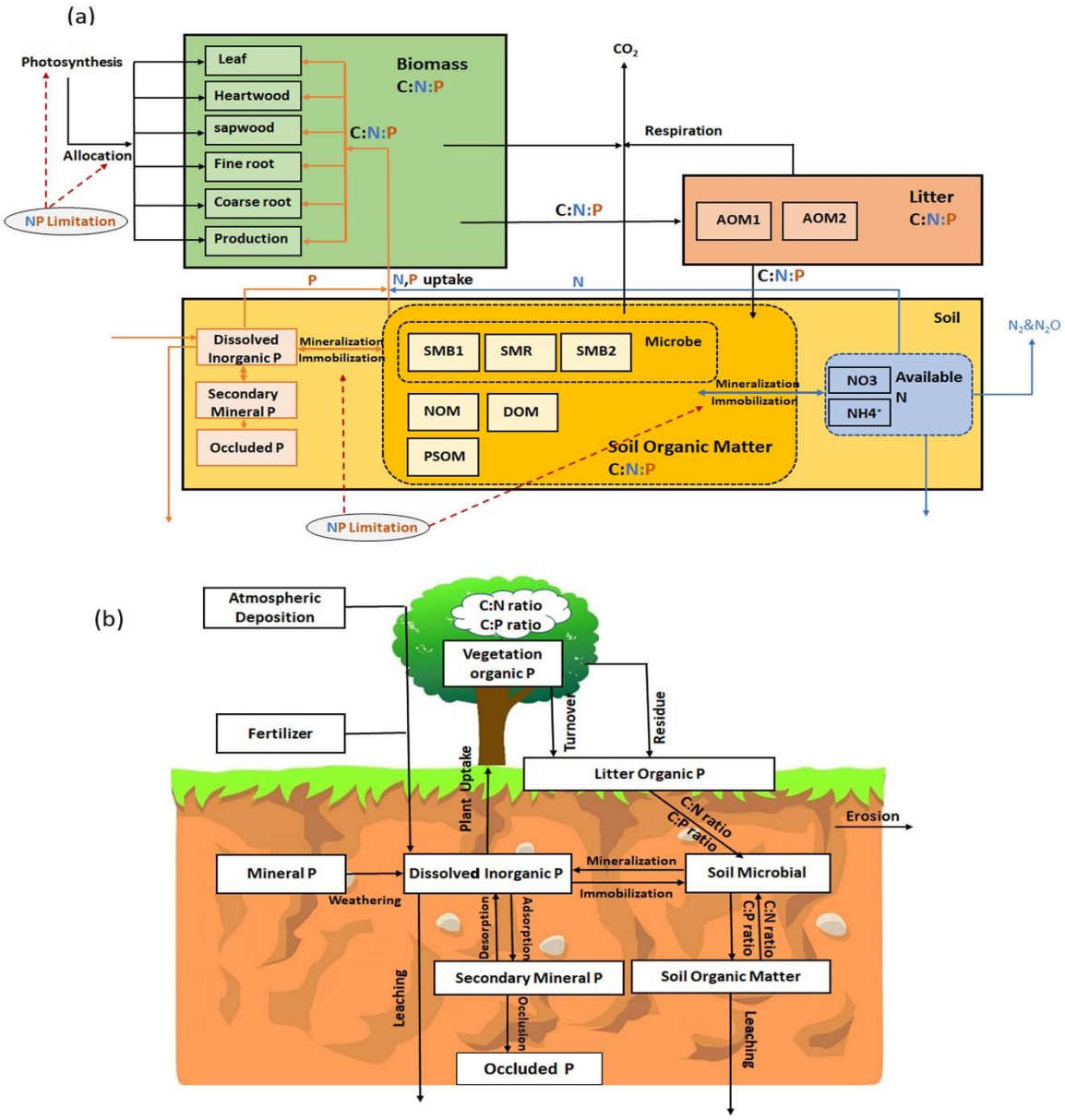

Figure2- 2 Structure of (a) CNP cycles in DLEM-CNP: C enters the ecosystems through vegetation CO_2 uptake during photosynthesis. The plant biomass box consists of six CNP pools: (leaf, heartwood, sapwood, fine root, coarse root, and production). Litters are grouped into two added organic matter pools (AOM1 and AOM2) with different residence times. Soil organic matter has six pools: three microbial pools, namely, soil microbial 1(SMB1), soil microbial 2 (SMB2), soil microbial residues (SMR), two slow soil organic matter pools, namely, native organic matter (NOM), passive soil organic matter (PSOM), one dissolved organic matter (DOM). All these pools have corresponding N, P pools with specific C: N: P ratios. Soil available N box includes ammonium (NH_4^+), nitrate (NO_3^-). P in soil includes dissolved inorganic P pool, secondary mineral P pool, and occluded P pool. NP limitation has impacts on photosynthesis, carbon allocation, soil mineralization and immobilization processes. (b) P module: P enters ecosystems in the form of dissolved inorganic P from weathering of minerals, atmospheric deposition and fertilizer. Dissolved inorganic P is the sole source for plants and

microbes and can be reversibly adsorbed (secondary mineral P) onto soil particles or lost through leaching. Secondary mineral P can transform into occluded P, which is irreversibly lost to biota. When plants take up P from soils, it enters the plant allocating to growing plant tissues. When plant tissue is shed, part of the phosphorus is resorbed, while the rest enters the litter pools, from where it is either transformed into soil organic matter or mineralized.

2.1 Vegetation P processes

In the DLEM-CNP, woody vegetation is composed of six pools (1: leaf, 2: sapwood, 3: fine root, 4: coarse root, 5: reproduction pool, 6: heartwood pool), and herbaceous vegetation is composed of five pools (leaf, stem, fine root, coarse root, and reproduction). The stoichiometric relationship in each pool is determined by P uptake from soil, P allocation, tissue turnover, and minimum C: N ratio and C: P ratio (Table 2-1). Here we describe leaf nutrients limitation on photosynthesis, P uptake and allocation processes.

Table 2- 1 DLEM-CNP parameter table for P-related processes for tropical evergreen broadleaf forests (TrBEF).

Parameter	Value	Units	Description	Source
P_{up_max}	0.0019	$gPm^{-2}\ day^{-1}$	maximum vegetation P uptake rate	Ducnuigeen et al., 1997; Goll et al., 2012; Kelly et al., 2007; Pellet & El-Sharkawy, 1993
k_{up}	1.0	$g\ P\ m^{-2}$	concentration of P_{dip} at which vegetation P uptake is half of the maximum rate	calibrated
k	0.65	-	canopy extinction coefficient	Pan et al. (2014, 2015)
$CP_{min,leaf}$	400	g C/g P	minimum C:P ratio in leaf	Wang et al. (2017); McGroddy et al., (2004)
$CP_{leaflitter}$	2000	g C/g P	C:P ratio in leaflitter	Calibrated
$CP_{min,sapwood}$	2625	g C/g P	minimum C:P ratio in sapwood	Wang et al. (2017)
$CP_{min,heartwood}$	2625	g C/g P	minimum C:P ratio in heartwood	Wang et al. (2017)
$CP_{min,fineroot}$	615	g C/g P	minimum C:P ratio in fineroot	Wang et al. (2017)
$CP_{min,coarseroot}$	2625	g C/g P	minimum C:P ratio in coarseroot	Wang et al. (2017)
$CP_{min,AOM1}$	1593	g C/g P	minimum C:P ratio in AOM1 pool	Cleveland and Liptzin (2007)
$CP_{min,AOM2}$	951	g C/g P	minimum C:P ratio in AOM2 pool	Cleveland and Liptzin (2007)
$CP_{min,SMB1}$	29	g C/g P	minimum C:P ratio in SMB1 pool	Cleveland and Liptzin (2007)
$CP_{min,SMB2}$	29	g C/g P	minimum C:P ratio in SMB2 pool	Cleveland and Liptzin (2007)
$CP_{min,SMR}$	29	g C/g P	minimum C:P ratio in SME pool	Cleveland and Liptzin (2007)
$CP_{min,NOM}$	54	g C/g P	minimum C:P ratio in NOM pool	Cleveland and Liptzin (2007)
$CP_{min,PSOM}$	54	g C/g P	minimum C:P ratio in PSOM pool	Cleveland and Liptzin (2007)
$lchb_{dop}$	3×10^{-5}	$g\ P\ g^{-1}soil$	desorption coefficient for dissolved organic P	calibrated
$lchb_{dip}$	1.2×10^{-6}	$g\ P\ g^{-1}soil$	desorption coefficient for inorganic P	calibrated

2.1.1 P and N co-limitation on photosynthesis

We adopted the N-P co-limitation equation from the MIKE 3 ecohydrodynamic 3-dimensional model developed by the Danish Hydraulics Institute, which is originally applied to modeling N and P limitation on phytoplankton growth (Lessin et al., 2007). Most models which incorporate N and P cycles simply describe nutrients limitation by using Liebig's law of minimum (e.g., ORCHIDEE, CLM). In comparison, our N and P interactive co-limitation scheme has the advantage of simulating the interaction effects of N, P limitation on photosynthesis.

Photosynthesis

The gross primary productivity (GPP) calculation method in the DLEM-CNP is the same as that in the DLEM (Tian et al., 2010a; Tian et al., 2010b). The DLEM uses a modified Farquhar's model to simulate GPP (Bonan, 1996; Collatz et al., 1991; Farquhar et al., 1980; Sellers et al., 1996). The canopy is divided into sunlit and shaded layers. GPP (g C m^{-2} day^{-1}) is calculated by scaling leaf assimilation rates (g C m^{-2} day^{-1}) up to the whole canopy:

$$GPP_{sun} = 12.01 \times 10^{-6} \times A_{sun} \times plai_{sun} \times dayl \times 3600 \quad (1)$$

$$GPP_{shade} = 12.01 \times 10^{-6} \times A_{shade} \times plai_{shade} \times dayl \times 3600 \quad (2)$$

$$GPP = GPP_{sun} + GPP_{shade} \quad (3)$$

where GPP_{sun} and GPP_{shade} are the GPP of sunlit and shaded canopy, respectively; A_{sun} and A_{shade} are assimilation rates of the sunlit and shaded canopy; $plai_{sum}$ and $plai_{shade}$ are sunlit and shaded leaf area indices, estimated as equations 4 and 5, respectively; $dayl$ is daytime length (second) in a day (h). 12.01×10^{-6} is a constant to change the unit from μmol CO_2 to gram C.

$$plai_{sun} = 1 - EXP(-proj_{LAI}) \quad (4)$$

$$plai_{shade} = proj_{LAI} - plai_{sun} \quad (5)$$

where $proj_{LAI}$ is the projected leaf area index, which is calculated as the product of leaf carbon content (g C m^{-2}) and PFT specific leaf area (SLA, m^2 g C^{-1}). Using similar methods to Collatz et al. (1991), DLEM determines the C assimilation rate (*A*) as the minimum of three limiting rates, w_c , w_j, w_e, which are functions that represent the assimilation rates as limited by the efficiency of the photosynthetic enzymes system (Rubisco-limited), the amount of photosynthetically active radiation (PAR) captured by leaf chlorophyll (light-limited), and the capacity of leaves to export or utilize photosynthesis products (export-limited) for C_3 species, respectively. For C_4 species, w_e refer to the phosphoenolpyruvate (PEP) carboxylase limited rate of carboxylation. Sunlit and the shaded canopy C assimilation rate can be estimated as:

$$A = \min(w_c, w_j, w_e) \times Index_{gs} \quad (6)$$

$$w_c = \begin{cases} \dfrac{(c_i - \Gamma_*)V_{max}}{c_i + K_c(1 + o_i/K_0)} & for\ C_3\ plants \\ V_{max} & for\ C_4\ plants \end{cases} \quad (7)$$

$$w_j = \begin{cases} \dfrac{(c_i - \Gamma_*)4.6\emptyset\alpha}{c_i + 2\Gamma_*} & for\ C_3\ plants \\ 4.6\emptyset\alpha & for\ C_4\ plants \end{cases} \quad (8)$$

$$w_j = \begin{cases} 0.5V_{max} & for\ C_3\ plants \\ 4000V_{max}\dfrac{c_i}{P_{atm}} & for\ C_4\ plants \end{cases} \quad (9)$$

where c_i is internal leaf CO_2 concentration (Pa); o_i is O_2 concentration (Pa); Γ_* is CO_2 compensation point (Pa); K_c and K_0 (Pa) are Michaelis-Menten constants for CO_2 and O_2 at 25 ^oC, respectively; α is quantum efficiency; $\emptyset$ is absorbed photosynthetically active radiation ($W \cdot M^{-2}$);

V_{max} (μmol CO_2 m^{-2} s^{-1}) is maximum rate of carboxylation varies with temperature, foliage nitrogen and phosphorus concentration, and soil moisture (Bonan, 1996), calculated as:

$$V_{max} = V_{max25} a_{vmax}^{\frac{T_{ave}-25}{10}} f(NP) f(T_{ave}) \beta_t \quad (10)$$

where V_{max25} is maximum rate of carboxylation at 25 °C (μmol CO_2 m^{-2} s^{-1}) and a_{vmax} is maximum temperature sensitivity parameter. $f(NP)$ adjusts the rate of photosynthesis, calculated in equation 25 and 26. The leaf nitrogen limitation coefficients are estimated for sunlit and shaded leaves and:

$$f_{sun}(N) = \frac{Ncon_{sun_{leaf}}}{Ncon_{leaf\_max}} \quad (11)$$

$$f_{shade}(N) = \frac{Ncon_{shade_{leaf}}}{Ncon_{leaf\_max}} \quad (12)$$

where $Ncon_{sun\_leaf}$ and $Ncon_{shade\_leaf}$ are N concentration (g N / g dry matter) for the sunlit and shaded leaves, and $Ncon_{leaf\_max}$ is maximum leaf N concentration (g N / g dry matter). The formulas of the three variables are:

$$Ncon_{sun_{leaf}} = \frac{\frac{0.45 \times N_{leaf}}{C_{leaf}}}{\frac{LAI_{sun}}{LAI} + \frac{LAI_{shade} e^{-0.5k}}{LAI}} \quad (13)$$

$$Ncon_{shade_{leaf}} = Ncon_{sun_{leaf}} \times e^{-0.5k} \quad (14)$$

$$Ncon_{leaf\_max} = \frac{0.45}{CN_{min,leaf}} \tag{15}$$

where LAI_{sun} and LAI_{shade} are leaf area index for sunlit and shaded leaves, LAI is total leaf area index of plant canopy, N_{leaf} is leaf N content (g N m^{-2}), C_{leaf} is leaf carbon content (g C m^{-2}), 0.45 is conversion factor from carbon to dry biomass, k is canopy extinction coefficient, and $CN_{min,leaf}$ is the minimum C : N ratio for leaves.

$f(T_{ave})$ is a function of temperature-related metabolic processes as the following:

$$f(T_{ave}) = \left[1 + \exp\left(\frac{-220000 + 710(T_{ave} + 273.16)}{8.314(T_{ave} + 273.16)}\right)\right]^{-1} \tag{16}$$

β_t is a function (0-1) that represents the soil moisture and the lower temperature effects on stomatal resistance and photosynthesis.

$$\beta_t = \beta(T_{min}) \times \beta(w) \tag{17}$$

$$\beta(T_{min}) = \begin{cases} 0 & for\ T_{min} < -8\ ℃ \\ 1 + 0.125T_{min} & for -8\ ℃ \le T_{min} \le 0\ ℃ \\ 1 & for\ \ T_{min} > 0\ ℃ \end{cases} \tag{18}$$

$$\beta(w) = \sum_{i=1}^{10} w_i\, r_i \tag{19}$$

$$w_i = \begin{cases} 0 & for\ ps_i > psi_{close} \\ \dfrac{psi_{close} - ps_i}{psi_{close} - psi_{open}} & for\ psi_{open} \le ps_i \le psi_{close} \\ 1 & for\ ps_i < psi_{close} \end{cases} \tag{20}$$

where T_{min} is daily minimum temperature; w_i is soil water stress of soil layer i; ps_i is soil water potential of soil layer i, estimated from Saxton and Rawls (2006). r_i is root fractions distributed in soil layer i; psi_{close} and psi_{open} are te plant functional specific tolerance of the soil water potential for stomata overall close and open. The water stress in plants is a function of soil water potential, which ranges from 0 to 1. Under no water limitations, the soil water stress of soil layer i (w_i) is equal to 1 where the soil water potential is at its maximum i.e., soil water potential when the stomata is opened (psi_{open}). Under frequent water stress, however, w_i is calculated based on wilting point potential of specific plant functional types and depends on the balance between psi_{close} and psi_{open}.

Leaf stomatal resistance and leaf photosynthesis are coupled together through the following (Bonan, 1996; Collatz et al., 1991; Sellers et al., 1996).

$$\frac{1}{r_s} = \mathrm{m}\frac{A}{C_s}\frac{e_s}{e_i}P_{atm} + b \tag{21}$$

where r_s is leaf stomatal resistance, m is an empirical parameter, A is leaf photosynthesis, C_s is leaf surface CO_2 concentration, e_s is leaf surface vapor pressure, e_i is saturated vapor pressure inside leaf, b is minimum stomatal conductance with $A = 0$, and P_{atm} is atmospheric pressure. Together in the following equations:

$$C_s = C_a - 1.37 r_b P_{atm} A \tag{22}$$

$$e_s = \frac{e_a' + e_i r_b}{r_b + r_s} \tag{23}$$

where C_a is atmospheric CO_2 concentration, r_b is boundary resistance, e_a is vapor pressure of air, and stomatal resistance is the larger of the two roots of this quadratic (Bonan, 1996).

$$\left(\frac{mAP_{atm}e_a^{'}}{C_s e_i} + b\right) {r_s}^2 + \left(\frac{mAP_{atm}r_b}{C_s} + br_b - 1\right) r_s - r_b = 0 \quad (24)$$

P and N co-limitation

Leaf P concentration is calculated separately for sunlit and shaded leaves to estimate P limitation on photosynthesis. To account for the interactive co-limitation effect of N and P, the joint nutrient scalar $f(NP)$is calculated as (Lessin et al., 2007):

$$f_{sun}(NP) = \frac{2}{\frac{1}{f_{sun}(N)} + \frac{1}{f_{sun}(P)}} \quad (25)$$

$$f_{shade}(NP) = \frac{2}{\frac{1}{f_{shade}(N)} + \frac{1}{f_{shade}(P)}} \quad (26)$$

where $f_{sun}(N)$ and $f_{shade}(N)$ are sunlit and shaded leaves N limitation coefficients, and $f_{sun}(P)$ and $f_{shade}(P)$ are sunlit and shaded leaves P limitation coefficients. Leaf nutrient limitation coefficients are applied to impact the maximum rate of carboxylation (V_{cmax}), through which the electron transport capacity (J_{max}) is also affected.

Specifically, leaf P limitation coefficients $f_{sun}(P)$ and $f_{shade}(P)$ are estimated in a similar way as the leaf N limitation coefficients in the DLEM (Pan et al., 2014a),

$$f_{sun}(P) = \frac{Pcon_{sun_{leaf}}}{Pcon_{leaf\_max}} \quad (27)$$

$$f_{shade}(P) = \frac{Pcon_{shade_{leaf}}}{Pcon_{leaf\_max}} \quad (28)$$

where $Pcon_{sun\_leaf}$ and $Pcon_{shade\_leaf}$ are P concentration (g P / g dry matter) for sunlit and shaded leaves, and $Pcon_{leaf\_max}$ is maximum leaf P concentration (g P / g dry matter). The formulas of the three variables are:

$$Pcon_{sun_{leaf}} = \frac{\frac{0.45 \times P_{leaf}}{C_{leaf}}}{\frac{LAI_{sun}}{LAI} + \frac{LAI_{shade}e^{-0.5k}}{LAI}} \quad (29)$$

$$Pcon_{shade_{leaf}} = Pcon_{sun_{leaf}} \times e^{-0.5k} \quad (30)$$

$$Pcon_{leaf\_max} = \frac{0.45}{CP_{min,leaf}} \quad (31)$$

where LAI_{sun} and LAI_{shade} are leaf area index for sunlit and shaded leaves, LAI is total leaf area index of plant canopy, P_{leaf} is leaf P content (g P m^{-2}), C_{leaf} is leaf carbon content (g C m^{-2}), 0.45 is conversion factor from carbon to dry biomass, k is canopy extinction coefficient, and $CP_{min,leaf}$ is minimum C : P ratio for leaves.

2.1.2 P uptake

Plant P uptake rate (P_{up}, g P m^{-2} day^{-1}) is determined by the potential uptake rate (P_{pot}, g P m^{-2} day^{-1}), vegetation P demand (P_{demand}, g P m^{-2} day^{-1}), and available dissolved soil inorganic P (P_{dip}, g P m^{-2} day^{-1}):

$$P_{up} = \min\left(P_{up\_pot}, P_{demand}, P_{dip}\right) \quad (32)$$

P_{up_pot} is maximum vegetation P uptake rate (P_{up_max}, g P m^{-2} day^{-1}) down-regulated by volumetric water content (W_{soil}, %), and P_{dip} :

$$P_{up\_pot} = P_{up\_max} f_{up}\left(W_{soil}, P_{dip}\right) \quad (33)$$

$$f_{up}\left(W_{soil}, P_{dip}\right) = \frac{f_{up}(W_{soil}) \times P_{dip}}{f_{up}(W_{soil}) \times P_{dip} + k_{up}} \quad (34)$$

$$f_{up}(W_{soil}) = 0.9\left(\frac{W_{soil}}{\theta_{fc}}\right)^3 + 0.1 \quad (35)$$

where k_{up} (g P m^{-2} day^{-1}) is P_{dip} concentration at which vegetation P uptake is half of its maximum rate; and θ_{fc} is volumetric water content at field capacity (%). The demanded P for vegetation to keep the minimum C:P ratio, P_{demand} (g P m^{-2} day^{-1}), is estimated as

$$P_{demand} = \sum_{i=1}^{5} \frac{C_i}{CP_{min,i}} - \sum_{i=1}^{5} P_i \quad (36)$$

where i denotes vegetation living pools (1: leaf, 2: sapwood, 3: fine root, 4: coarse root, 5: reproduction root); C_i and P_i are organic C and P pool of vegetation (g C m^{-2}, g P m^{-2}); $CP_{min,i}$ is a prescribed parameter representing minimum C : P ratio in each plant pool.

2.1.3 P allocation

The P uptaken by vegetation from soil is allocated to vegetation pools. The total allocable vegetation P (P_{alloc} g P m^{-2}) is calculated as the sum of P in each pool after resorbing from shed leaf and P uptaken from soil. Part of vegetation P is transferred to litter organic P pools according to leaf litter C:P ratio (Table 2-1) during vegetation turnover processes (such as leaf shedding, and tree mortality, etc.). The nutrient resorption from leaf is simulated based on the difference in C:P ratio between leaf and leaf litter. For simplification purposes, we assumed that the P in plant is redistributed at daily allocation time step after P resorbing from shed tissue and being uptaken from soil.

$$P_{resorption} = \frac{C_{leaflitter}}{C:P_{\text{leaf}}} - \frac{C_{leaflitter}}{C:P_{\text{leaflitter}}} \tag{37}$$

$$P_{alloc} = \sum_{i=1}^{5} P_i + P_{up} \tag{38}$$

P_{alloc} is allocated to vegetation living pools (leaf, sapwood, coarseroot, fineroot, and reproduction) according to the stoichiometric relationship of C and P in each vegetation pool. P content in each vegetation pool after P allocation (P_i^*, g P m^{-2}) is calculated as:

$$P_i^* = P_{alloc} \times \left(\frac{\frac{C_i}{CP_{min,i}}}{\sum_{i=1}^{5} \frac{C_i}{CP_{min,i}}} \right) \tag{39}$$

where $CP_{min,i}$ is the minimum C:P ratio and i represents the ith vegetation pool.

2.2 Soil P processes

In soil, we define three inorganic P pools, including dissolved inorganic P (P_{dip}, g P m^{-2}), secondary mineral P (P_{sm}, g P m^{-2}), and occluded P (P_{oc}, g P m^{-2}) (Figure 2-2). We assume that soil P_{dip} is the only readily available P for plant uptake:

$$\frac{dP_{dip}}{dt} = P_w + P_{dep} + P_{fer} + P_{des} + P_{min} - P_{up} - P_{imb} - P_{ads} - P_{ocl} - P_{lose\_p} \quad (40)$$

P_{dip} is replenished by apatite rock weathering (P_w, g P m^{-2} day^{-1}), atmospheric deposition (P_{dep}, g P m^{-2} day^{-1}), fertilizer application (P_{fer}, g P m^{-2} day^{-1}), desorption of phosphorus from secondary mineral P pool (P_{des}, g P m^{-2} day^{-1}), and mineralization of organic phosphorus (P_{min}, g P m^{-2} day^{-1}). Meanwhile, P_{dip} is consumed by plant root uptake (P_{up}, g P m^{-2} day^{-1}), microbial immobilization (P_{imb}, g P m^{-2} day^{-1}), adsorbed by fine soil partials or cations (P_{ads}, g P m^{-2} day^{-1}), occluded (P_{ocl}, g P m^{-2} day^{-1}), and lost by leaching and erosion (P_{lose_p}, g P m^{-2} day^{-1}).

For the soil organic matter (SOM), DLEM includes three microbial pools (SMB1, SMB2, and SMR), one dissolved organic matter pool (DOM), one native organic matter pool (NOM), and one passive organic matter pool (PSOM) (Figure 2-2a). Each soil organic pool has a prescribed stoichiometric relationship for C, N, and P (Table 2-1). Soil organic P comes from litter P; it transfers to soil inorganic P through mineralization processes and leaves soil column through leaching and erosion processes.

2.2.1 Weathering

Parent material weathering is the primary source of soil inorganic P, which is controlled by the quantity of apatite rock substrate and physical soil conditions (Guidry & Mackenzie, 2003). In DLEM-CNP, the P weathering algorithm is adopted from the Century model (Parton et al.,

1988), which considers the influences of phosphate rock availability, soil temperature and moisture, and soil texture:

$$P_w = P_{par} f_{weather}(T_{soil}, \Theta_{soil}) f_{weather}(clay + silt) \quad (41)$$

where P_{par} is parent P in a soil column (g P m^{-2}), which is input data for DLEM-CNP and from soil P synthesis data (Yang et al., 2014), $f_{weather}(T_{soil}, \Theta_{soil})$ represents effect of soil temperature and moisture on weathering, $f_{weather}(clay + silt)$ is soil texture factor on weathering, $clay$ and $silt$ are fractions of clay and silt in soil. The effect of soil temperature and moisture is estimated as:

$$f_{weather}(T_{soil}, \Theta_{soil}) = f_{weather}(\Theta_{soil})\, f_{weather}(T_{soil}) \quad (42)$$

$$f_{weather}(\Theta_{soil}) = \begin{cases} 1, & \frac{\Theta - \Theta_{wilt}}{\Theta_{fc} - \Theta_{wilt}} > 13 \\ \frac{1}{1 + 10 \times e^{-6\frac{\Theta - \Theta_{wilt}}{\Theta_{fc} - \Theta_{wilt}}}}, & \frac{\Theta - \Theta_{wilt}}{\Theta_{fc} - \Theta_{wilt}} \leq 13 \end{cases} \quad (43)$$

$$f_{weather}(T_{soil}) = \max\left(\frac{11.75 + \left(\frac{29.7}{3.14}\right) \times \tan\left(3.14 \times 0.031 \times (T_{soil} - 15.4)\right)}{11.75 + \left(\frac{29.7}{3.14}\right) \times \tan\left(3.14 \times 0.031 \times (30 - 15.4)\right)}, 0.01 \right) \quad (44)$$

where Θ_{wilt} is volumetric water content at wilting point (%), Θ_{fc} is volumetric water content at field capacity, Θ is volumetric water content.

$$f_{weather}(clay + silt) = \frac{0.1 + \left(\frac{0.1}{3.14}\right) \times \tan\left(3.14 \times 2 \times (clay + silt - 0.7)\right)}{365} \quad (45)$$

2.2.2 P exchange between dissolved inorganic P and secondary mineral P

The dissolved inorganic P can be adsorbed by fine soil particles and cations to form secondary mineral P (McGechan & Lewis, 2002; Smeck, 1985). Meanwhile, adsorbed P can be released to the dissolve inorganic P pool when the balance of adsorption and desorption is disturbed (Lewis & McGechan, 2002; Williams et al., 1980). DLEM-CNP simulates the bidirectional P fluxes ($R_{des-ads}$, g P m^{-2} day^{-1}) between soil dissolve inorganic P pool and secondary mineral P pool using the algorithm in Knisel (1993),

$$P_{des-ads} = 0.1 f_{ad-de}(T_{soil}) f_{ad-de}(W_{soil}) \left(P_{dip} - P_{sm} \left(\frac{PAI}{1 - PAI} \right) \right), \quad (46)$$

$$f_{ad-de}(T_{soil}) = e^{0.115 \times T_{soil} - 2.88} \quad (47)$$

$$f_{ad-de}(W_{soil}) = \begin{cases} 0 , & W_{soil} \geq \Theta_{fc} \\ \dfrac{\Theta - \Theta_{wilt}}{\Theta_{fc} - \Theta_{wilt}}, & W_{soil} < \Theta_{fc} \end{cases} \quad (48)$$

The secondary mineral P pool is initialized as:

$$P_{sm} = P_{dip} \left(\frac{1 - PAI}{PAI} \right) \quad (49)$$

$$PAI = \begin{cases} 0.0054 \times (22 \times pH + 10 \times clay - 53) + 0.116 \times pH - 0.73, & P_{par} > 100 \\ 0.46 - 0.0916 \times \ln(100 \times clay) , & P_{par} < 100 \end{cases} \quad (50)$$

where positive values of $P_{des-ads}$ represent adsorption (P_{ads}) and negative values represent desorption (P_{des}), $f_{ad-de}(T_{soil})$ and $f_{ad-de}(W_{soil})$ are soil temperature and soil moisture coefficients for inorganic P adsorption and desorption processes, and PAI is soil chemical coefficient as a function of soil pH and clay fraction.

2.2.3 P occlusion

In soil, iron (Fe), aluminum (Al), and calcium (Ca) compounds have a large binding capacity for P adsorption (Filippelli, 2008). The occluded P by these compounds is unavailable for plant uptake. In DLEM-CNP, occlusion of P sources from P_{sm}, and P occlusion rate (P_{ocl}) is calculated following Knisel (1993) and Chaubey et al. (2006):

$$P_{ocl} = \begin{cases} K_{as} \times (ras \times P_{sm} - P_{oc}); & ras \times P_{sm} \geq P_{oc} \\ 0 \quad ; & ras \times P_{sm} < P_{oc} \end{cases}, \tag{51}$$

where ras is ratio between occluded P pool and secondary mineral P pool, and K_{as} is a flow coefficient parameterized as:

$$K_{as} = \begin{cases} e^{-1.77 \times PAI - 7.08} & , \quad non-calcareous\ soils \\ 0.00076 & , \quad calcareous\ soils \end{cases} \tag{52}$$

2.2.4 P mineralization and immobilization

The competition between microbes and plants for dissolved inorganic P is handled analogously to the competition for soil mineral N in DLEM. Gross P immobilization, gross P mineralization, as well as plant P uptake are calculated daily. In each timestep, microbes are given a higher priority in accessing nutrients than plants.

Soil P can either be mineralized (organic P to inorganic P) or immobilized (inorganic P to organic P), depending on carbon decomposition rate (C_{dec}) and C: P ratios of the source and destination organic carbon pools ($C:P_{\text{source}}$ and $C:P_{\text{destination}}$):

$$P_{min-imm} = \frac{C_{\text{dec}}}{C:P_{\text{source}}} - \frac{C_{dec}(1-f_{CO2})}{C:P_{\text{destination}}} \quad (53)$$

where $P_{min-imm}$ is P mineralization or immobilization rate (g P m^{-2}) with a positive value representing mineralization (P_{min}) and a negative value representing immobilization (P_{imb}), f_{CO2} is fraction of the decomposed carbon emitted from soil as CO_2. The decomposition rate of organic pools is simulated following the classic first-order decay algorithm (Parton et al., 1987; Parton et al., 1988):

$$C_{dec} = C_{pool}K_{dec} \quad (54)$$

where C_{dec} is decomposed carbon (g C m^{-2} day^{-1}), C_{pool} is the size of carbon pool (g C m^{-2}), and $K_{dec}$is decomposition rate (day^{-1}) of each pool regulated by soil temperature, soil moisture, nutrient availability, and soil texture:

$$K_{dec} = \frac{K_{max}}{365} \times f(T) \times f(W) \times f(NP) f(clay) \quad (55)$$

$f(NP)$ is nutrient scalar which is controlled by N limitation and P limitation:

$$f(NP) = \frac{2}{\frac{1}{f(N)} + \frac{1}{f(P)}} \quad (56)$$

$$f(PI) = \frac{avp}{P_{imm}} \tag{57}$$

$$f(PM) = \begin{cases} 1 - \dfrac{avp - avp_{opt}}{avp_{opt}} & avp > avp_{opt} \\ 1 & \dfrac{avp_{opt}}{2} \le avp \le avp_{opt} \\ 1 + \dfrac{0.5avp_{opt} - avp}{avp_{opt}} & avp \le \dfrac{avp_{opt}}{2} \end{cases} \tag{58}$$

where K_{max} is maximum decay rate (day^{-1}); $f(PM)$and $f(PI)$ are P scalars in mobilization and immobilization, respectively; P_{imm} is potential P immobilization rate; avp is available soil inorganic P (g P m^{-2}); and avp_{opt} is optimum available soil P (g P m^{-2}). The N related equations and detailed equations in soil decomposition can be found in Appendix 1.

2.2.5 P loss

The loss of P in dissolved forms may occur with surface runoff or leaching. And the loss of P in particulate forms is usually associated with erosion of soil mineral or organic particles (McDowell et al., 2004). Dissolved inorganic P leaching (P_{lch_dip}, g P m^{-2} day^{-1}) is calculated as:

$$P_{lch_{dip}} = P_{dip} \times f_{flow} \times \frac{P_{dipc}}{P_{dipc} + lchb_{dip}} \tag{59}$$

where f_{flow} is runoff and drainage coefficient for leaching, P_{dipc} is total inorganic P content in soil (g P g^{-1} soil), and $lchb_{dip}$ is desorption coefficient for inorganic P. $f_{flow}$is calculated as:

$$f_{flow} = \frac{q_{srun} + q_{drain}}{\theta + q_{srun} + q_{drain}} \quad (60)$$

$$P_{dipc} = \frac{P_{dip}}{Wt_{soil}} \quad (61)$$

where q_{srun} is surface runoff (mm); q_{drain} is subsurface runoff (mm); θ is soil water content (mm); q_{srun}, q_{drain}, and θ are simulated by the DLEM soil hydrology procedures (Liu et al., 2013). Wt_{soil} is soil mass in the top 50 cm (g m^{-2}).

Similarly, dissolved organic P leaching (P_{lch_dop}, g P m^{-2} day^{-1}) is simulated as:

$$P_{lch_{dop}} = P_{dop} \times f_{flow} \times \frac{P_{dopc}}{P_{dopc} + lchb_{dop}} \quad (62)$$

where P_{dop} is total amount of soil dissolved organic P (g P m^{-2}); $lchb_{dop}$ is desorption coefficient for dissolved organic P (DOP, g P g^{-1}soil); P_{dopc} is concentration of DOP concentration in the soil column (g P g^{-1} soil):

$$P_{dopc} = \frac{P_{dop}}{Wt_{soil}} \quad (63)$$

Export of particular organic P (P_{lch_pop}, g P m^{-2} day^{-1}) is assumed to occur with soil erosion ($R_{erosion}$, g soil m^{-2} day^{-1}), which is calculated using the Modified Universal Soil Loss Equation in DLEM (Liu et al., 2013; Yang et al., 2015):

$$P_{lch_{pop}} = P_{opc} \times R_{erosion} \quad (64)$$

$$P_{opc} = \frac{P_{op}}{Wt_{soil}} \quad (65)$$

where P_{opc} is total organic P content in soil column (g P g^{-1} soil), and P_{op} (g P m^{-2}) is total organic P in soil P pools at a depth of 1m.

3. Summary

In this study, we developed a process-based P module on the platform of the Dynamic Land Ecosystem Model (DLEM) by considering P impacts on vegetation and soil biogeochemical processes, which upgraded the coupled CN model (DLEM-CN) into the coupled CNP model (DLEM-CNP). Phosphorus cycle has been successfully coupled with C and N cycles in the DLEM. The DLEM-CNP fully incorporates CNP cycles in all pools (plant, litter, and soil organic/inorganic pools) and key biogeochemical processes. The DLEM-CNP model had an outstanding innovation point that it first time introduces the interactive co-limitation of N and P on vegetation C assimilation in the TBMs, overcoming the shortcoming of using Liebig's law of minimum.

Reference

Bonan, G. B. (1996). *Land surface model (LSM version 1.0) for ecological, hydrological, and atmospheric studies: Technical description and user`s guide. Technical note*. Retrieved from United States: https://www.osti.gov/servlets/purl/442360

Chaubey, I., Migliaccio, K., Green, C., Arnold, J., & Srinivasan, R. (2006). Phosphorus modeling in soil and water assessment tool (SWAT) model. *Book Modeling Phosphorus in the Environment*, 163-187.

Cleveland, C. C., & Liptzin, D. (2007). C: N: P stoichiometry in soil: is there a “Redfield ratio” for the microbial biomass? *Biogeochemistry, 85*(3), 235-252.

Collatz, G. J., Ball, J. T., Grivet, C., & Berry, J. A. (1991). Physiological and environmental regulation of stomatal conductance, photosynthesis and transpiration: a model that includes a laminar boundary layer. *Agricultural and Forest Meteorology, 54*(2), 107-136. https://doi.org/https://doi.org/10.1016/0168-1923(91)90002-8

Ducnuigeen, J., Williard, K., & Steiner, R. C. (1997). *Relative nutrient requirements of plants suitable for riparian vegetated buffer strips*: Interstate Commission on the Potomac River Basin Rockville, Maryland.

Farquhar, G. D., von Caemmerer, S., & Berry, J. A. J. P. (1980). A biochemical model of photosynthetic CO2 assimilation in leaves of C3 species. *149*(1), 78-90. journal article. https://doi.org/10.1007/bf00386231

Filippelli, G. M. (2008). The global phosphorus cycle: past, present, and future. *Elements, 4*(2), 89-95.

Goll, D. S., Brovkin, V., Parida, B. R., Reick, C. H., Kattge, J., Reich, P. B., et al. (2012). Nutrient limitation reduces land carbon uptake in simulations with a model of combined carbon, nitrogen and phosphorus cycling. *Biogeosciences, 9*(9), 3547-3569. https://doi.org/10.5194/bg-9-3547-2012

Guidry, M. W., & Mackenzie, F. T. (2003). Experimental study of igneous and sedimentary apatite dissolution: control of pH, distance from equilibrium, and temperature on dissolution rates. *Geochimica et Cosmochimica Acta, 67*(16), 2949-2963.

Kelly, J. M., Kovar, J. L., Sokolowsky, R., & Moorman, T. B. (2007). Phosphorus uptake during four years by different vegetative cover types in a riparian buffer. *Nutrient Cycling in Agroecosystems, 78*(3), 239-251. https://doi.org/10.1007/s10705-007-9088-4

Knisel, W. G. (1993). *GLEAMS: Groundwater Loading Effects of Agricultural Management Systems: Version 2.10*: University of Georgia Coastal Plain Experiment Station, Bio. & Ag. Engineering.

Lessin, G., Lips, I., & Raudsepp, U. (2007). Modelling nitrogen and phosphorus limitation on phytoplankton growth in Narva Bay, south-eastern Gulf of Finland. *Oceanologia, 49*(2).

Lewis, D., & McGechan, M. (2002). A review of field scale phosphorus dynamics models. *Biosystems engineering, 82*, 359-380.

Liu, M., Tian, H., Yang, Q., Yang, J., Song, X., Lohrenz, S. E., & Cai, W. J. (2013). Long‐term trends in evapotranspiration and runoff over the drainage basins of the Gulf of Mexico during 1901–2008. *Water Resources Research, 49*(4), 1988-2012.

Lu, C., & Tian, H. (2013). Net greenhouse gas balance in response to nitrogen enrichment: perspectives from a coupled biogeochemical model. *Global Change Biology, 19*(2), 571-588. https://doi.org/10.1111/gcb.12049

Lu, C., Tian, H., Liu, M., Ren, W., Xu, X., Chen, G., & Zhang, C. (2012). Effect of nitrogen deposition on China's terrestrial carbon uptake in the context of multifactor environmental changes. *Ecological applications, 22*(1), 53-75.

McDowell, R., Biggs, B., Sharpley, A., Nguyen, L. J. C., & Ecology. (2004). Connecting phosphorus loss from agricultural landscapes to surface water quality. *20*(1), 1-40.

McGechan, M., & Lewis, D. (2002). SW—soil and water: sorption of phosphorus by soil, part 1: principles, equations and models. *Biosystems engineering, 82*(1), 1-24.

McGroddy, M. E., Daufresne, T., & Hedin, L. O. (2004). Scaling of C: N: P stoichiometry in forests worldwide: implications of terrestrial redfield‐type ratios. *Ecology, 85*(9), 2390-2401.

Pan, S., Tian, H., Dangal, S. R., Ouyang, Z., Tao, B., Ren, W., et al. (2014a). Modeling and monitoring terrestrial primary production in a changing global environment: toward a multiscale synthesis of observation and simulation. *Advances in Meteorology, 2014*.

Pan, S., Tian, H., Dangal, S. R., Yang, Q., Yang, J., Lu, C., et al. (2015). Responses of global terrestrial evapotranspiration to climate change and increasing atmospheric CO2 in the 21st century. *Earth's Future, 3*(1), 15-35.

Pan, S., Tian, H., Dangal, S. R., Zhang, C., Yang, J., Tao, B., et al. (2014b). Complex spatiotemporal responses of global terrestrial primary production to climate change and increasing atmospheric CO2 in the 21st century. *PloS one, 9*(11), e112810.

Pan, S., Yang, J., Tian, H., Shi, H., Chang, J., Ciais, P., et al. (2020). Climate Extreme Versus Carbon Extreme: Responses of Terrestrial Carbon Fluxes to Temperature and Precipitation. *Journal of Geophysical Research: Biogeosciences, 125*(4), e2019JG005252. https://doi.org/10.1029/2019JG005252

Parton, W. J., Schimel, D. S., Cole, C. V., & Ojima, D. S. (1987). Analysis of Factors Controlling Soil Organic Matter Levels in Great Plains Grasslands1. *Soil Science Society of America Journal, 51*(5), 1173-1179. https://doi.org/10.2136/sssaj1987.03615995005100050015x

Parton, W. J., Stewart, J. W. B., & Cole, C. V. (1988). Dynamics of C, N, P and S in grassland soils: a model. *Biogeochemistry, 5*(1), 109-131. https://doi.org/10.1007/BF02180320

Pellet, D., & El-Sharkawy, M. A. (1993). Cassava varietal response to phosphorus fertilization. II. Phosphorus uptake and use efficiency. *Field crops research, 35*(1), 13-20. https://doi.org/https://doi.org/10.1016/0378-4290(93)90132-7

Ren, W., Tian, H., Liu, M., Zhang, C., Chen, G., Pan, S., et al. (2007). Effects of tropospheric ozone pollution on net primary productivity and carbon storage in terrestrial ecosystems of China. *Journal of Geophysical Research: Atmospheres, 112*(D22).

Saxton, K. E., & Rawls, W. J. (2006). Soil Water Characteristic Estimates by Texture and Organic Matter for Hydrologic Solutions. *Soil Science Society of America Journal, 70*(5), 1569-1578. https://doi.org/10.2136/sssaj2005.0117

Sellers, P. J., Randall, D. A., Collatz, G. J., Berry, J. A., Field, C. B., Dazlich, D. A., et al. (1996). A Revised Land Surface Parameterization (SiB2) for Atmospheric GCMS. Part I: Model Formulation. *Journal of climate, 9*(4), 676-705. https://doi.org/10.1175/1520-0442(1996)009<0676:ARLSPF>2.0.CO;2

Smeck, N. E. (1985). Phosphorus dynamics in soils and landscapes. *Geoderma, 36*(3-4), 185-199.

Tian, H., Chen, G., Liu, M., Zhang, C., Sun, G., Lu, C., et al. (2010a). Model estimates of net primary productivity, evapotranspiration, and water use efficiency in the terrestrial ecosystems of the southern United States during 1895–2007. *Forest ecology and management, 259*(7), 1311-1327. https://doi.org/https://doi.org/10.1016/j.foreco.2009.10.009

Tian, H., Liu, M., Zhang, C., Ren, W., Xu, X., Chen, G., et al. (2010b). The dynamic land ecosystem model (DLEM) for simulating terrestrial processes and interactions in the context of multifactor global change. *Acta Geographica Sinica, 65*(9), 1027-1047.

Tian, H., Xu, X., Liu, M., Ren, W., Zhang, C., Chen, G., & Lu, C. (2010c). Spatial and temporal patterns of CH_4 and N_2O fluxes in terrestrial ecosystems of North America during 1979–2008: application of a global biogeochemistry model. *Biogeosciences, 7*(9), 2673-2694. https://doi.org/10.5194/bg-7-2673-2010

Tian, H., Xu, X., Lu, C., Liu, M., Ren, W., Chen, G., et al. (2011). Net exchanges of CO2, CH4, and N2O between China's terrestrial ecosystems and the atmosphere and their contributions to global climate warming. *Journal of Geophysical Research: Biogeosciences, 116*(G2). https://doi.org/10.1029/2010JG001393

Tian, H., Yang, Q., Najjar, R. G., Ren, W., Friedrichs, M. A., Hopkinson, C. S., & Pan, S. (2015). Anthropogenic and climatic influences on carbon fluxes from eastern North America to the Atlantic Ocean: A process‐based modeling study. *Journal of Geophysical Research: Biogeosciences, 120*(4), 757-772.

Wang, R., Goll, D., Balkanski, Y., Hauglustaine, D., Boucher, O., Ciais, P., et al. (2017). Global forest carbon uptake due to nitrogen and phosphorus deposition from 1850 to 2100. *Global Change Biology, 23*(11), 4854-4872. https://doi.org/10.1111/gcb.13766

Williams, J., Shear, H., & Thomas, R. (1980). Availability to Scenedesmus quadricauda of different forms of phosphorus in sedimentary materials from the Great Lakes 1. *Limnology and Oceanography, 25*(1), 1-11.

Yang, Q., Tian, H., Friedrichs, M. A., Hopkinson, C. S., Lu, C., & Najjar, R. G. (2015). Increased nitrogen export from eastern North America to the Atlantic Ocean due to

climatic and anthropogenic changes during 1901–2008. *Journal of Geophysical Research: Biogeosciences, 120*(6), 1046-1068.

Yang, X., Post, W. M., Thornton, P. E., & Jain, A. K. (2014). Global Gridded Soil Phosphorus Distribution Maps at 0.5-degree Resolution. In: ORNL Distributed Active Archive Center.

Chapter 3. The Coupling of Carbon, Nitrogen and Phosphorus in the Terrestrial Biosphere: Model Validation, Parameterization, Sensitivity and Evaluation in Tropical Forests

Abstract

The biological processes of phosphorous (P), carbon (C), and nitrogen (N) in the Earth system are fully coupled, which shapes the structure, functioning, and dynamics of terrestrial ecosystems. However, incorporating P-related processes into terrestrial biosphere models (TBMs) is still in an early stage. Through incorporating P processes and C-N-P interactions into the Dynamic Land Ecosystem Model (DLEM), DLEM was upgraded from a coupled C-N model into a coupled C-N-P model (DLEM-CNP), with a major advantage of representing the interactive co-limitation of N and P on vegetation C assimilation. DLEM-CNP was calibrated and validated at four eddy covariance flux sites, two Hawaii sites along a chronosequence of soils, and another 13 tropical forest sites at daily to annual time scale. The results indicated that DLEM-CNP was capable of reproducing the forest productivity (eddy covariance flux sites daily GPP Root Mean Square Error (RMSE) range from 1.1-1.5 g C m^{-2} yr^{-1}; 13 tropical forest sites annual NPP R^2 = 0.92, RMSE = 176.7 g C m^{-2} yr^{-1}), biomass, leaf N: P ratio, and plant response to fertilizer addition. A sensitivity analysis suggested that these results were reasonably robust against uncertainties in model parameter estimates and the model was most sensitive to parameters on P uptake. These results suggest that the inclusion of P processes in DLEM-CNP is important for accurately representing C dynamics in tropical forests, avoiding overestimation of tropical forest productivity by CN models. Additionally, N and P fertilizer addition experiment demonstrate that the feature of interactive co-limitation of N and P on vegetation C assimilation in DLEM-CNP is an important innovation for TBMs.

1. Introduction

In many terrestrial ecosystems, the availability of soil nutrients shapes their structure and functions, including productivity, diversity, dynamics, and interactions of plant, animal, and microbial communities (Vitousek, 2004). Phosphorus comes primarily from parent material weathering and atmospheric deposition and is lost through nutrient leaching, soil erosion, and fire (Filippelli, 2008; Newman, 1995; Wang et al., 2015). Ecosystems with longtime development can reach a final steady-state with P limitation, in which the ecosystem becomes depleted in parent P and a large fraction of the P should be bound up in occluded fraction (Buendía et al., 2010; Porder et al., 2007; Walker & Syers, 1976). P limitation on primary productivity at the level of individual species is recognized to be widespread in tropical forests because of the absence of glaciation and the relatively rapid weathering of parent material P as a result of warmer and wetter climate (Davidson et al., 2004; Tanner et al., 1998; Turner et al., 2018; Vitousek et al., 2010). Research on soil P fractions and fertilization addition experiments also demonstrates P limitation on plant productivity widely exists in tropical areas (Vitousek, 2004; Yang et al., 2013). P limitation on primary productivity, therefore, plays a key role in the global carbon (C) cycle (Lloyd et al., 2001; Wieder et al., 2015). Moreover, P limitation on primary productivity may intensify in the future as a result of rising atmospheric CO_2 and nitrogen (N) deposition, which can weaken the carbon sequestration capability of terrestrial ecosystems (Goll et al., 2012; Zhang et al., 2014).

The interactions of C, N, and P play critical roles in regulating carbon uptake and storage and N, P biogeochemical processes in terrestrial ecosystems (Ågren et al., 2012; Guignard et al., 2017; Wang et al., 2017). P and N are both involved in critical C processes such as photosynthesis and decomposition. Leaf N and P can determine leaf photosynthetic capacity by regulating the

maximum rate of carboxylation (V_{cmax}) and the electron transport capacity (J_{max}) (Domingues et al., 2010). N limitation could limit carboxylation capacity and electron transport rates (Hikosaka, 2004; Wang et al., 2018). P is required for many transformations of P-rich molecules (ATP, NADP, and sugar phosphates from the Calvin cycle) and the regeneration of ribulose-1,5-bisphosphate (RUBP) (Farquhar et al., 1980). P limitation could reduce light-use efficiency, electron transport rates, regeneration of ribulose bisphosphate, and the allocation of leaf N to photosynthetic processes (Wang et al., 2018). Field experiments demonstrate N and P fertilizer addition can increase forest trunk growth and biomass increment (Harrington et al., 2001; Newbery et al., 1999; Tanner et al., 1990; Vitousek et al., 1993). Additionally, multiple lines of evidence show that N and P interactions play important roles in affecting available N and P in soil (Marklein & Houlton, 2012; Reed et al., 2007; Treseder & Vitousek, 2001). The supply of P can influence N fixation rates, such that more supply of P can increase the N inputs and N availability in terrestrial ecosystems (Reed et al., 2007). Additionally, extra N is required by plants and microbes to produce more N-rich extracellular phosphatase enzymes that cleave ester-P bonds in soil organic matter increasing availability of P (Mcgill & Cole, 1981; Olander & Vitousek, 2000; Wang et al., 2007).

Since the industrial revolution in the 1850s, the global P cycle has been substantially disturbed and altered by anthropogenic activities (Cordell et al., 2009). Humans have unprecedentedly accelerated the P cycle by fertilizer production and application in the agricultural lands to increase food production (Elser & Bennett, 2011). The P scarcity was exacerbated because of the increased P demand in the context of increasing atmospheric CO_2 concentration and N deposition indirectly induced by human activities (Jiang et al., 2019). Thus, there is an important need to represent P processes in the terrestrial biosphere models (TBMs) for better understanding and simulating C, N, and P interactions. This endeavor can help to improve the predictions of the

C cycle in terrestrial ecosystems under a changing global environment. Meanwhile, a more in depth understanding of the P cycle will be important for decision-makers to develop feasible policies to manage P nutrient sustainability in the context of the enhanced anthropogenic disturbances.

The incorporation of the P cycle is an important task in the development of terrestrial biosphere models, particularly in tropical forests where P availability is often presumed to limit ecosystem primary production (Reed et al., 2015). Within the past decades, TBMs have evolved from the first-generation C only models (Houghton et al., 2001; Lieth, 1975) to CN interactions models (Gerber et al., 2010; Thornton et al., 2007; Tian et al., 2010; Yang et al., 2009; Zaehle & Dalmonech, 2011; Zaehle et al., 2010). In recent years, the P cycle has been incorporated into several TBMs, such as Community Land Model (CLM -CNP) (Yang et al., 2014b), CABLE-CNP (Wang et al., 2007), CASA-CNP (Wang et al., 2010), and Organizing Carbon and Hydrology In Dynamic Ecosystems (ORCHIDEE) (Goll et al., 2017), etc. There is mounting evidence that the representation of P in TBMs is important for our understanding and prediction of ecosystem dynamics, particularly for tropical forests with strong P limitation (Fleischer et al., 2019; Goll et al., 2018; Goll et al., 2012). Wang et al. (2010), Goll et al. (2012), and Yang et al. (2014) highlighted the importance of incorporating the P cycle in TBMs, particularly in tropical ecosystems. Several studies also demonstrated that coupling P dynamics into TBMs could reduce the simulated terrestrial C sink due to increasing atmospheric CO_2 concentrations in the Amazon basin and other areas (Fleischer et al., 2019; Yang et al., 2019; Yang et al., 2016; Zhang et al., 2011). However, it is still challenging for terrestrial ecosystem modelers to provide more realistic CNP models because some P processes and their interactions on C and N processes are still not well understood (Achat et al., 2016; Jiang et al., 2019; Reed et al., 2015).

Here, we first describe the major advantage of representing the interactive co-limitation of N and P on vegetation C assimilation of the P module in the DLEM-CNP. Then we evaluate the performance of the model to reproduce daily and seasonal C fluxes at four eddy covariance flux sites. After that, we evaluate model performance against field data collected from long-term fertilization experiments in a soil formation chronosequence in Hawaii (Harrington et al., 2001; Ostertag, 2001). Finally, we test the robustness of the model by systematically varying key parameters related to P processes.

2. Materials and Methods

2.1 The Dynamic Land Ecosystem Model with C-N-P coupled (DLEM-CNP)

The DLEM-CNP is detailed described in chapter 2. Phosphorus processes were coupled into the DLEM, and the cycles of C, N, and P are fully coupled in DLEM-CNP during photosynthesis, allocation, turnover, nutrient uptake, and decomposition. In DLEM-CNP, organic P transfers into inorganic forms through mineralization in the soil, while inorganic P converts to organic form through immobilization and vegetation uptake.

2.2 P and N co-limitation on photosynthesis in DLEM-CNP

We adopted the NP co-limitation equation from the MIKE 3 ecohydrodynamic 3-dimensional model developed by the Danish Hydraulics Institute, which is originally applied to modeling N and P limitation on phytoplankton growth (Lessin et al., 2007). Most models which incorporate N and P cycles simply describe nutrients limitation by using Liebig's law of minimum (e.g., ORCHIDEE, CLM). In comparison, our N and P interactive co-limitation scheme has the advantage of simulating the interaction effects of N, P limitation on photosynthesis. The detailed processes and equations are described in chapter 2.

2.3 Model implementation

2.3.1 Site information

FLUXNET sites

FLUXNET data are a standard terrestrial biosphere model benchmark (Friend et al., 2007), and the effects of N-P limitation on the daily and seasonal cycles of C fluxes are analyzed for these four sites. We selected four FLUXNET sites located in tropical areas with the vegetation type of tropical forests (BR-Sa3, BR-Sa1, MY-PSO, PA-SPn, Figure 3-1, Table 3-1).

Table 3- 1 FLUXNET sites information

Sites	BR-Sa3	BR-Sa1	MY-PSO	PA-SPn
latitude	-3.0180	-2.8567	2.9730	9.3181
longitude	-54.9714	-54.9589	102.3062	-79.6346
altitude (m)	100	88	192	78
Mean annual temperature (^oC)	26.12	26.13	25.3	26.5
mean annual precipitation ($mmyr^{-1}$)	2043.77	2074.79	1864.8	2350
Dominant vegetation	Evergreen Broadleaf Forests	Evergreen Broadleaf Forests	Evergreen Broadleaf Forests	Deciduous Broadleaf Forests
soil pH	3.85	3.85	4.7	4.8
soil bulk density ($kg\ m^{-2}$)	1.3	1.3	1.36	1.49
soil texture (clay: silt: sand)	0.49，0.1,0.41	0.49，0.1,0.41	0.3，0.25，0.45	0.19，0.07，0.75
Parent P(gP/m^2)	0.57	1.12	10.24	0.62
Data DOIs	FLUXNET 2015 DOI: 10.18140/FLX/1440033	FLUXNET2015 DOI: 10.18140/FLX/1440032	FLUXNET2015 DOI: 10.18140/FLX/1440240	FLUXNET2015 DOI: 10.18140/FLX/1440180

Hawaii sites

The two forest sites (Thurston and Kokee) at Hawaiian Islands (Figure 3-1, Table 3-2) provide an excellent chance for nutrient cycle research as they have similar climate but different soil development stages (Vitousek, 2004). The soil at the Thurston site (latitude = 19.41 °N,

longitude = 155.24 °W) is 300 years old (0.3 ky), and vegetation growth is limited mainly by N, while soil at the Kokee site (latitude = 22.14 °N, longitude = 159.62 °W) is 4 million years old (4100 ky) and vegetation growth is limited mainly by P (Harrington et al., 2001; Ostertag, 2001). The annual mean temperature at the two sites is around 16 ^{o}C, and the mean annual precipitation is about 2500 mm. Both sites have similar parent material, and *Metrosideros polymorpha* is the major tree species (Crews et al., 1995). Field observations, including plant production, vegetation biomass, soil organic matters, and leaf N: P ratio, are available (Goll et al., 2017; Harrington et al., 2001; Ostertag, 2001). In addition, long-term (6–11 years) factorial fertilization experiments were conducted at the two sites (at the Thurston site since 1985 for 12 years fertilization addition and at the Kokee site since 1991 for six years fertilization addition) (Harrington et al., 2001; Ostertag, 2001; Vitousek, 2004). The fertilization experiments used a factorial design that consisted of all four combinations of zero or 100 kg ha^{-1} yr^{-1} N (half as urea, half as ammonium nitrate) and zero or 100 kg ha^{-1} yr^{-1} P (as triple superphosphate) (Harrington et al., 2001). These fertilization experiments can help validate model performance in representing the N and P limitation interactive effects.

Table 3- 2 Hawaiian Islands sites information

	Thurston	Kokee	Source
latitude (^{o} N)	19.4	22.1	Vitousek (2004)
longitude (^{o} W)	155.2	59.6	Vitousek (2004)
altitude (m)	1176	1134	Crews et al. (1995)
age (years)	300	4.1×10^{6}	Vitousek (2004)
mean annual temperature (^{o}C)	16	16	Crews et al. (1995)
mean annual precipitation (mmyr^{-1})	2500	2500	Crews et al. (1995)
soil pH	5.0	3.8	Chorover et al. (2004)
soil bulk density (kg m^{-2})	300	575	Olander and Vitousek (2004)
soil texture (clay: silt: sand)	0.25, 0.25, 0.5	0.17, 0.79, 0.4	Olander and Vitousek (2004)

N deposition (g m^{-2} yr^{-1})	0.6	0.6	Chadwick et al. (1999)
P deposition (mg m^{-2} yr^{-1})	0.9	0.9	Chadwick et al. (1999)

Clark Tropical sites

Clark et al. (2001) synthesized the data in the literature on NPP in old-growth tropical forests to produce a consistent dataset on NPP. They developed consistent, documented estimates of the upper and lower bounds around total NPP for 39 diverse tropical forest sites to serve as benchmarks for calibrating and evaluating biogeochemical models. These estimates are based on existing field measurements and judgment that belowground production is bounded by the range of 0.2–1.2 ANPP (aboveground NPP) (Clark et al., 2001). As total NPP has frequently been estimated by assuming that aboveground NPP (BNPP) equals ANPP (Esser et al., 1997), we used the upper bound for BNPP in Clark et al. (2001) (1.2 * estimated ANPP). We extracted site data from Clark et al. (2001) based on longitude and latitude information. For the sites with the same longitude and latitude, we averaged the NPP value. We excluded sites without longitude and latitude information. As we evaluate more detailed NPP and C cycle features at the Hawaii fertilization section, so we excluded the Hawaii sites here. A summary of site information can be found in Table 3-3 (site name, location, rainfall, temperature).

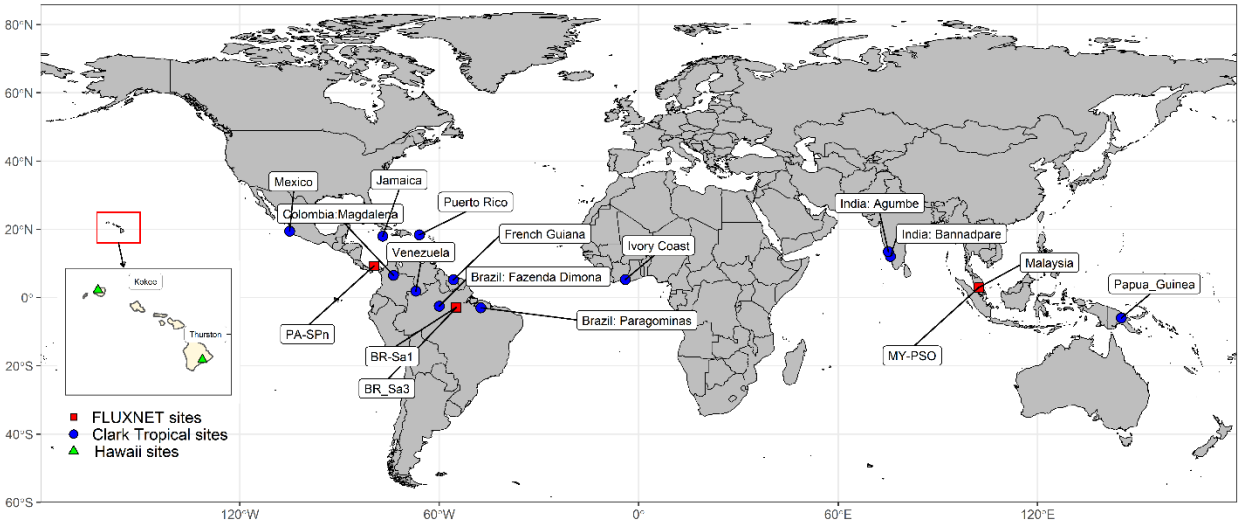

Figure 3- 1 Location of tropical forest sites for model validation.

Table 3- 3 Compiled Clark tropical sites information

	Site	Latitude	Longitude	Elevation(m)	Mean annual temperature(°C)	Mean annual precipitation(mm)	Estimated NPP (gC/m^2yr^{-1})	Reference
1	Brazil: Fazenda Dimona	2.5 S	60 W	…	26.7	2300	1462.5 ±210.5	Chambers (1998), Sizer (1992)
2	Brazil: Paragominas	2.98 S	47.52 W	…	…	1750	1440.0 ± 42.4	Trumbore et al. (1995)
3	Colombia: Magdalena	6.5 N	73.8 W	…	27.5	3150	1885 ± 332.3	Folster et al. (1976)
4	French Guiana: Piste de Saint-Elie	5.25 N	55.75 W	…	26	3450	1470 ± 0	Lescure et al. (1983)
5	India: Bannadpare	12.08 N	75.7 E	200	27	5310	865 ± 7.1	Rai and Procto (1986*a*,*b*)
6	India: Agumbe	13.5 N	75.1 E	575	22.2	7670	790 ± 99.0	Rai and Proctor (1986*a*,*b*)
7	Ivory Coast: Banco	5.28 N	4.03 W	100	26.2	2095	2326.7 ± 73401	Bernhard (1970),
8	Jamaica: Blue Mt.	18 N	77 W	1600	15.8	2230	1177.5 ± 90.3	Tanner (1980a, 1980b, 1985)
9	Malaysia: Pasoh	2.98 N	102.3 E	…	25	1807	1940 ± 0	Kira (1978.)
10	Mexico: Chamela	19.5 N	105.05 W	110	24.9	707	773.3 ± 92.9	Martinez-Yrizar et al. (1996); Martinez-Yrizar et al. (1992)

11	Papua New Guinea: Mt. Kerigomma	6 S	145.18 E	2450	13	3985	1350 ± 0	Edwards and Grubb (1977)
12	Puerto Rico: palm fl forest	18.42 N	66 W	750	19.7	3725	1410 ± 240.4	Lugo and Murphy (1986)
13	Venezuela: San Carlos	1.9 N	67.05 W	119	26	3550	1250 ± 91.7	Jordan and Escalante (1980)

2

2.3.2 Input data

Input data for FLUXNET sites

At the four FLUXNET sites, climate variables (daily precipitation, daily shortwave radiation, daily maximum temperature, daily average temperature, and daily minimum temperature) and elevation were extracted from the site observation (https://fluxnet.fluxdata.org/). Atmospheric CO_2 concentration data was obtained from NOAA (https://www.esrl.noaa.gov/gmd/ccgg/trends/data.html). Soil property data, including soil texture, pH, and bulk density, was extracted from the Global Soil Data Task (https://daac.ornl.gov/). Soil parent P data was from Global Gridded Soil Phosphorus Distribution Maps at a half-degree resolution (Yang et al., 2014a).

Input data for Hawaii chronosequence sites

At the two Hawaii sites, climate variables (daily precipitation, daily shortwave radiation, daily maximum temperature, daily average temperature, and daily minimum temperature) were extracted from the Daily Surface Weather Data on a 1-km Grid for North America, Version 3 (Thornton et al., 2017). Atmospheric CO_2 concentration data was obtained from NOAA (https://www.esrl.noaa.gov/gmd/ccgg/trends/data.html). The elevation, slope, and aspect were extracted from the USGS 10-meter DEM product (https://gis.ess.washington.edu/data/raster/tenmeter/hawaii/). The other input data, such as soil bulk density, soil texture, soil pH, was obtained from Goll et al. (2017). (Table 3-2)

Clark tropical sites forcing data

For these tropical sites, climate data was obtained from the National Centers for Environmental Prediction (NCEP) Climate Forecast System Reanalysis (CFSR) product

(https://globalweather.tamu.edu/), which has 0.3° resolution and has been widely used in watershed modeling research (Dile & Srinivasan, 2014; Fuka et al., 2014). Other data use the same data source as FLUXNET and Hawaii sites.

2.3.3 Simulation set-up

Model simulation at each site followed a three-step procedure: an equilibrium run, a spin-up run, and a transient run. The equilibrium run was carried out to obtain an equilibrium state with cycled average climate data, which is assumed to be reached when the plant and soil C pool with atmosphere C pool net carbon exchange is less than 0.1 g C m^{-2} yr^{-1}, the change in soil water pool is less than 0.1 mm yr^{-1}, the change in total plant and soil N content is less than 0.1 g N m^{-2} yr^{-1} and the change in total plant and soil P content is less than 0.01 g P m^{-2} between two consecutive 20-year periods. The aim of the model spin-up is to smooth the transition between the equilibrium run and transient run. After the spin-up run, we conducted the transient run with all the driving forces changed year by year.

At the two Hawaii sites, we designed the fertilizer addition experiments using the DLEM-CNP, including adding 100 kg ha^{-1} yr^{-1} N fertilizer only, adding 100 kg ha^{-1} yr^{-1} P fertilizer only, and adding 100 kg ha^{-1} yr^{-1} N and 100 kg ha^{-1} yr^{-1} P fertilizer together. The fertilizer was applied on every day with 1/365 of the annual rate.

A one-at-a-time (OAT) sensitivity analysis was performed for the 4 FLUXNET sites. In one simulation, we only modified one parameter by ± 10% with respect to the reference value and held other parameters constantly. Phosphorus related model parameters (Table 2-1, definition of the parameters) included the maximum vegetation P uptake rate (P_{up_max}); the C:P ratio in leaflitter ($CP_{leaflitter}$); concentration of P_{dip} at which vegetation P uptake is half of the maximum

rate (k_{up}); the minimum C:P ratio in sapwood ($CP_{min,sapwood}$); the minimum C:P ratio in leaf ($CP_{min,leaf}$); the desorption coefficient for inorganic P ($lchb_{dip}$).

2.4 Statistical Analysis

Nutrient use efficiency is a measurement of how well plants use the available mineral nutrients. The N and P use efficiency (NUE and PUE) are calculated based on Goll et al. (2017) as:

$$NUE = \frac{NPP}{N_{up}} \quad (1)$$

$$PUE = \frac{NPP}{P_{up}} \quad (2)$$

where NPP is annual plant net primary production, N_{up} is annual plant nitrogen uptake, P_{up} is annual plant phosphorus uptake.

Response ratio (RR) represents the measured or modeled plant production in the fertilizer treatment divided by its value under unfertilized conditions (Yang et al., 2014b). We use RR to evaluate the response of vegetation to fertilizer addition. The NPP with fertilizer and without fertilizer used here as a multiple year average during the experiment period.

$$RR = \frac{NPP_{fertilized}}{NPP_{unfertilized}} \quad (3)$$

The coefficient of determination (R^2), root mean square error (RMSE) are used to evaluate the model performance.

3. Results

3.1 Simulated and observed GPP at FLUXNET sites

The capacity of DLEM-CNP to reproduce observed daily and seasonal cycles of GPP was tested at the 4 FLUXNET sites. To compare the effects of the representation of P-related processes with DLEM-CN, a reference simulation was performed using the DLEM-CN model. Generally, DLEM-CNP performed well with respect to R^2 and RMSE at all sites. For all four sites, the DLEM-CNP reduced the RMSE (g C m^{-2} d^{-1}) with respect to DLEM-CN (BR-Sa1:1.49 vs. 4.15; BR-Sa3: 1.1 vs. 1.67; MY-PSO: 1.14 vs. 1.29; PA-SPn: 1.23 vs. 1.48). Figure 3-2 demonstrates this for the daily step GPP stimulation. Explicitly accounting for the effects of P limitation on photosynthesis does not change the shape of either the simulated daily or seasonal cycle of carbon fluxes. The simulated leaf nutrient limitation factor at the four sites shows that, including P limitation, the leaf NP limitation factor is stronger than the leaf N limitation factor in DLEM-CN, thus lowering the simulated GPP. At these sites, we output daily average foliar N content, foliar P content, and V_{cmax}, P mineralization, P weathering rate, plant P uptake rate, available PO_4 to show more information about P pools and fluxes (Table 3-4). The V_{cmax} ranges from 39.1 to 43.3 μmol CO_2 m^{-2} s^{-1}. Walker (2014) compiled global data set of photosynthetic rates and leaf nutrient traits include estimates of V_{cmax}, leaf nitrogen content, leaf phosphorus content data from both experimental and ambient field conditions. We filtered Walker's dataset to get tropical forests V_{cmax}, leaf N, leaf P, then compared with our results at FLUXNET sites with daily output. Walker's dataset indicates the V_{cmax} of tropical forests ranges from 33.66 to 140.88 μmol/m^2 s^{-1}, the leaf N range from 1.10 to 2.81 g/$m^{2,}$ and the leaf P range from 0.06 to 0.18 g/m^2. Our simulation results of V_{cmax} and leaf nutrient concentration fell within their ranges (Table 3-4).

Table 3- 4 Vegetation characteristics and P pools, fluxes at the 4 FLUXNET sites

sites	BR-Sa1	BR-Sa3	MY-PSO	PA-SPn
V_{cmax} (μmol $CO_2 m^{-2} s^{-1}$)	39.1	43.0	43.3	42.5
Leaf P content (g N/m^2)	0.083	0.129	0.086	0.103
Leaf N content (g P/m^2)	2.12	2.62	2.42	2.66
Leaf N:P ratio	25.6	20.3	28.2	25.9
P mineralization (g $P/m^2 yr^{-1}$)	0.30	0.35	0.19	0.10
P weathering (g $P/m^2 yr^{-1}$)	0.063	0.087	0.164	0.304
P uptake (g $P/m^2 yr^{-1}$)	0.20	0.32	0.20	0.24
available PO_4 (g P/m^2)	0.67	0.94	1.00	1.01

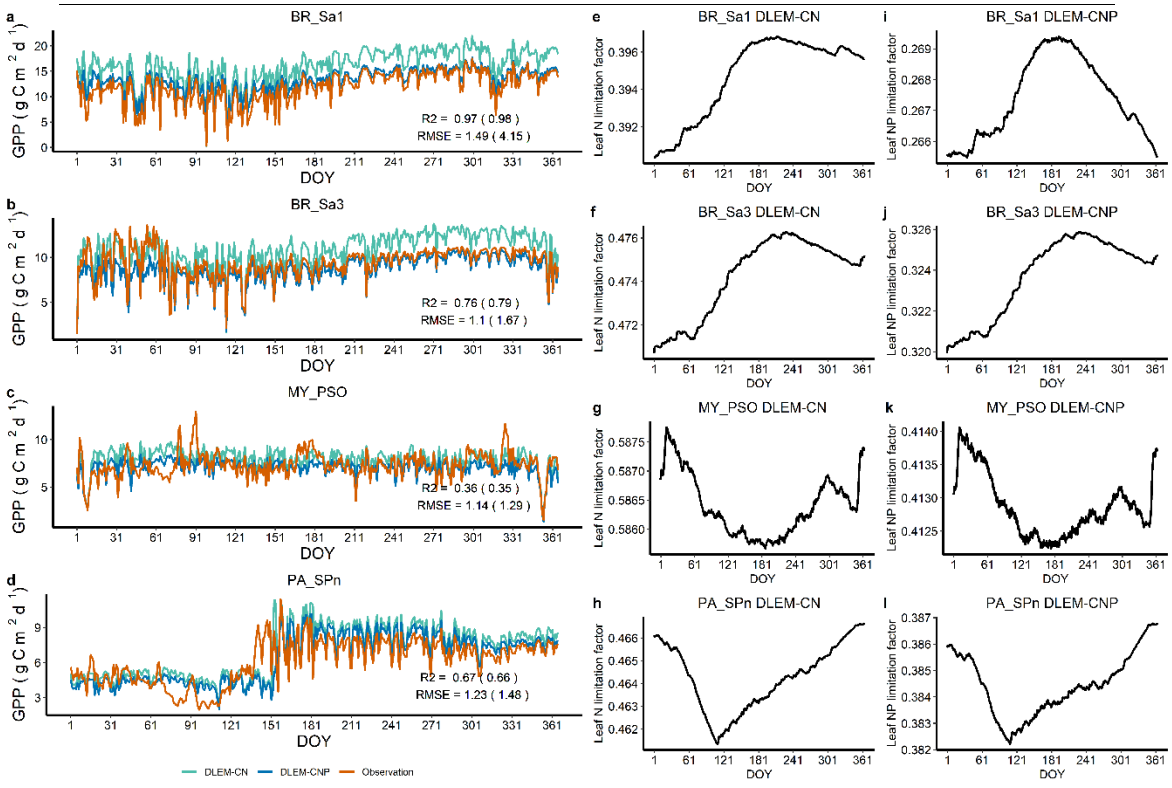

Figure 3- 2 Comparison of daily GPP between DLEM-CNP, DLEM-CN simulations, and FLUXNET observations (a, b, c, d). The leaf nutrient limitation factor of DLEM-CN, DLEM-CNP (e, f, g, h, i, j, k, l). The DLEM-CN model corresponds to performances given within parenthesis.

3.2 Carbon stocks and fertilizer addition experiments at Hawaiian sites

The NPP and carbon stocks simulated by the DLEM-CNP at Thurston and Kokee sites are consistent with observations for both sites (Table 3-5; Figure 3-3). The average NPP from the model simulation is 785.8 ± 14.8 g C m^{-2} y^{-1} at Thurston and 725.7 ± 40.1 g C m^{-2} y^{-1} at Kokee, the observed NPP is 789 ± 63.0 g C m^{-2} y^{-1} and 757 ± 73.0 g C m^{-2} y^{-1} at corresponding sites. The woody biomass (8535.2 ± 37.9 g C m^{-2}) was reasonably reproduced by the model with a slightly higher value (4.6%) than observation at the Thurston site. While the simulated woody biomass (8875.9 ± 74.4 g C m^{-2}) showed a 9.4% lower value than observation at the Kokee site (Figure 3-3). The soil organic carbon simulated by the DLEM-CNP is 13301.6 g C m^{-2} at Thurston and 18075.1 g C m^{-2} at Kokee, which is 12.9% and 24.5% lower than field measurements, respectively.

Nutrient use efficiencies (NPP divided by plant nutrient uptake) is an implicit plant property that depends on the tissue stoichiometry (Goll et al., 2017). The DLEM-CNP simulated NUE is 184.8 ± 8.8 g C g^{-1} N at Thurston site and 124.5 ± 20.5 g C g^{-1} N at Kokee site, which is underestimated by 19.6% and 44.6%, respectively, implying lower carbon productivity per plant nitrogen simulated by our model. The N uptake (4.26 ± 0.22 g N m^{-2} y^{-1} at Thurston site and 5.94 ± 0.90 g N m^{-2} y^{-1} at Kokee site) is overestimated by the model at both sites. The simulated PUE was comparable to observations (2.07 ± 0.04 g C mg^{-1} P vs. 3.22 ± 0.23 g C mg^{-1} P; 3.47 ± 0.08 g C mg^{-1} P vs. 3.86 ± 0.53 g C mg^{-1} P). The simulations of DLEM-CNP captured the pattern of higher NUE at N limited site and higher PUE at P limited site, which is consistent with Vitousek (2004) reporting that forests could acquire and use nutrients more efficiently at nutrient scarcity sites. Besides, the simulated P uptake (0.38 ± 0.01 g P m^{-2} y^{-1} at Thurston and 0.21 ± 0.02 g P m^{-2} y^{-1} at Kokee) is consistent with observations across two sites (Table 3-5).

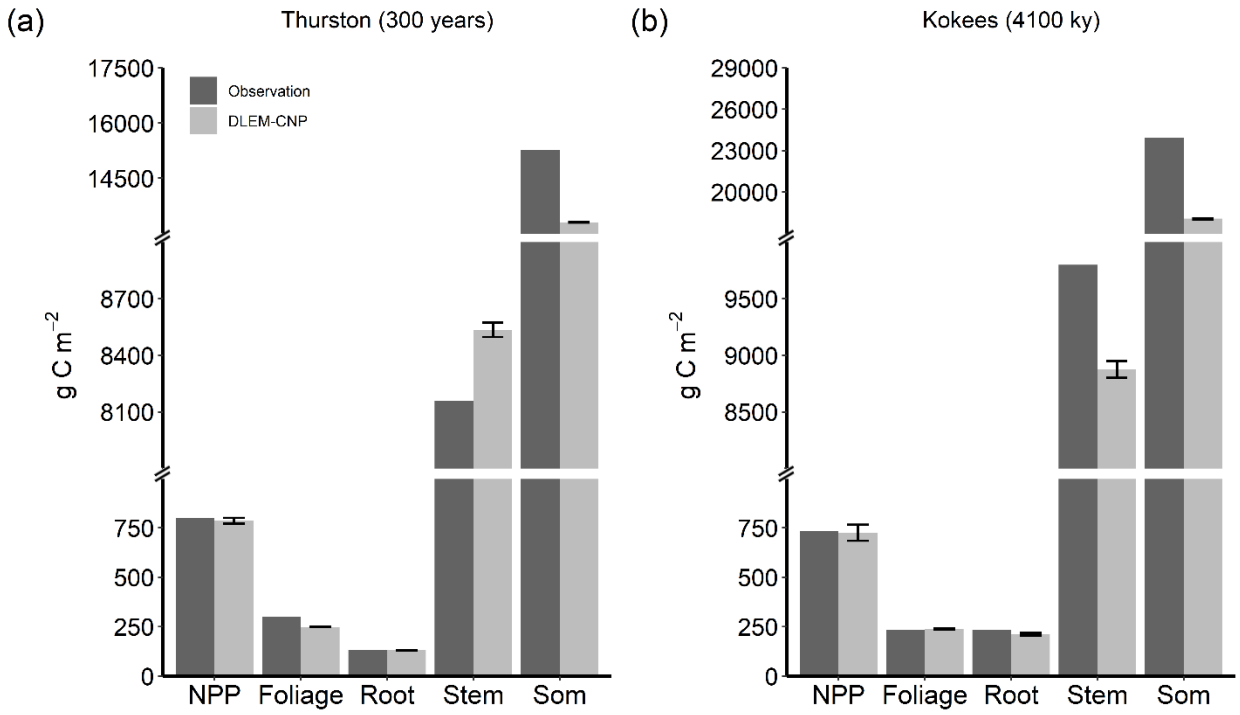

Figure 3- 3 Comparison between model simulations and observations at (a) Thurston and (b) Kokee Hawaiian sites. DLEM-CNP data indicates annual mean ± SD. Ky = 1000 years.

Table 3- 5 Vegetation characteristics at the two Hawaiian Islands sites

	Thurston		Kokee	
	simulated	observed	simulated	observed
NPP (g C m^{-2} yr^{-1})	785.8 ± 14.8	789 ± 63.0	725.7 ± 40.1	757 ± 73.0
N uptake (g N m^{-2} yr^{-1})	4.26 ± 0.22	3.43	5.94 ± 0.90	3.21
P uptake (g P m^{-2} yr^{-1})	0.38 ± 0.01	0.24	0.21 ± 0.02	0.19
NUE (g C g^{-1} N)	184.8 ± 8.8	229.9 ± 17.9	124.5 ± 20.5	224.8 ±32.7
PUE (g C mg^{-1} P)	2.07 ± 0.04	3.22 ± 0.23	3.47 ± 0.08	3.86 ± 0.53
Leaf N:P ratio	13.3 ± 0.2	12.6 ± 1.6	17.9 ± 0.4	17.3 ±2.7

Note: NPP is Net Primary Production; N uptake is plant nitrogen uptake rate; P uptake is plant phosphorus uptake rate; NUE is nitrogen use efficiency; PUE is phosphorus use efficiency; Leaf N:P ratio with g/g.

The simulated leaf N: P ratio at Thurston and Kokee is 13.3 ± 0.17 g N g^{-1} P and 17.9 ± 0.44 g N g^{-1} P, respectively. The values are close to the field observations, which are 12.6 ± 1.6 g

N g^{-1} P, 17.3 ± 2.7 g N g^{-1} P, indicating a good simulation regarding leaf nutrient condition. Tissue N: P ratios are widely used as an indicator of nutrient availability (Koerselman & Meuleman, 1996; McGroddy et al., 2004). Commonly, foliage N: P ratio of less than 14 indicates N limitation and above 16 indicates P limitation (Koerselman & Meuleman, 1996). The modeled leaf N: P ratio shows that N limits plant growth at the 0.3 ky site (leaf N: P ratio < 14), and P limits plant growth at the 4100 ky site (leaf N:P ratio > 16).

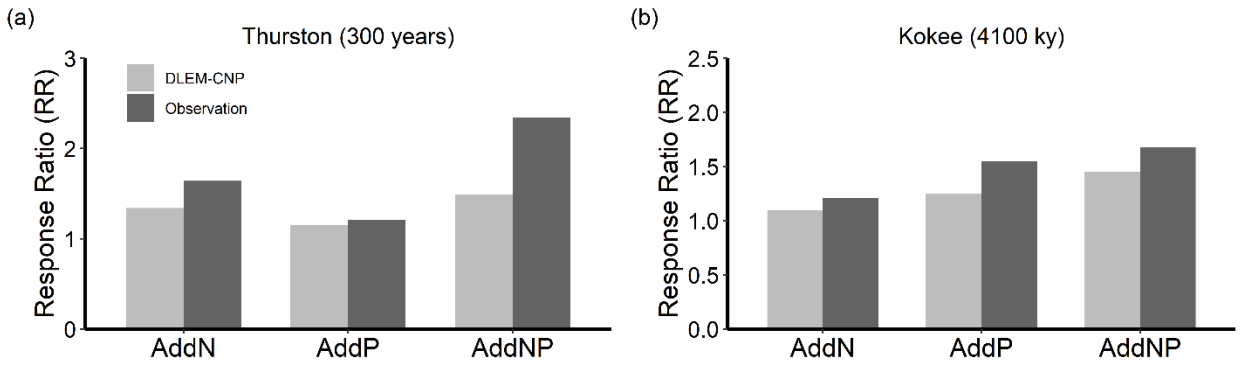

Figure 3- 4 Fertilizer addition experiments response ratio (RR) of net primary production (NPP) at (a) Thurston and (b) Kokee. Ky = 1000 years.

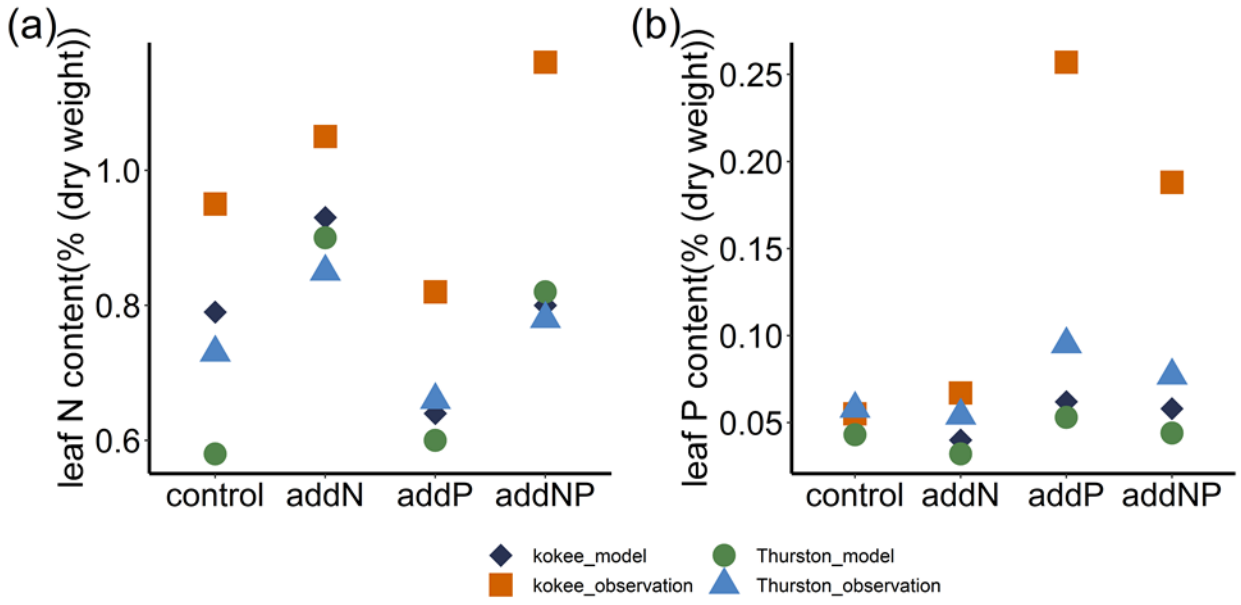

Figure 3- 5 (a) Leaf N content and (b) leaf P content during fertilizer addition experiments at Thurston and Kokee.

For fertilizer addition experiments, at Thurston site, which is N-limited, adding N significantly increased plant production (RR = 1.34), meanwhile adding P also increased plant production with a much smaller amount than adding N (RR = 1.15) (Figure 3-4). At the Kokee site, which is P limited, adding P resulted in a greater increase in plant production (RR = 1.46) and adding N slightly enhanced the plant production (RR = 1.10). At both sites, the simultaneous N and P addition resulted in the maximum increase of plant production, with RR being 1.48 at Thurston site and 1.45 at Kokee site.

Leaf N content and leaf P content can reflect the nutrient status of the plant and can have direct effects on leaf photosynthesis and vegetation productivity. At both sites, model simulations show leaf N content increase when the N fertilizer added and leaf P content increase when the P fertilizer added, which agrees with the observation. Overall, leaf N, P contents are realistically simulated by the DLEM-CNP. The variation of Leaf N content and leaf P content is roughly captured by the DLEM-CNP under all nutrient treatment conditions (add N, add P, and add NP). However, the model cannot catch the amplitude of leaf P content increment when P and NP fertilizers were added to P limited site (Figure 3-5). At the P limited Kokee site, after P and NP fertilizers were added the observation of leaf P content was 0.260 ± 0.1000 (%, dry weight) and 0.190 ± 0.040 (%, dry weight), but model results are only 0.062 ± 0.008 and 0.058 ± 0.004 (%, dry weight).

3.3 Simulations at tropical sites by DLEM-CNP and DLEM-CN

We expanded the model validation to more tropical forest sites and examined model performance on the multi-year average NPP. We compiled NPP records at 13 tropical forest sites in Clark et al. (2001), ranging from 800 g C yr^{-1} to 1600 g C yr^{-1} (Figure 3-6). The NPP simulated

by the DLEM-CNP is consistent with the observational datasets (R^2= 0.92). The introduction of the P module improved NPP simulation at the tropical forest sites, decreasing the overestimated NPP by the DLEM-CN model across all the 13 sites. The R^2 is 0.92 for DLEM-CNP and 0.87 for DLEM-CN. Root Mean Square Error is 176.7 g C m^{-2} yr^{-1} for DLEM-CNP and 364.1.5 g C m^{-2} yr^{-1} for DLEM-CN. All three statistical indicators (R^2, RMSE) demonstrate the DLEM-CNP has better performance in modeling tropical forest NPP by including P processes and considering CNP interactions.

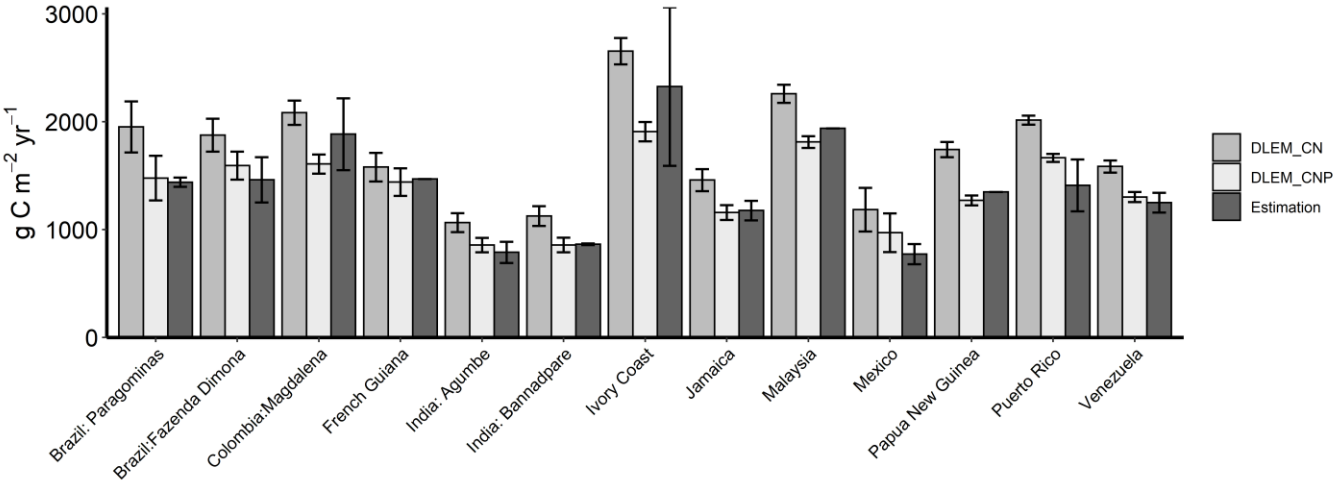

Figure 3- 6 Comparisons of net primary production (NPP) from the DLEM-CN, DLEM-CNP, and observations at tropical sites.

3.4 Model sensitivity to parameters

A one-at-a-time (OAT) sensitivity analysis was performed for the 4 FLUXNET sites. In one simulation, we only modified one parameter by ± 10% with respect to the reference value and held other parameters constantly. Sensitivity of different variables to parameters calculated as difference between output from modified parameters and default parameter divided by output from default parameters. Figure 3-7 shows the sensitivity of simulated GPP, foliage P, available PO_4, leaf N: P ratio to P-related parameters, and potential uncertainties in model parameterization.

Simulated GPP varies between -2.7% and 2.5% in relative to the simulated values in the default model parameterization, (Figure 3-7a). GPP is most sensitive to the P uptake (P_{up_max}, k_{up}), reflecting the important role of plant P uptake on P limitation and GPP. Leaf P content (Figure 3-7b) is predominantly controlled by the P uptake (P_{up_max}, k_{up}) and P allocation ($CP_{min,sapwood}$, $CP_{min,leaf}$) processes. P_{up_max} lead to -5.4% to 5.1% changes in Leaf P content. And leaf P content varies with change of -5.3% ~ 6.2% and -5.0% ~ 5.9% for parameter k_{up} and $CP_{min,leaf}$ respectively. Available PO_4 shows a slight response to the different parameter set. Sensitivity of available PO_4 to parameters shows the biggest differences between sites. The potential reason may be that available PO_4 is impacted by every processes in soil and plant uptake. Thus, different sites with different properties can have different impacts on the available PO_4. Notably, $lchb_{dip}$ is among the most sensitivity for available PO_4 leading to a relatively small change -1.1% ~ 0.7%. Leaf N: P ratio shows a similar pattern with leaf P content of sensitivity to parameters. The sensitivity analysis demonstrates that changes in parameters result in small changes in model outcomes, and model is most sensitive to parameters on P uptake.

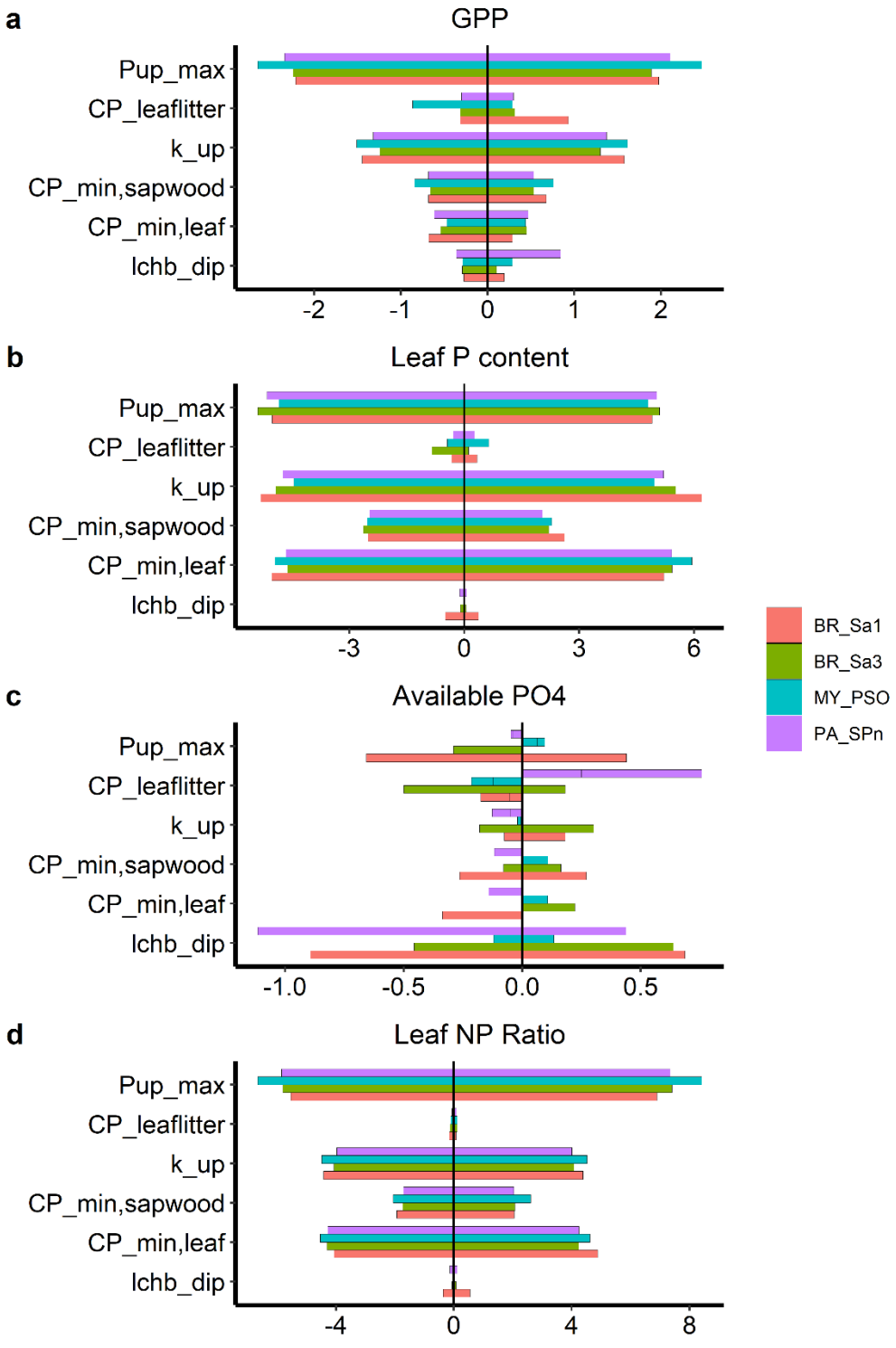

Figure 3- 7 Sensitivity analysis at 4 FLUXNET sites.

4. Discussion

4.1 Model Evaluation at the Site Scale

The results presented here demonstrate the incorporation of key P dynamics within the DLEM. The model simulations are consistent with the observed ranges of GPP, NPP, P tissue concentrations, NUE, net N mineralization, and the response to the fertilizer addition experiments at the FLUXNET sites, Hawaii sites, and other tropical sites.

Some TBMs with coupled CNP cycles have been reported before (Goll et al., 2012; Goll et al., 2017; Wang et al., 2010; Yang et al., 2014). The DLEM-CNP model distinguishes itself from these models in that there is an explicit consideration of the NP co-limitation (Equation 1 and 2) on photosynthesis. With this NP co-limitation scheme, DLEM-CNP has better potential for simulating NP interaction effects on C assimilation in contrast to models without considering P effects on photosynthesis, only considering leaf P to calculate GPP, or describing nutrients limitation on plant growth by using the Liebig's law of minimum (e.g., CLM-CNP, ORCHIDEE). In the Hawaii site fertilizer addition experiments, the addition of P at the N limited Thurston site alleviated N limitation on vegetation growth. Also, the N addition at P limited site slightly increased NPP. These responses demonstrated the innovative improvements of introducing the N and P interactive co-limitation effect. Field experiments support this N and P interactive co-limitation and therefore it needs to be considered in models (Domingues et al., 2010; Jiang et al., 2019; Walker et al., 2017; Wang et al., 2018). Considering N, P co-limitation may increase the capability of models to predict future conditions in P-limited tropical forests, especially when combined with other environmental drivers (Domingues et al., 2010; Jiang et al., 2019). However, the mechanisms are not fully clear. Therefore, more data and experiments on foliar N, P

concentrations and photosynthetic parameters are needed to help molders develop more robust relationships.

In DLEM-CNP, GPP is regulated through the NP limitation on V_{cmax}. Our simulation results of daily V_{cmax} is at the lower end of the observation range. However, there are a range of V_{cmax} values from different studies indicating our simulated V_{cmax} is reasonable. Kattge et al. (2009) reported the observed V_{cmax} for tropical broadleaf evergreen trees at 41 μmol CO_2 m^{-2} s^{-1} (Bonan et al., 2012). Some modeling studies for Amazonia also reported various V_{cmax} values: 43 μmol CO_2 m^{-2} s^{-1} (Carswell et al., 2000); 58 μmol CO_2 m^{-2} s^{-1} (Mercado et al., 2006); 64 μmol CO_2 m^{-2} s^{-1}, based on the Lloyd et al. (2010) analysis of Domingues et al. (2005); and 68 μmol CO_2 m^{-2} s^{-1} (Lloyd et al., 1995). Mercado et al. (2009) used values of 32, 40, 47, 52, and 52 μmol CO_2 m^{-2} s^{-1} for five Amazonian sites. Fisher et al. (2007) used values of 24–44 μmol CO_2 m^{-2} s^{-1} for simulations in eastern Amazonia.

At the Hawaii sites, the underestimated NUE could be due to the overestimation of N uptake, which is related to C: N ratio of biomass and biological N fixation rate. The C: N ratio of biomass is a species dependent parameter; thus, it may tend to introduce bias at site level. Moreover, the biological N fixation rate is described as a plant-type-specific parameter in DLEM, which may not reflect the reality at Hawaii sites.

Our model underestimated the absolute value of RR in fertilization experiments. Also, the model didn't catch the amplitude of leaf P content increase when P or NP fertilizer was added to P limited site (Figure 3-4b). Leaf N and P concentrations determine the leaf NP limitation on GPP. Hence, the smaller increase in leaf P content than observation resulted in the underestimated RR. Two reasons explain the underestimated of leaf P content increase. DLEM-CNP simulated

fertilizer application by assuming that annual fertilizer input was applied evenly each day. Specifically, in our simulation, the N and P fertilizers were added at a rate of 0.027 (10/365) gN/gP m^{-2} per day. These fertilizers directly entered soil available N pool and soil dissolve inorganic P pool. The 0.027 gN/gP m^{-2} per day fertilizers did not lead to a substantial increase in soil available N and dissolve inorganic P pool, which impeded the nutrient uptake by plant. In addition, Harrington et al. (2001) observed P limitation results in disproportionally significant increases in P uptake after fertilization during the fertilization experiment. However, this mechanism strongly depends on species, it has not been included in our model. In the future, we will improve our model to simulate fertilizer with monthly or daily data to more accurately capture the fertilization effect.

The mismatch between the modeled SOM and observed values at Hawaii can be attributed to the uncertainties in modeling decomposition process. In contrast to first-order decomposition models (Parton et al., 1987), SOC decomposition rates should depend not only on the SOC stock size but also on the size and composition of the decomposer microbial pool (Schimel & Weintraub, 2003) as well as carbon nutrients interactions (Six et al., 2002). Therefore, the SOC stocks are still far from certain in TBMs. Some research demonstrated P could have impacts on the microbial decomposition rate, e.g., Qualls and Richardson (2000) suggested P enrichment influences the litter decomposition rate in the Everglades. Tian et al. (2015) also emphasized that nutrient limitation on microbial activities are important structural uncertainties but being ignored or poorly represented by most models leading to uncertainties in the modeled SOC. All these studies implying a more realistic decomposition process is needed.

4.2 Uncertainty and Future Research

Although DLEM-CNP could well reproduce the observed forest productivity and biomass, several issues need to be addressed in the future. First, our model does not consider biochemical

mineralization, a process that plants and microbes can produce phosphatase enzymes to mineralize P in soil organic matter but without mineralizing C and N (Mcgill & Cole, 1981). Wang et al. (2007) showed that neglecting biochemical P mineralization tended to overestimate the fraction of soil organic P and underestimated the fractions of the labile P. Neglect of biochemical mineralization may underestimate available P, causing stronger P limitation on plant productivity. Second, DLEM-CNP did not consider P effects on some N processes, such as the biological N fixation process. Several studies indicate that P availability may impact N fixation (Edwards et al., 2006; Reed et al., 2007). Edwards et al. (2006) examined biological N fixation of swards response to elevated CO_2 under both high and low P availability, showing high P increased biological N fixation. Reed et al. (2007) suggested that P availability, possibly via regulation of N fixation, strongly influence N availability in recovering prairie soils. However, the mechanisms of P influence on N fixation have not yet been fully understood. Third, plants' adaptation to P limitation can change vegetation physiological characteristics (Vance et al., 2003). Plants evolve strategies for P acquisition and use in P-limiting environments, including decreased growth rate, increased growth per unit of P uptake, remobilization of internal P, modifications in carbon metabolism that bypass P-requiring steps, and alternative respiratory pathways (Vance et al., 2003). All these adaption strategies are supposed to lead to vegetation parameters change (e.g., V_{cmax}, minimum leaf C: N ratio, and minimum leaf C: P ratio). Last, in model we didn't consider trace elements, such as Potassium (K), Calcium (Ca), Magnesium (Mg). However, trace elements also have impacts on plant productivity.

In tropical areas, forests in different places have different P limitation levels and highly variable NPP (Castanho et al., 2013; Fyllas et al., 2009; Tanner et al., 1998). Our results at various tropical forest sites demonstrated that using a uniform value for key ecological parameters of

tropical forests would decrease the simulation accuracy. In future work, a more detailed forest classification scheme could be developed to represent the spatial heterogeneity of tropical forests.

As P limitation on productivity is recognized to be widespread in tropical forests, at this stage, we only focus our model development in tropical forest areas. In the future, we will expand the model application to other terrestrial ecosystems.

5. Conclusions

P cycle has been successfully coupled with C and N cycles in the DLEM. The DLEM-CNP fully incorporates CNP cycles in all pools (plant, litter, and soil organic/inorganic pools) and key biogeochemical processes. Evaluation of model performance at FLUXNET sites, Hawaii sites, and comparison of NPP simulated by the DLEM-CNP and DLEM-CN with benchmarks at tropical forests demonstrate the improvement of the model's performance. Furthermore, we simulated the response of plants to fertilizer addition for evaluating the mechanisms of nutrient limitation on plants. Results imply a significant P impact on ecosystem C dynamics and highlight the innovative improvements of introducing the N and P interactive co-limitation effect. Our results reveal interactions between C, N, P processes, indicating that the inclusion of the P cycle in the current TBMs is essential to better understand the impacts of global change on terrestrial ecosystems. With adequate parameterization, the DLEM-CNP model can be applied to simulate and predict the productivity of terrestrial ecosystems and C, N, P dynamics across the global land surface.

Reference

Achat, D. L., Augusto, L., Gallet-Budynek, A., & Loustau, D. (2016). Future challenges in coupled C–N–P cycle models for terrestrial ecosystems under global change: a review. *Biogeochemistry, 131*(1), 173-202. https://doi.org/10.1007/s10533-016-0274-9

Ågren, G. I., Wetterstedt, J. Å. M., & Billberger, M. F. K. (2012). Nutrient limitation on terrestrial plant growth – modeling the interaction between nitrogen and phosphorus. *New Phytologist, 194*(4), 953-960. https://doi.org/10.1111/j.1469-8137.2012.04116.x

Bonan, G. B., Oleson, K. W., Fisher, R. A., Lasslop, G., & Reichstein, M. (2012). Reconciling leaf physiological traits and canopy flux data: Use of the TRY and FLUXNET databases in the Community Land Model version 4. *Journal of Geophysical Research: Biogeosciences, 117*(G2). https://doi.org/10.1029/2011JG001913

Buendía, C., Kleidon, A., & Porporato, A. (2010). The role of tectonic uplift, climate, and vegetation in the long-term terrestrial phosphorous cycle. *Biogeosciences, 7*(6), 2025-2038. https://doi.org/10.5194/bg-7-2025-2010

Carswell, F. E., Meir, P., Wandelli, E. V., Bonates, L. C. M., Kruijt, B., Barbosa, E. M., et al. (2000). Photosynthetic capacity in a central Amazonian rain forest. *Tree Physiology, 20*(3), 179-186. https://doi.org/10.1093/treephys/20.3.179

Castanho, A. D. A., Coe, M. T., Costa, M. H., Malhi, Y., Galbraith, D., & Quesada, C. A. (2013). Improving simulated Amazon forest biomass and productivity by including spatial variation in biophysical parameters. *Biogeosciences, 10*(4), 2255-2272. https://doi.org/10.5194/bg-10-2255-2013

Chorover, J., Amistadi, M. K., & Chadwick, O. A. (2004). Surface charge evolution of mineral-organic complexes during pedogenesis in Hawaiian basalt. *Geochimica et Cosmochimica Acta, 68*(23), 4859-4876. https://doi.org/https://doi.org/10.1016/j.gca.2004.06.005

Clark, D. A., Brown, S., Kicklighter, D. W., Chambers, J. Q., Thomlinson, J. R., Ni, J., & Holland, E. A. (2001). Net primary production in tropical forests: an evaluation and synthesis of existing field data. *Ecological applications, 11*(2), 371-384.

Cordell, D., Drangert, J.-O., & White, S. (2009). The story of phosphorus: Global food security and food for thought. *Global Environmental Change, 19*(2), 292-305. https://doi.org/https://doi.org/10.1016/j.gloenvcha.2008.10.009

Crews, T. E., Kitayama, K., Fownes, J. H., Riley, R. H., Herbert, D. A., Mueller-Dombois, D., & Vitousek, P. M. (1995). Changes in soil phosphorus fractions and ecosystem dynamics across a long chronosequence in Hawaii. *Ecology, 76*(5), 1407-1424.

Davidson, E. A., Reis de Carvalho, C. J., Vieira, I. C. G., Figueiredo, R. d. O., Moutinho, P., Yoko Ishida, F., et al. (2004). NITROGEN AND PHOSPHORUS LIMITATION OF

BIOMASS GROWTH IN A TROPICAL SECONDARY FOREST. *Ecological applications, 14*(sp4), 150-163. https://doi.org/10.1890/01-6006

Domingues, T. F., Berry, J. A., Martinelli, L. A., Ometto, J. P. H. B., & Ehleringer, J. R. (2005). Parameterization of Canopy Structure and Leaf-Level Gas Exchange for an Eastern Amazonian Tropical Rain Forest (Tapajós National Forest, Pará, Brazil). *Earth Interactions, 9*(17), 1-23. https://doi.org/10.1175/EI149.1

Domingues, T. F., Meir, P., Feldpausch, T. R., Saiz, G., Veenendaal, E. M., Schrodt, F., et al. (2010). Co-limitation of photosynthetic capacity by nitrogen and phosphorus in West Africa woodlands. *Plant, Cell & Environment, 33*(6), 959-980. https://doi.org/10.1111/j.1365-3040.2010.02119.x

Edwards, E. J., McCaffery, S., & Evans, J. R. (2006). Phosphorus availability and elevated CO2 affect biological nitrogen fixation and nutrient fluxes in a clover-dominated sward. *New Phytologist, 169*(1), 157-167. https://doi.org/10.1111/j.1469-8137.2005.01568.x

Edwards, P., & Grubb, P. (1977). Studies of mineral cycling in a montane rain forest in New Guinea: I. The distribution of organic matter in the vegetation and soil. *The Journal of Ecology*, 943-969.

Elser, J., & Bennett, E. J. N. (2011). Phosphorus cycle: a broken biogeochemical cycle. *478*(7367), 29.

Esser, G., Lieth, H. F. H., Scurlock, J. M. O., & Olson, R. J. (1997). *Worldwide estimates and bibliography of net primary productivity derived from pre-1982 publications*. Retrieved from United States: https://www.osti.gov/servlets/purl/631208

Farquhar, G. D., von Caemmerer, S., & Berry, J. A. J. P. (1980). A biochemical model of photosynthetic CO2 assimilation in leaves of C3 species. *149*(1), 78-90. journal article. https://doi.org/10.1007/bf00386231

Filippelli, G. M. (2008). The global phosphorus cycle: past, present, and future. *Elements, 4*(2), 89-95.

Fisher, R. A., Williams, M., Da Costa, A. L., Malhi, Y., Da Costa, R. F., Almeida, S., & Meir, P. (2007). The response of an Eastern Amazonian rain forest to drought stress: results and modelling analyses from a throughfall exclusion experiment. *Global Change Biology, 13*(11), 2361-2378. https://doi.org/10.1111/j.1365-2486.2007.01417.x

Fleischer, K., Rammig, A., De Kauwe, M. G., Walker, A. P., Domingues, T. F., Fuchslueger, L., et al. (2019). Amazon forest response to CO2 fertilization dependent on plant phosphorus acquisition. *Nature Geoscience*. https://doi.org/10.1038/s41561-019-0404-9

Friend, A. D., Arneth, A., Kiang, N. Y., Lomas, M., OgÉE, J., RÖDenbeck, C., et al. (2007). FLUXNET and modelling the global carbon cycle. *Global Change Biology, 13*(3), 610-633. https://doi.org/10.1111/j.1365-2486.2006.01223.x

Fyllas, N. M., Patino, S., Baker, T., Bielefeld Nardoto, G., Martinelli, L., Quesada, C., et al. (2009). Basin-wide variations in foliar properties of Amazonian forest: phylogeny, soils and climate. *6*, 2677-2708.

Gerber, S., Hedin, L. O., Oppenheimer, M., Pacala, S. W., & Shevliakova, E. (2010). Nitrogen cycling and feedbacks in a global dynamic land model. *Global Biogeochemical Cycles, 24*(1). https://doi.org/10.1029/2008GB003336

Goll, D., Joetzjer, E., Huang, M., & Ciais, P. (2018). Low Phosphorus Availability Decreases Susceptibility of Tropical Primary Productivity to Droughts. *Geophysical Research Letters, 45*(16), 8231-8240.

Goll, D., Vuichard, N., Maignan, F., Jornet-Puig, A., Sardans, J., Violette, A., et al. (2017). A representation of the phosphorus cycle for ORCHIDEE (revision 4520). *Geoscientific Model Development Discussions, 10*(10), 3745-3770.

Goll, D. S., Brovkin, V., Parida, B. R., Reick, C. H., Kattge, J., Reich, P. B., et al. (2012). Nutrient limitation reduces land carbon uptake in simulations with a model of combined carbon, nitrogen and phosphorus cycling. *Biogeosciences, 9*(9), 3547-3569. https://doi.org/10.5194/bg-9-3547-2012

Guignard, M. S., Leitch, A. R., Acquisti, C., Eizaguirre, C., Elser, J. J., Hessen, D. O., et al. (2017). Impacts of Nitrogen and Phosphorus: From Genomes to Natural Ecosystems and Agriculture. *Frontiers in Ecology and Evolution, 5*(70). Review. https://doi.org/10.3389/fevo.2017.00070

Harrington, R. A., Fownes, J. H., & Vitousek, P. M. J. E. (2001). Production and Resource Use Efficiencies in N- and P-Limited Tropical Forests: A Comparison of Responses to Long-term Fertilization. *4*(7), 646-657. journal article. https://doi.org/10.1007/s10021-001-0034-z

Hikosaka, K. (2004). Interspecific difference in the photosynthesis–nitrogen relationship: patterns, physiological causes, and ecological importance. *Journal of Plant Research, 117*(6), 481-494. https://doi.org/10.1007/s10265-004-0174-2

Houghton, J. T., Ding, Y., Griggs, D., Noguer, M., van der Linden, P., Dai, X., et al. (2001). Climate Change 2001: The Scientific Basis, Cambridge Uni. In: Press.

Jiang, M., Caldararu, S., Zaehle, S., Ellsworth, D. S., & Medlyn, B. E. (2019). Towards a more physiological representation of vegetation phosphorus processes in land surface models. *New Phytologist*.

Jordan, C. F., & Escalante, G. (1980). Root productivity in an Amazonian rain forest. *Ecology, 61*(1), 14-18.

Kattge, J., Knorr, W., Raddatz, T., & Wirth, C. (2009). Quantifying photosynthetic capacity and its relationship to leaf nitrogen content for global-scale terrestrial biosphere models. *Global Change Biology, 15*(4), 976-991. https://doi.org/10.1111/j.1365-2486.2008.01744.x

Kira, T. (1978.). *Community architecture and organic matter dynamics in tropical lowland rain forests of Southeast Asia with special reference to Pasoh Forest,West Malaysia.* (P. B. T. a. M. H. Zimmerman Ed.): Cambridge University Press, New York, .

Koerselman, W., & Meuleman, A. F. (1996). The vegetation N: P ratio: a new tool to detect the nature of nutrient limitation. *Journal of applied Ecology, 33*(6), 1441-1450.

Lessin, G., Lips, I., & Raudsepp, U. (2007). Modelling nitrogen and phosphorus limitation on phytoplankton growth in Narva Bay, south-eastern Gulf of Finland. *Oceanologia, 49*(2).

Lieth, H. (1975). Modeling the Primary Productivity of the World. In H. Lieth & R. H. Whittaker (Eds.), *Primary Productivity of the Biosphere* (pp. 237-263). Berlin, Heidelberg: Springer Berlin Heidelberg.

Lloyd, J., Bird, M., Veenendaal, E., & Kruijt, B. (2001). Should phosphorus availability be constraining moist tropical forest responses to increasing CO2 concentrations? In *Global biogeochemical cycles in the climate system* (pp. 95-114): Elsevier.

Lloyd, J., Grace, J., Miranda, A. C., Meir, P., Wong, S. C., Miranda, H. S., et al. (1995). A simple calibrated model of Amazon rainforest productivity based on leaf biochemical properties. *Plant, Cell & Environment, 18*(10), 1129-1145. https://doi.org/10.1111/j.1365-3040.1995.tb00624.x

Lloyd, J., Patiño, S., Paiva, R. Q., Nardoto, G. B., Quesada, C. A., Santos, A. J. B., et al. (2010). Optimisation of photosynthetic carbon gain and within-canopy gradients of associated foliar traits for Amazon forest trees. *Biogeosciences, 7*(6), 1833-1859. https://doi.org/10.5194/bg-7-1833-2010

Lugo, A. E., & Murphy, P. G. (1986). Nutrient dynamics of a Puerto Rican subtropical dry forest. *Journal of Tropical Ecology, 2*(1), 55-72.

Marklein, A. R., & Houlton, B. Z. (2012). Nitrogen inputs accelerate phosphorus cycling rates across a wide variety of terrestrial ecosystems. *New Phytologist, 193*(3), 696-704. https://doi.org/10.1111/j.1469-8137.2011.03967.x

Martinez-Yrizar, A., Maass, J., Pérez-Jiménez, L., & Sarukhán, J. (1996). Net primary productivity of a tropical deciduous forest ecosystem in western Mexico. *Journal of Tropical Ecology, 12*(1), 169-175.

Martinez-Yrizar, A., Sarukhan, J., Perez-Jimenez, A., Rincon, E., Maass, J. M., Solis-Magallanes, A., & Cervantes, L. (1992). Above-ground phytomass of a tropical deciduous forest on the coast of Jalisco, Mexico. *Journal of Tropical Ecology, 8*(1), 87-96.

Mcgill, W. B., & Cole, C. V. (1981). Comparative Aspects of Cycling of Organic C, N, S and P through Soil Organic-Matter. *Geoderma, 26*(4), 267-286. https://doi.org/Doi 10.1016/0016-7061(81)90024-0

McGroddy, M. E., Daufresne, T., & Hedin, L. O. (2004). Scaling of C: N: P stoichiometry in forests worldwide: implications of terrestrial redfield‐type ratios. *Ecology, 85*(9), 2390-2401.

Mercado, L., Lloyd, J., Carswell, F., Malhi, Y., Meir, P., & Nobre, A. D. (2006). Modelling Amazonian forest eddy covariance data: a comparison of big leaf versus sun/shade models for the C-14 tower at Manaus I. Canopy photosynthesis. *Acta Amazonica, 36*, 69-82.

Mercado, L. M., Lloyd, J., Dolman, A. J., Sitch, S., & Patiño, S. (2009). Modelling basin-wide variations in Amazon forest productivity – Part 1: Model calibration, evaluation and upscaling functions for canopy photosynthesis. *Biogeosciences, 6*(7), 1247-1272. https://doi.org/10.5194/bg-6-1247-2009

Newbery, D. M., Clutton–Brock, T. H., Prance, G. T., Mirmanto, E., Proctor, J., Green, J., et al. (1999). Effects of nitrogen and phosphorus fertilization in a lowland evergreen rainforest. *Philosophical Transactions of the Royal Society of London. Series B: Biological Sciences, 354*(1391), 1825-1829. https://doi.org/10.1098/rstb.1999.0524

Newman, E. I. (1995). Phosphorus Inputs to Terrestrial Ecosystems. *Journal of Ecology, 83*(4), 713-726. https://doi.org/10.2307/2261638

Olander, L. P., & Vitousek, P. M. (2000). Regulation of soil phosphatase and chitinase activityby N and P availability. *Biogeochemistry, 49*(2), 175-191. https://doi.org/10.1023/A:1006316117817

Ostertag, R. (2001). Effects of nitrogen and phosphorus availability on fine‐root dynamics in Hawaiian montane forests. *Ecology, 82*(2), 485-499.

Porder, S., Vitousek, P. M., Chadwick, O. A., Chamberlain, C. P., & Hilley, G. E. (2007). Uplift, Erosion, and Phosphorus Limitation in Terrestrial Ecosystems. *Ecosystems, 10*(1), 159-171. https://doi.org/10.1007/s10021-006-9011-x

Qualls, R. G., & Richardson, C. J. (2000). Phosphorus enrichment affects litter decomposition, immobilization, and soil microbial phosphorus in wetland mesocosms. *Soil Science Society of America Journal, 64*(2), 799-808.

Reed, S. C., Seastedt, T. R., Mann, C. M., Suding, K. N., Townsend, A. R., & Cherwin, K. L. (2007). Phosphorus fertilization stimulates nitrogen fixation and increases inorganic nitrogen concentrations in a restored prairie. *Applied Soil Ecology, 36*(2), 238-242. https://doi.org/https://doi.org/10.1016/j.apsoil.2007.02.002

Reed, S. C., Yang, X., & Thornton, P. E. (2015). Incorporating phosphorus cycling into global modeling efforts: a worthwhile, tractable endeavor. *New Phytologist, 208*(2), 324-329.

Schimel, J. P., & Weintraub, M. N. (2003). The implications of exoenzyme activity on microbial carbon and nitrogen limitation in soil: a theoretical model. *Soil Biology and Biochemistry, 35*(4), 549-563. https://doi.org/https://doi.org/10.1016/S0038-0717(03)00015-4

Six, J., Conant, R. T., Paul, E. A., & Paustian, K. (2002). Stabilization mechanisms of soil organic matter: Implications for C-saturation of soils. *Plant and Soil, 241*(2), 155-176. https://doi.org/10.1023/A:1016125726789

Tanner, E. V. J. (1980a). Litterfall in Montane Rain Forests of Jamaica and its Relation to Climate. *Journal of Ecology, 68*(3), 833-848. https://doi.org/10.2307/2259459

Tanner, E. V. J. (1980b). Studies on the Biomass and Productivity in a Series of Montane Rain Forests in Jamaica. *Journal of Ecology, 68*(2), 573-588. https://doi.org/10.2307/2259423

Tanner, E. V. J. (1985). Jamaican Montane Forests: Nutrient Capital and Cost of Growth. *Journal of Ecology, 73*(2), 553-568. https://doi.org/10.2307/2260493

Tanner, E. V. J., Kapos, V., Freskos, S., Healey, J. R., & Theobald, A. M. (1990). Nitrogen and Phosphorus Fertilization of Jamaican Montane Forest Trees. *Journal of Tropical Ecology, 6*(2), 231-238.

Tanner, E. V. J., Vitousek, P. M., & Cuevas, E. (1998). EXPERIMENTAL INVESTIGATION OF NUTRIENT LIMITATION OF FOREST GROWTH ON WET TROPICAL MOUNTAINS. *Ecology, 79*(1), 10-22. https://doi.org/10.1890/0012-9658(1998)079[0010:EIONLO]2.0.CO;2

Thornton, P. E., Lamarque, J.-F., Rosenbloom, N. A., & Mahowald, N. M. (2007). Influence of carbon-nitrogen cycle coupling on land model response to CO2 fertilization and climate variability. *Global Biogeochemical Cycles, 21*(4). https://doi.org/10.1029/2006GB002868

Thornton, P. E., Thornton, M. M., Mayer, B. W., Wei, Y., Devarakonda, R., Vose, R. S., & Cook, R. B. (2017). Daymet: Daily Surface Weather Data on a 1-km Grid for North America, Version 3. In: ORNL Distributed Active Archive Center.

Tian, H., Liu, M., Zhang, C., Ren, W., Xu, X., Chen, G., et al. (2010). The dynamic land ecosystem model (DLEM) for simulating terrestrial processes and interactions in the context of multifactor global change. *Acta Geographica Sinica, 65*(9), 1027-1047.

Tian, H., Lu, C., Yang, J., Banger, K., Huntzinger, D. N., Schwalm, C. R., et al. (2015). Global patterns and controls of soil organic carbon dynamics as simulated by multiple terrestrial biosphere models: Current status and future directions. *Global Biogeochemical Cycles, 29*(6), 775-792. https://doi.org/10.1002/2014GB005021

Treseder, K. K., & Vitousek, P. M. (2001). EFFECTS OF SOIL NUTRIENT AVAILABILITY ON INVESTMENT IN ACQUISITION OF N AND P IN HAWAIIAN RAIN FORESTS. *Ecology, 82*(4), 946-954. https://doi.org/10.1890/0012-9658(2001)082[0946:EOSNAO]2.0.CO;2

Turner, B. L., Brenes-Arguedas, T., & Condit, R. (2018). Pervasive phosphorus limitation of tree species but not communities in tropical forests. *Nature, 555*, 367. https://doi.org/10.1038/nature25789

Vance, C. P., Uhde-Stone, C., & Allan, D. L. (2003). Phosphorus acquisition and use: critical adaptations by plants for securing a nonrenewable resource. *New Phytologist, 157*(3), 423-447. https://doi.org/10.1046/j.1469-8137.2003.00695.x

Vitousek, P. M. (2004). *Nutrient cycling and limitation: Hawai'i as a model system*: Princeton University Press.

Vitousek, P. M., Porder, S., Houlton, B. Z., & Chadwick, O. A. (2010). Terrestrial phosphorus limitation: mechanisms, implications, and nitrogen–phosphorus interactions. *Ecological applications, 20*(1), 5-15.

Vitousek, P. M., Walker, L. R., Whiteaker, L. D., & Matson, P. A. (1993). Nutrient limitations to plant growth during primary succession in Hawaii Volcanoes National Park. *Biogeochemistry, 23*(3), 197-215. https://doi.org/10.1007/BF00023752

Walker, A. P., Quaife, T., van Bodegom, P. M., De Kauwe, M. G., Keenan, T. F., Joiner, J., et al. (2017). The impact of alternative trait-scaling hypotheses for the maximum photosynthetic carboxylation rate (Vcmax) on global gross primary production. *New Phytologist, 215*(4), 1370-1386. https://doi.org/10.1111/nph.14623

Walker, T., & Syers, J. K. (1976). The fate of phosphorus during pedogenesis. *Geoderma, 15*(1), 1-19.

Wang, J., Wen, X., Zhang, X., Li, S., & Zhang, D.-Y. (2018). Co-regulation of photosynthetic capacity by nitrogen, phosphorus and magnesium in a subtropical Karst forest in China. *Scientific Reports, 8*(1), 7406. https://doi.org/10.1038/s41598-018-25839-1

Wang, R., Balkanski, Y., Boucher, O., Ciais, P., Peñuelas, J., & Tao, S. (2015). Significant contribution of combustion-related emissions to the atmospheric phosphorus budget. *Nature Geoscience, 8*(1), 48-54. https://doi.org/10.1038/ngeo2324

Wang, R., Goll, D., Balkanski, Y., Hauglustaine, D., Boucher, O., Ciais, P., et al. (2017). Global forest carbon uptake due to nitrogen and phosphorus deposition from 1850 to 2100. *Global Change Biology, 23*(11), 4854-4872.

Wang, Y. P., Houlton, B. Z., & Field, C. B. (2007). A model of biogeochemical cycles of carbon, nitrogen, and phosphorus including symbiotic nitrogen fixation and phosphatase production. *Global Biogeochemical Cycles, 21*(1). https://doi.org/10.1029/2006GB002797

Wang, Y. P., Law, R., & Pak, B. (2010). A global model of carbon, nitrogen and phosphorus cycles for the terrestrial biosphere. *Biogeosciences, 7*(7), 2261-2282.

Wieder, W. R., Cleveland, C. C., Smith, W. K., & Todd-Brown, K. (2015). Future productivity and carbon storage limited by terrestrial nutrient availability. *Nature Geoscience, 8*, 441. https://doi.org/10.1038/ngeo2413

Yang, X., Post, W. M., Thornton, P. E., & Jain, A. (2013). The distribution of soil phosphorus for global biogeochemical modeling. *Biogeosciences, 10*(4), 2525-2537. https://doi.org/10.5194/bg-10-2525-2013

Yang, X., Post, W. M., Thornton, P. E., & Jain, A. K. (2014a). Global Gridded Soil Phosphorus Distribution Maps at 0.5-degree Resolution. In: ORNL Distributed Active Archive Center.

Yang, X., Ricciuto, D. M., Thornton, P. E., Shi, X., Xu, M., Hoffman, F., & Norby, R. J. (2019). The effects of phosphorus cycle dynamics on carbon sources and sinks in the Amazon region: a modeling study using ELM v1. *Journal of Geophysical Research: Biogeosciences, 0*(ja). https://doi.org/10.1029/2019JG005082

Yang, X., Thornton, P., Ricciuto, D., & Post, W. (2014b). The role of phosphorus dynamics in tropical forests–a modeling study using CLM-CNP. *Biogeosciences, 11*(6), 1667-1681.

Yang, X., Thornton, P. E., Ricciuto, D. M., & Hoffman, F. M. (2016). Phosphorus feedbacks constraining tropical ecosystem responses to changes in atmospheric CO2 and climate. *Geophysical Research Letters, 43*(13), 7205-7214. https://doi.org/10.1002/2016GL069241

Yang, X., Wittig, V., Jain, A. K., & Post, W. (2009). Integration of nitrogen cycle dynamics into the Integrated Science Assessment Model for the study of terrestrial ecosystem responses to global change. *Global Biogeochemical Cycles, 23*(4). https://doi.org/10.1029/2009GB003474

Zaehle, S., & Dalmonech, D. (2011). Carbon–nitrogen interactions on land at global scales: current understanding in modelling climate biosphere feedbacks. *Current Opinion in Environmental Sustainability, 3*(5), 311-320. https://doi.org/https://doi.org/10.1016/j.cosust.2011.08.008

Zaehle, S., Friend, A. D., Friedlingstein, P., Dentener, F., Peylin, P., & Schulz, M. (2010). Carbon and nitrogen cycle dynamics in the O-CN land surface model: 2. Role of the nitrogen cycle in the historical terrestrial carbon balance. *Global Biogeochemical Cycles, 24*(1). https://doi.org/10.1029/2009gb003522

Zhang, Q., Wang, Y. P., Matear, R. J., Pitman, A. J., & Dai, Y. J. (2014). Nitrogen and phosphorous limitations significantly reduce future allowable CO2 emissions. *Geophysical Research Letters, 41*(2), 632-637. https://doi.org/10.1002/2013GL058352

Zhang, Q., Wang, Y. P., Pitman, A. J., & Dai, Y. J. (2011). Limitations of nitrogen and phosphorous on the terrestrial carbon uptake in the 20th century. *Geophysical Research Letters, 38*(22). https://doi.org/10.1029/2011GL049244

Chapter 4 Phosphorus limitation on the CO_2 fertilization effect in tropical forests as informed by a coupled biogeochemical model

Abstract

Tropical forests store more than half of the world's terrestrial carbon (C) pool and account for one-third of global net primary productivity (NPP). With their significant contribution to the global C cycle, tropical forests maintain a critical negative feedback to climate warming through the CO_2 fertilization effect. Many terrestrial biosphere models (TBMs) estimate increased productivity in tropical forests throughout the 21st century due to the CO_2 fertilization. However, phosphorus (P) limitation on vegetation photosynthesis and productivity have not been considered by most current TBMs. Here, we used a process-based Dynamic Land Ecosystem Model with coupled C-N-P dynamics (DLEM-CNP) to examine how P limitation has affected C fluxes of tropical rainforests during 1860-2018. Our model results showed that consideration of the P cycle reduced the CO_2 fertilization effect on tropical rainforests gross primary production (GPP) by 25% and 45%, NPP by 25% and 46%, and net ecosystem production (NEP) by 28% and 41% relative to CN-only and C-only models. During the period from the 1860s to the 2010s, the DLEM-CNP estimated that for per unit area, the tropical rainforest GPP increased by 17 %, Ra increased by 18%, NPP increased by 16 %, Rh increased by 13%, and NEP increased by 121%, respectively. Additionally, factorial experiments with DLEM-CNP showed that the enhanced GPP and NPP benefiting from the CO_2 fertilization effect (1.9 and 1.0 Pg C year^{-1}) had been offset by deforestation (-2.9 and -1.4 Pg C year^{-1}) from the 1860s to the 2010s. Our study highlights the importance of P limitation on the C cycle and the weakened CO_2 fertilization effect as a result of the P limitation in tropical forests.

1. Introduction

Tropical forests store about 72% of global forest biomass carbon (C) (Pan et al., 2011) and account for about one-third of global net primary productivity (NPP) (Field et al., 1998). As essential C reservoirs in the Earth system, tropical forests maintain a critical negative feedback to climate warming by slowing the rate of increasing CO_2 concentration in the atmosphere. The CO_2 fertilization effect that increases CO_2 concentrations in leaves enhances plants' capacity in fixing carbon through photosynthesis and has been considered as a primary mechanism that maintains and enhances tropical forest productivity (Schimel et al., 2015). In recent decades, however, tropical forests are suffering from the combination of deforestation (Pan et al., 2011), increases in temperature and frequent droughts as well as nutrient limitation (Liu et al., 2017; Yang et al., 2018), which have reduced their ability to respond to the rising CO_2 concentration (Cox et al., 2013; Mitchard, 2018). Given their importance in mitigating climate warming, an accurate estimation of C uptake in the tropical forests and its temporal variations is critical for designing effective climate mitigation policies or implementing management activities.

Both field and satellite observations (De Kauwe et al., 2016; Kolby Smith et al., 2016; Norby et al., 2005; Norby et al., 1999) and model simulations (Friedlingstein et al., 2019; Thornton et al., 2007) have shown the CO_2 fertilization effect supports a critical negative feedback to climate change, particularly in the tropics (Ciais et al., 2013; Schimel et al., 2015). Multiple lines of evidence suggest that the CO_2 fertilization effect on the global land ecosystems has substantial contributions from tropical forests (Liu et al., 2019; Lloyd, 1999; Schimel et al., 2015). However, uncertainties of this effect still exist, which limit our capacity to understand and predict tropical forest response to climate changes. For example, Free-air CO_2 enrichment (FACE) experiments that observe the CO_2 fertilization effect have been primarily conducted in temperate forests (Norby

& Zak, 2011) but have not been conducted in tropical forests so far (Cernusak et al., 2013; Hofhansl et al., 2016; Jiang et al., 2020). Tropical forests are subject to very different environmental conditions from temperate forests, especially soil nutrient availability, leading to potentially different responses to rising atmospheric CO_2. FACE experiments in temperate areas indicated that soil nutrient availability, particularly nitrogen (N), limits the magnitude of forest productivity increase (Norby et al., 2010). It is noteworthy that N limitation on productivity mostly occurs in temperate and boreal forests, whereas phosphorus (P) limitation has been primarily observed in tropical forests (Hofhansl et al., 2016; Vitousek et al., 2010; Walker & Syers, 1976; Wang et al., 2020a). The increasing CO_2 fertilization effect on the tropical forests simulated by terrestrial biosphere models (TBMs) has been questioned due to the missed P cycle representation (Cox et al., 2013; Huntingford et al., 2013). Meanwhile, the CO_2 fertilization effect on vegetation photosynthesis has been weakened in recent decades, partially attributable to nutrient limitations (Wang et al., 2020b).

Available P is crucial to maintain tropical forest structure and functions, affecting many key processes, including photosynthesis, respiration, decomposition, etc., (Vitousek, 2004). Phosphorus limitation on primary productivity is recognized to be widespread in tropical forests because of the long-term weathering of parent material P in the warm and humid climate conditions (Davidson et al., 2004; Tanner et al., 1998; Turner et al., 2018; Vitousek et al., 2010). Due to the importance of the P cycle to tropical forests, an increasing number of TBMs have started to include P dynamics and impacts on vegetation growth (Thornton et al., 2007; Zaehle & Friend, 2010). Recent progress in developing the quantitative frameworks in TBMs to represent the P cycle has been achieved, such as the Community Land Model (CLM -CNP) (Yang et al., 2014b), CABLE-CNP (Wang et al., 2007), Organizing Carbon and Hydrology In Dynamic Ecosystems

(ORCHIDEE) (Goll et al., 2017), and DLEM-CNP (Wang et al., 2020c). However, there are divergences in model structures and the simulated ecosystem dynamics. For example, TBMs differ in their assumptions on how nutrient limitation controls productivity and C allocation and their representation of soil P acquisition mechanisms (Fleischer et al., 2019).

Most TBMs represent tropical rainforests as one plant function type (PFT), i.e., the tropical broadleaf evergreen forest. This single PFT has a uniform set of parameters, which do not account for variations in space and, thus, inadequately represent its spatial heterogeneity (Castanho et al., 2013). In most TBMs, the parameter of V_{cmax25} (the maximum carboxylation rate at 25˚C), one of the most important parameters controlling photosynthesis processes (Bonan et al., 2012; Farquhar et al., 1980; Pan et al., 2014), is usually prescribed as a constant for a specific PFT based on field measurements or empirical relationships with plant properties (Bonan et al., 2012; Kattge et al., 2009; Walker et al., 2014). However, field data showed that V_{cmax25} is highly variable even for the same PFT (He et al., 2019; Kattge et al., 2009; Walker et al., 2014). This is particularly true for tropical rainforests because there are significant differences in soil properties and species composition (Fyllas et al., 2009; Quesada et al., 2010). Castanho et al. (2013) demonstrated that using single values for V_{cmax} in the tropical forests constrained the simulation accuracy in a dynamic vegetation model. V_{cmax} was found to be the most important property determining the modeled spatial variation of aboveground NPP. Therefore, it is necessary to represent the spatial variations of this critical parameter in tropical rainforests in TBMs for improving the accuracy of the simulated C cycle.

Building upon a previous study (Chapter 3 in this study), we partitioned the tropical rainforests into four tropical rainforest groups assigned with different V_{cmax25}. We used the improved Dynamic Land Ecosystem Model (DLEM-CNP) to 1) examine the P limitation on CO_2

fertilization effect in tropical forests comparing with C, C-N model; 2) estimate the spatial and temporal patterns of C fluxes in tropical rainforests with integrated C-N-P cycles during 1860 to 2018; and 3) explore the different factors' impacts with the CO_2 fertilization effect in the tropical rainforests, including climate, atmospheric N deposition, deforestation, and soil P during the historical period from 1860 to 2018.

2. Methods

2.1. Tropical Rainforests Subdivision

In this study, tropical forests were defined as the tropical evergreen broadleaf forests residing between the Tropic of Cancer and the Tropic of Capricorn (Fu et al., 2018). The Amazon rainforests are the most extensive tropical rainforests, while other tropical rainforests reside in western and central Africa, western India, Southeast Asia and the Pacific Islands, and Australia. We obtained site-level tropical forest NPP from the synthesized data of primary forests compiled by Clark et al. (2003). We excluded sites without longitude and latitude information. NPP values were averaged for the sites with the same longitude and latitude information. Finally, we obtained 13 tropical rainforest sites with NPP data and geographic coordinates. We calibrated the V_{cmax25} parameter at each site for the DLEM-CNP model based on their NPP values. A summary of site information can be found in Appendix 2, Table S2-1.

K-means clustering (MacQueen, 1967) is a method commonly used to automatically partition a data set into *k* groups. It proceeds by selecting *k* initial cluster centers and then iteratively refining them. The algorithm converges when there is no further change in assignment of instances to clusters. We selected five types of environmental factors to conduct the K-means clustering, including climate conditions (annual precipitation, the standard deviation of inter-annual precipitation, annual mean temperature, annual maximum temperature, annual minimum

temperature, and solar radiation), geospatial information (longitude, latitude), soil texture information from Harmonized World Soil Database (Wieder, 2014), parent P content from Global Gridded Soil Phosphorus Distribution Maps (Yang et al., 2014a), and elevation data from Global 30 Arc-Second Elevation product (GTOPO30, https://lta.cr.usgs.gov/GTOPO30). We used k-means clustering to partition the 13 tropical rainforest sites into four groups (Figure S2-1, S2-2). Finally, we calculated the Euclidean distance of these environmental factors of each grid of tropical evergreen broadleaf forest (TrEBF) to the four groups centers, grouping TrEBF into four subdivisions based on the closest group center (Figure 4-1).

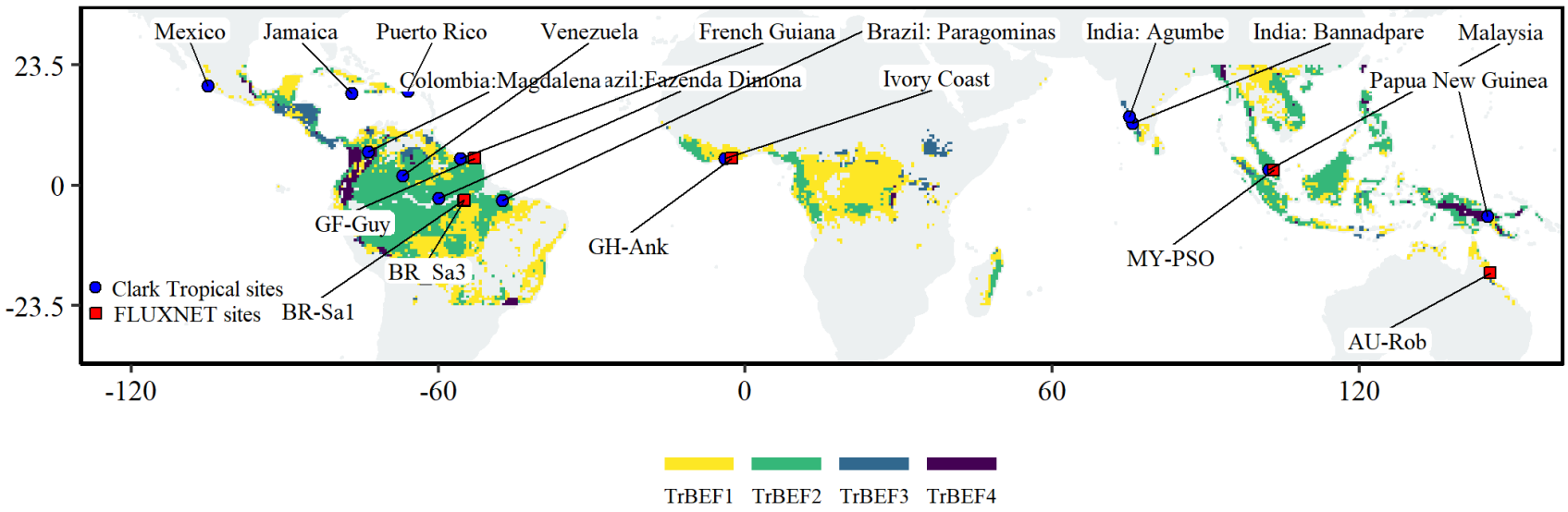

Figure 4- 1 Map of global tropical rainforests with four subdivisions (TrBEF1-4) and the location of 13 tropical forest sites from Clark et al. (2001) and six FLUXNET sites used in this study.

2.2. Model Description

The Dynamic Land Ecosystem Model-CNP (DLEM-CNP) is a highly integrated process-based terrestrial biosphere model, includes N and P controls on vegetation and soil biogeochemical processes (Figure 2-2). DLEM-CNP has a major advantage of representing the interactive co-limitation of N and P on vegetation C assimilation (Wang et al., 2020c).

2.3. Input Data

The model input datasets include climate conditions (daily mean temperature, maximum temperature, and minimum temperature, daily precipitation, and solar radiation), atmospheric CO_2 concentrations, annual land cover, and land use (LCLU) maps, nitrogen deposition, soil properties (parent P content, texture, pH, and bulk density), and topographical information (e.g., elevation, slope, and aspect). The climate conditions at the spatial resolution of 0.5°x 0.5° latitude/longitude from 1860 to 2018 were obtained from the CRU-JRA55 climate data from the 2019 Global Carbon Budget Project (Friedlingstein et al., 2019). Atmospheric CO_2 concentrations from 1860 to 2018 were obtained from the National Oceanic and Atmospheric Administration (NOAA). Atmospheric N deposition data were from the N_2O Model Intercomparison Project (NMIP) (Tian et al., 2018). The potential vegetation map was constructed with Synergetic Land Cover Product (SYNMAP; (Jung et al., 2006)). LULC data was from LUH2-GCB2019 data, which used the most recent HYDE–FAO release and was applied in the 2019 Global Carbon Budget Project (Friedlingstein et al., 2019). Soil physical properties were taken from ISRIC-WISE Harmonized Global Soil Profile Data Set (Batjes, 2009). Parent P content data was obtained from Global Gridded Soil Phosphorus Distribution Maps (Yang et al., 2014a). The elevation, slope, and aspect were derived from the Global 30 Arc-Second Elevation product (GTOPO30; https://lta.cr.usgs.gov/GTOPO30).

2.4. Field Observation Data for Model evaluation

FLUXNET data is a standard TBMs benchmark (Friend et al., 2007). We selected six FLUXNET sites in tropical areas with the vegetation type of evergreen broadleaf forests (BR-Sa3, BR-Sa1, MY-PSO, GF-Guy, GH-Ank, AU-Rob, Figure 4-1) for model validation and performance evaluation. Daily gross primary production (GPP) from the Daytime partitioning method (Pastorello et al., 2020) was used to evaluate DLEM-CNP performance. In order to identify the effects of the representation of P-related processes in DLEM-CNP, we also simulated the site-level GPP using the DLEM-CN model for comparison purposes.

2.5. Model simulation experiments

DLEM-CNP simulations include three steps: (1) an equilibrium run driven by the first 20-year mean climate (1860–1879) to develop the initial conditions for ecosystem C, N, P, and water pools, (2) a spin-up simulation of 30 years before 1860 to eliminate noise caused by the simulation shift from the equilibrium simulation mode to the transient simulation mode, and (3) a transient simulation using input data sets from 1860-2018 to generate simulation results. First, the DLEM-C (without N and P limitations, which was executed with the same model code without N and P limitations on photosynthesis or decomposition), DLEM-CN (without P limitation, assuming P saturation), DLEM-CNP (with N and P limitations) were driven by contemporary CO_2 from 1860-2018 to examine the effects of nutrients limitation on the CO_2 fertilization effect. To simulate the effects of individual environmental factors on C fluxes, we use DLEM-CNP to implement six numerical experiments (S0 to S5) (Table 4-1). The S0 is baseline run with cycled input data in 1860. The S1 experiment included the temporal variations of all time-varying driving forces and represent the model's "best estimate" of ecosystem dynamics. The combined effect of all environmental factors was calculated as S1 - S0. The individual effects of deforestation (DEF),

atmospheric CO_2 (CO_2), N deposition (NDEP), and climate (CLIM) were calculated as S1 - S2, S1 - S3, S1 - S4, and S1- S5, respectively.

Table 4- 1 Simulation protocol with the Dynamic Land Ecosystem Model

Experiments	CLIM	CO_2	NDEP	DEF
S0	1860	1860	1860	1860
S1	1860-2018	1860-2018	1860-2018	1860-2018
S2	1860-2018	1860-2018	1860-2018	1860
S3	1860-2018	1860	1860-2018	1860-2018
S4	1860-2018	1860-2018	1860	1860-2018
S5	1860	1860-2018	1860-2018	1860-2018

Note: CLIM is climate; NDEP is N deposition; CO_2 is atmospheric CO_2; and DEF is deforestation.

2.6. Path analysis model

To quantify the direct and indirect effects of CO_2 and climate with NPP, P uptake, and available P, path analysis model (PAM) was applied in this study. Path analysis model is a multivariate quantitative statistical technique and belongs to the structural equation model. Compared to common statistical methods such as simple or multiple regressions, it is capable of quantifying the complex and dynamic relationships among multiple dependent and independent variables, and it allows to separate the direct and indirect effects of the explanatory variable on the response variable (Alwin & Hauser, 1975; Hoyle, 1995; You et al., 2020). Before performing PAM, a conceptual model needs to be established based on prior knowledge of the empirical relationships between variables. In this study, we developed a conceptual model by specifying the relationship between CO_2, climate, NPP, P uptake, and available P while considering the interactions between these factors. In this study, PAM was conducted in R using the "lavaan" package (Rosseel, 2012), and all variables were standardized before analysis.

3. Results

3.1. Model validation using FLUXNET GPP

To evaluate our tropical rainforests subdivision strategy, we simulated GPP at FLUXNET sites with uniform V_{cmax25} (41 μmol m^{-2} s^{-1}, averaged value of all the 13 sites) and varied V_{cmax25} from calibration (BR-Sa3, BR-Sa1: 48 μmol m^{-2} s^{-1}; GF-Guy, MY-PSO, AU-Rob: 35 μmol m^{-2} s^{-1}; GH-Ank: 45 μmol m^{-2} s^{-1}), respectively, for subdivided TrEBFs (Figure 4-2). Field observations showed that average daily GPP tended to be higher in the Amazon region (BR-Sa3, BR-Sa1, GF-Guy) with an average of 10.5 g C m^{-2} d^{-1}. The simulated daily GPP with the average V_{cmax25} showed less variation among FLUXNET sites. In comparison, the simulations with subdivided TrEBF and assigned different V_{cmax25} were able to catch the tendency that higher daily GPP for the Amazon sites than the sites in Southeast Asia and Africa (Figure 4-2). This tendency is consistent with observations. Comparison with the site-level observations of all the selected FLUXNET sites showed that simulation with varied V_{cmax25} improved simulation accuracy with the root mean squared error (RMSE) decreasing from 2.19 to 0.53 g C m^{-2} d^{-1}.

The ability of the DLEM-CNP to reproduce the observed daily and seasonal cycles of GPP at the six FLUXNET sites was demonstrated in Figure 4-2. Generally, the DLEM-CNP performed well with respect to R^2 and RMSE for all sites. The model captured the pattern of the observed daily and seasonal cycle of carbon fluxes via the representation of the P effects on photosynthesis. Incorporating the P cycle lowered the model-simulated GPP compared to the DLEM-CN simulation and significantly increased its accuracy. This evaluation gives us the confidence that the DLEM-CNP is capable of simulating C fluxes in the tropical rainforests.

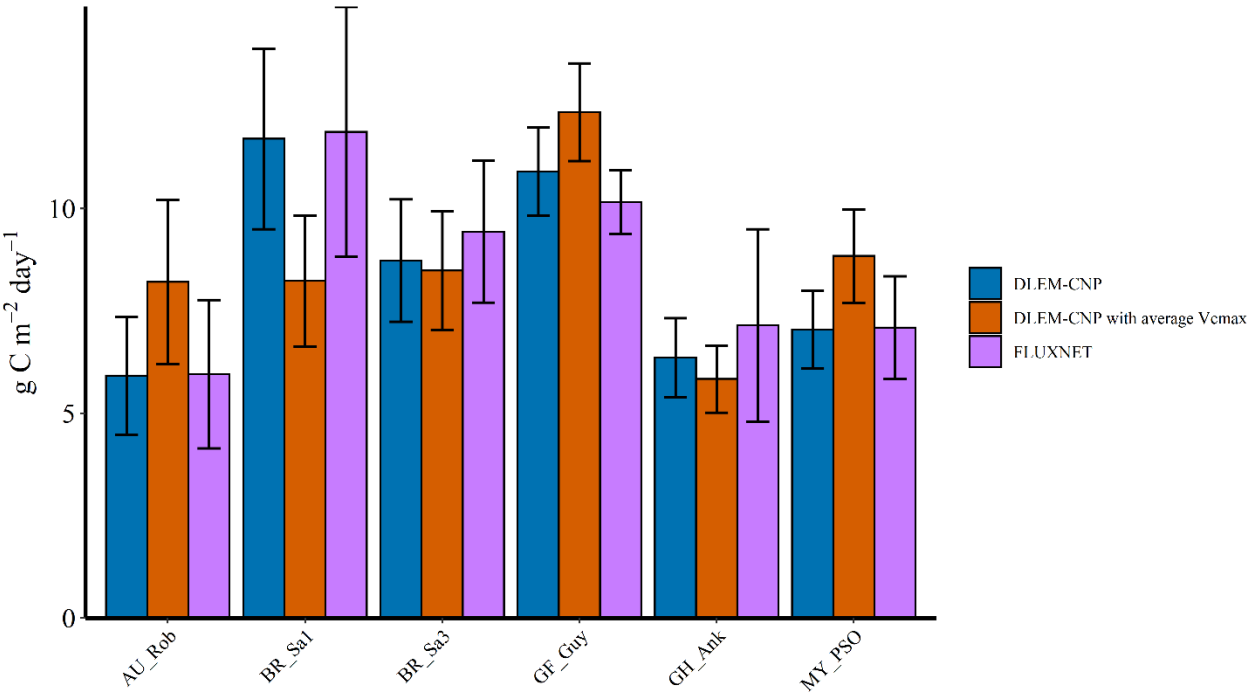

Figure 4- 2 Comparison of the daily average GPP between observations at FLUXNET sites and model simulations. Model simulations are derived using the average $V_{cmax25,}$ and varied V_{cmax25} in the four subdivided TrEBFs zones, respectively

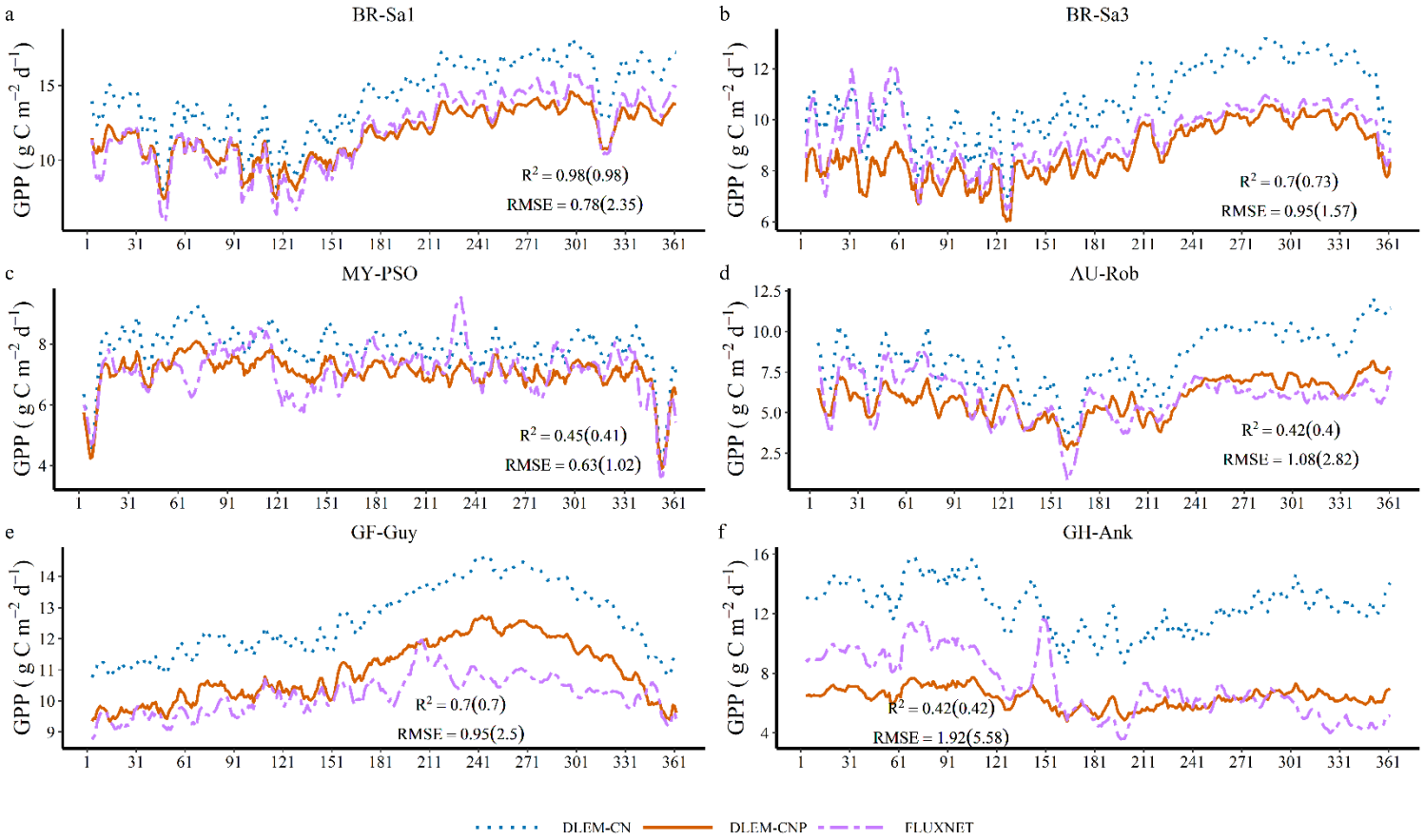

Figure 4- 3 Comparison of the daily gross primary productivity (GPP) between observations and model simulations at the selected FLUXNET sites. (a) BR-Sa1 (R^2: 0.98(0.98), RMSE: 0.78(2.35) g C m^{-2} d^{-1}), (b) BR-Sa3 (R^2: 0.70(0.73), RMSE: 0.95(1.57) g C m^{-2} d^{-1}), (c) MY-PSO (R^2: 0.45(0.41), RMSE: 0.63(1.02) g C m^{-2} d^{-1}) , (d) AU-Rob (R^2: 0.42(0.4), RMSE: 1.08(2.82) g C m^{-2} d^{-1}) , (e) GF-Guy (R^2: 0.70(0.70), RMSE: 0.95(2.50) g C m^{-2} d^{-1}), (f) GH-Ank (R^2: 0.42(0.42), RMSE: 1.92(5.58) g C m^{-2} d^{-1}). Statistics and plotted values are a 7-day running mean. RMSE is the root-mean-squared error. The DLEM-CN model corresponds to performances given within parenthesis.

3.2. Reduced CO_2 fertilization effects by nutrient limitation

Model simulations showed that increasing CO_2 led to a sustained increase of GPP, NPP, and NEP in the tropical rainforests due to the CO_2 fertilization effect in all DLEM-C, DLEM-CN, and DLEM-CNP simulations (Figure 4-4). The DLEM-CNP simulated lower GPP, NPP, and NEP increases (amount and rate) in the tropical rainforests than that of the DLEM-C and DLEM-CN models between 1860 and 2018, indicating that the P limitation reduced the response of GPP, NPP, and NEP to the CO_2 fertilization effect. For DLEM-C, DLEM-CN, and DLEM-CNP, the GPP increased by 21%, 18%, and 16%, autotrophic respiration (Ra) increased by 19%, 17%, and 15%, and NPP increased by 23%, 20%, and 18%, respectively, from 1860 to 2018 (Figure 4-4). During 1860-2018, the DLEM-C modeled GPP and NPP increased gradually by 0.10 and 0.06 Pg C $year^{-1}$, respectively. For DLEM-CN and DLEM-CNP, in contrast, the simulated GPP and NPP increased by 0.08 and 0.06 Pg C $year^{-1}$, and by 0.04 and 0.03 Pg C $year^{-1}$, respectively (Figure 4-4 g, h). Net ecosystem production (NEP) is the difference between NPP and heterotrophic respiration (Rh), and it represents the total amount of organic carbon in an ecosystem available for storage, export, or nonbiological oxidation through fire (Lovett et al., 2006). NEP is potentially controlled by N and P availability via C-N-P interactions on NPP and Rh. For DLEM-C, DLEM-CN, and DLEM-CNP, the simulated Rh grew by 18%, 16%, 14%, respectively. The NEP simulated by DLEM-CNP in 2018 was 0.95 Pg C $year^{-1}$ with considering N, P limitation, which was 51% lower than the simulated CO_2 fertilization effect on NEP without considering nutrient limitation (1.95 Pg C $year^{-1}$) and 25% lower than the DLEM-CN simulation only considering N limitation (1.27 Pg C $year^{-1}$) in 2018. The CO_2 fertilization effect was most pronounced after 1960 when the CO_2 concentration accelerated (Figure 4-4 f).

Comparison between DLEM-CNP and DLEM-C simulations suggested that considering N and P limitation lowered the CO_2 fertilization effect on GPP, NPP, and NEP by 45%, 46%, and 41%, respectively. Compared with the DLEM-CN, the DLEM-CNP lowered the CO_2 fertilization effect on GPP, NPP, and NEP by 25%, 25%, and 28%, respectively. In addition, simulation with the DLEM-CNP showed a larger spatial variation of CO_2 fertilization effect on GPP and NPP and a different spatial pattern of CO_2 fertilization effect on NEP compared to that without considering the P limitation. The DLEM-CNP simulated a higher than average CO_2 fertilization effect on GPP, NPP and NEP in the west Amazon, the eastern part of central Africa, and west Indonesia than other areas (Figure 4-5).

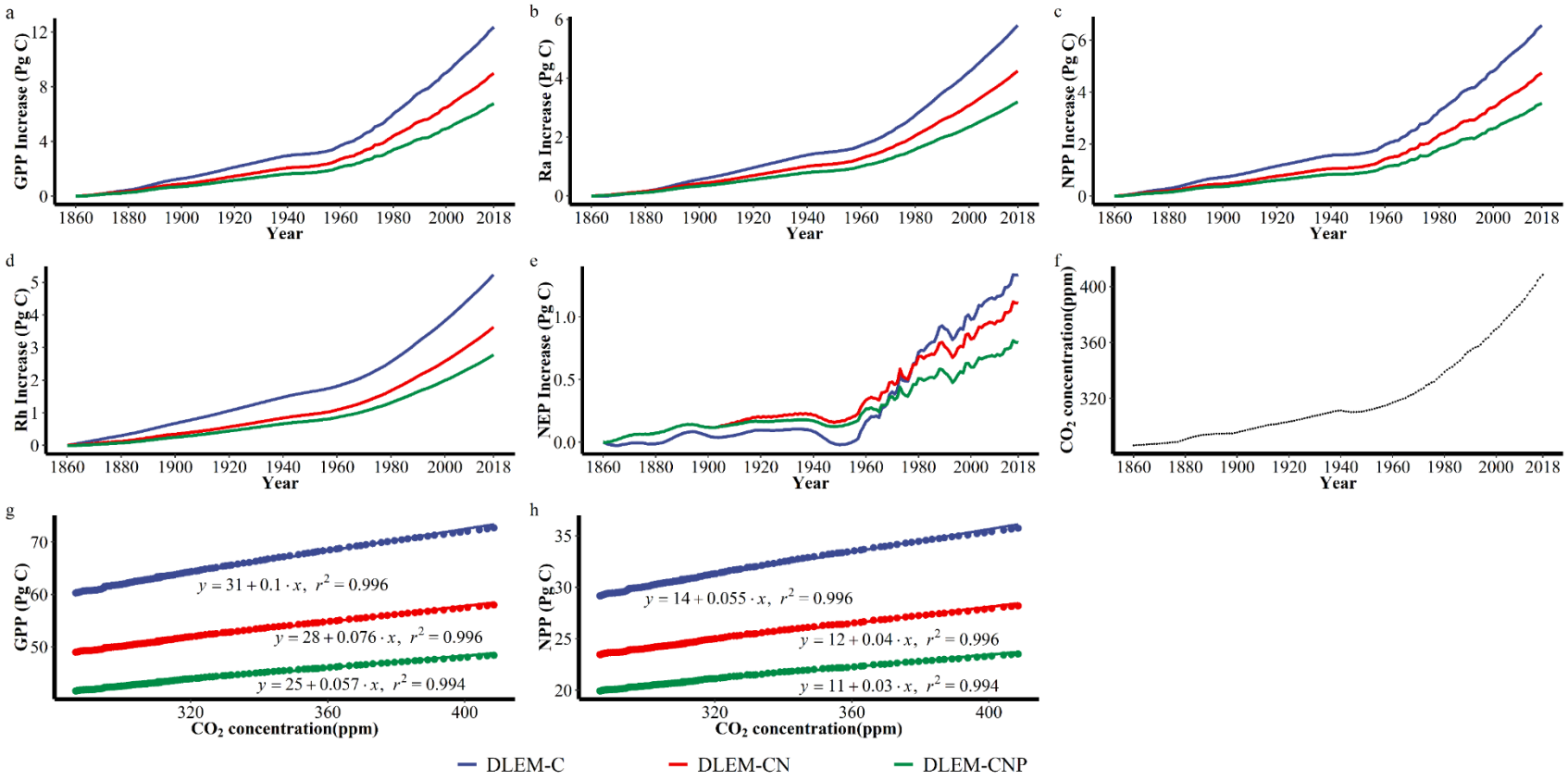

Figure 4- 4 The increased GPP (a), Ra (b), NPP (c), Rh (d), and annual NEP (e) in the tropical rainforest from 1860-2018 under historical atmospheric CO_2 concentration, simulated by DLEM-C (blue), DLEM-CN (red), and DLEM-CNP (green), respectively; figure (a,b,c,d,e) are with reference to 1860. Figure (f) is the CO_2 concentration from 1860-2018. Figures (g) and (h) are plots of annual GPP and NPP against CO_2 concentration

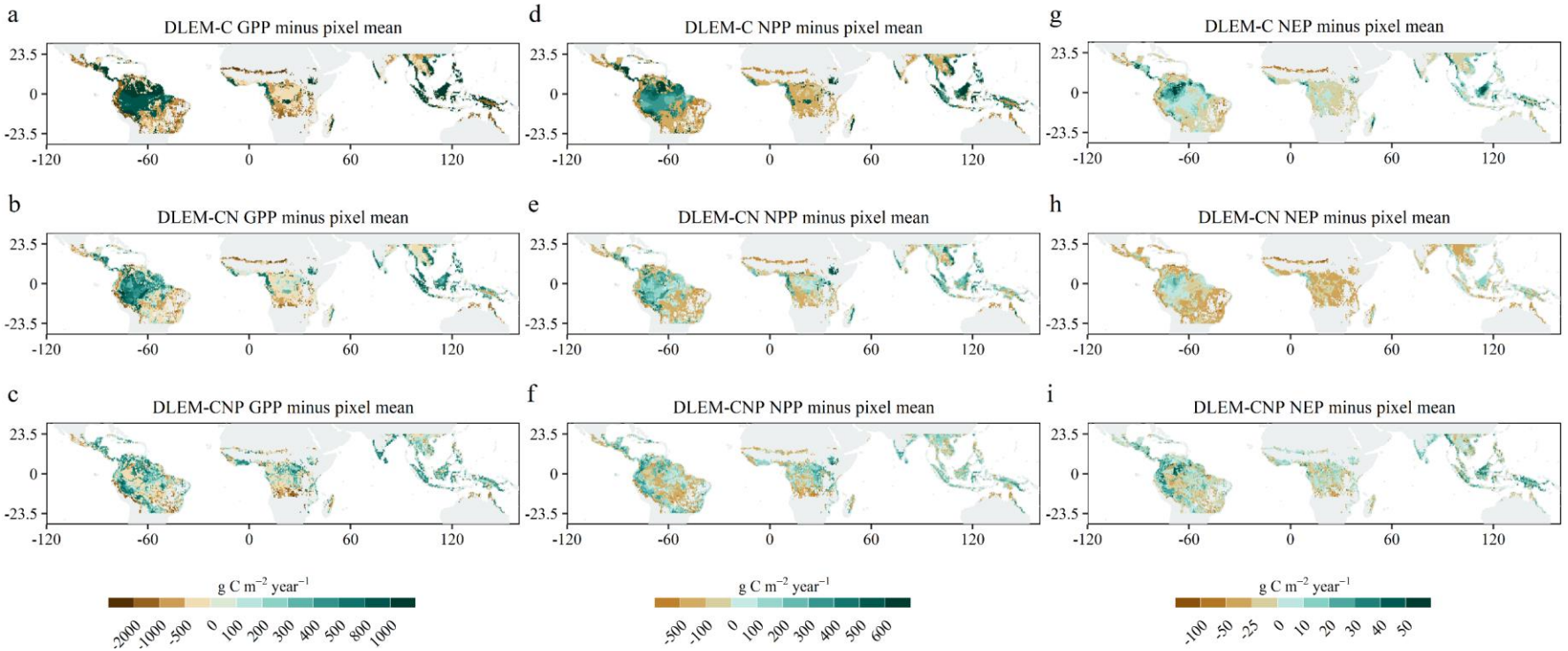

Figure 4- 5 Spatial pattern of the annual GPP, NPP, and NEP simulated by the DLEM-C (a, d, g), DLEM-CN (b, e, h), DLEM-CNP (c, f, i) in the 2010s with 1860-2018 atmospheric CO_2 concentration. To better show the spatial variations, we further processed the original GPP, NPP, and NEP values in each pixel by subtracting the mean GPP, NPP, and NEP of all tropical forest pixels of the corresponding simulation

3.3. The best estimate of temporal and spatial variability of tropical rainforest carbon fluxes

The DLEM-CNP was driven by time-varying environmental factors (climate, atmospheric CO_2 concentration, N deposition, and deforestation) in the simulation S1, which provided the "best estimate" of ecosystem carbon fluxes. Over the period 1860-2018, tropical rainforest areas declined at a rate of 1.7 million hectares per year (Figure 4-6). The area of tropical rainforests in the 1950s presented the largest decline of 35.5 Mha over the study period. However, the per unit area C fluxes of tropical rainforests had an increasing trend. From the 1860s to the 2010s, tropical rainforest GPP per unit area increased by 17% from 2464 $\pm$ 9 g C m^{-2} $year^{-1}$ to 2881 $\pm$ 25 g C m^{-2} $year^{-1}$; Ra per unit area increased by 18%; NPP per unit area increased by 16 % from 1192 $\pm$ 10 g C m^{-2} $year^{-1}$ to 1383 $\pm$ 21 g C m^{-2} $year^{-}$; Rh per unit area increased by 13%, and NEP per unit area increased by 121% from 29 $\pm$ 13 g C m^{-2} $year^{-1}$ to 65 $\pm$ 23 g C m^{-2} $year^{-1}$. The total NEP had an increasing trend of 0.003 Pg C $year^{-1}$ in the study period and reached the highest value of 0.82 $\pm$ 0.28 Pg C $year^{-1}$ in the 2000s and the 2010s. The NEP of the tropical rainforests has significant interannual variation related to ENSO cycles. In the El Niño years of 1998, 1987, 1983, 1969, 1958, 1941, 1931, 1926, 1871, the tropical rainforests had negative NEP, implying that the tropical rainforests are a C source during most El Niño years.

The DLEM-CNP simulation that was driven by time-varying environmental factors showed that NPP, GPP, and NEP of the tropical rainforests presented great spatial variability across the tropical regions (Figure 4-7). Higher GPP was located in the western and northern parts of the Amazonia, the eastern part of tropical Africa, and some areas in Southeast Asia and the Pacific Islands. By contrast, the lowest GPP was in the southeast part of the Amazonia and west tropical Africa. As NPP is closely related to GPP, the general spatial pattern of the tropical

rainforests NPP was similar to the spatial pattern of GPP. We found that the higher NEP was located in Central America, the western part of South America, the eastern part of tropical Africa, and Southeast Asia and the Pacific Islands, likely because of more parent P and less P limitation in these areas (Figure 4-7). The Mann-Kendall (MK) trend test showed that, in most tropical rainforests, GPP and NPP showed significant increasing trends (Figure 4-8). Also, the trends of GPP and NPP had similar spatial patterns. Although the Sen's slope of the NEP showed increasing trends in most tropical rainforests, there was no significant NEP trend (p-value $\geqslant 0.05$) in some areas of the central Amazonia, the edge of Africa rainforests, Southeast Asia and the Pacific Islands, Australia (Figure 4-8).

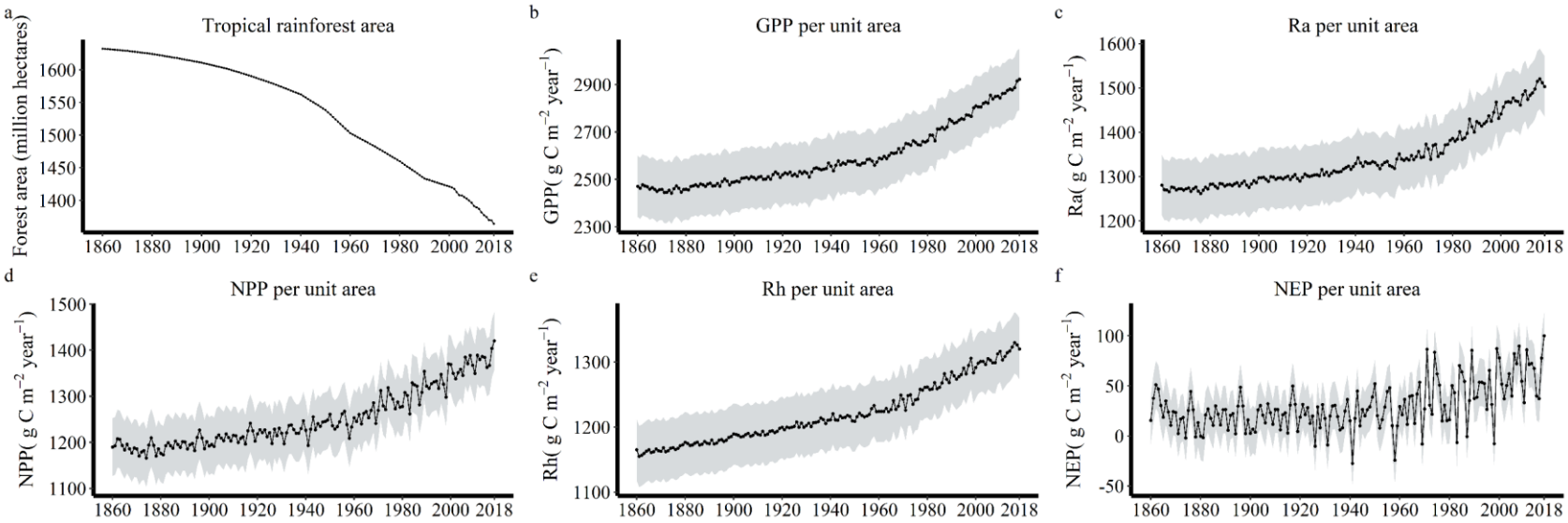

Figure 4- 6 Inter-annual variations of tropical forest GPP (a), NPP (b), and NEP (c; Pg C per year) for 1860–2018 simulated by the DLEM-CNP driven by all historical environmental factors. The shade means one standard deviation (sd) of each simulation.

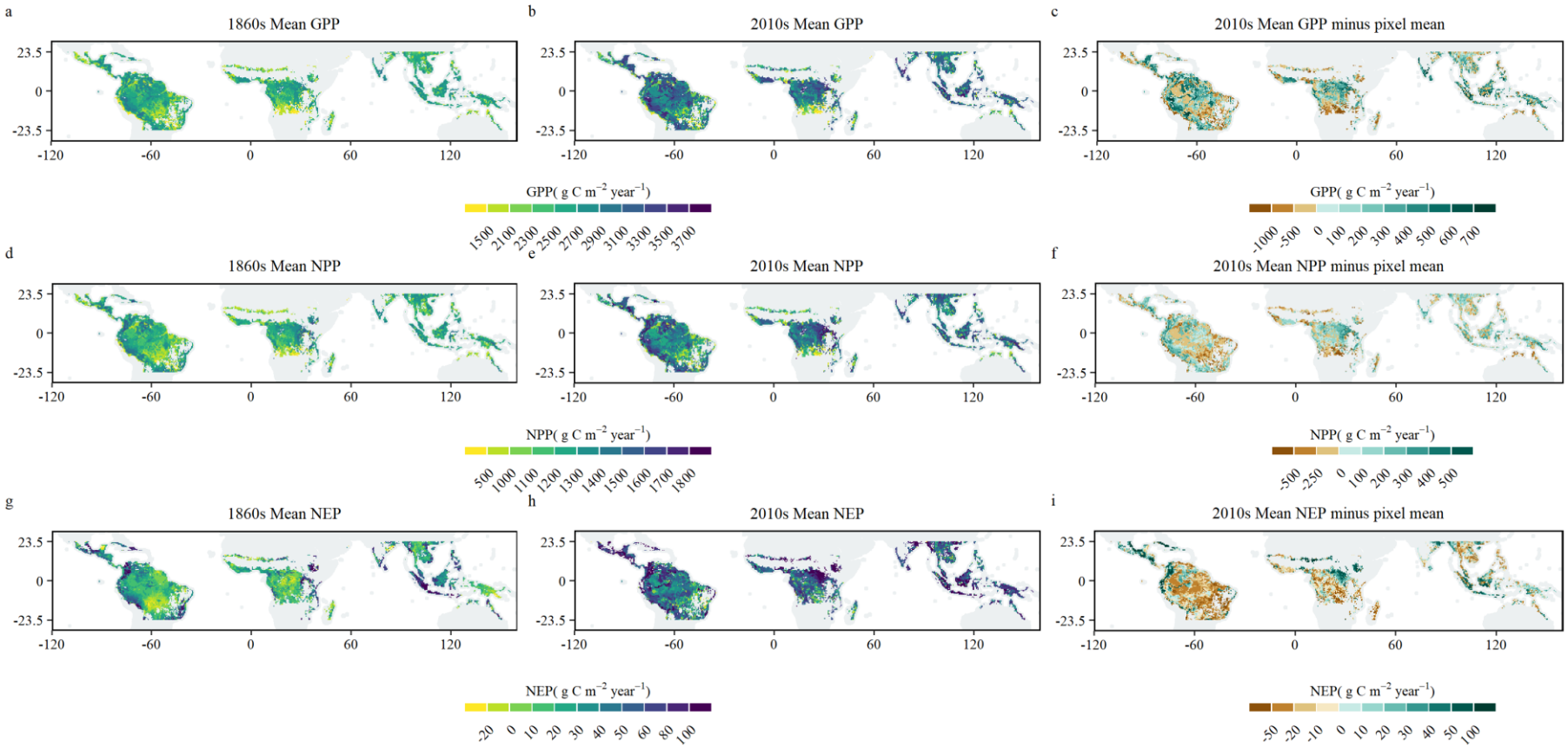

Figure 4- 7 Spatial distribution of the annual mean GPP (a; g C/m^2/year), NPP (c; g C/m^2/year), and NEP (e; g C/m^2/year) in the tropical forests in the 1860s and the 2010s simulated by the DLEM-CNP with all historical environmental forcing. In the 2010s, annual mean GPP minus the mean of all grids (e), the annual mean NPP minus the mean of all grids (f), and the annual mean NEP minus the mean of all grids (i).

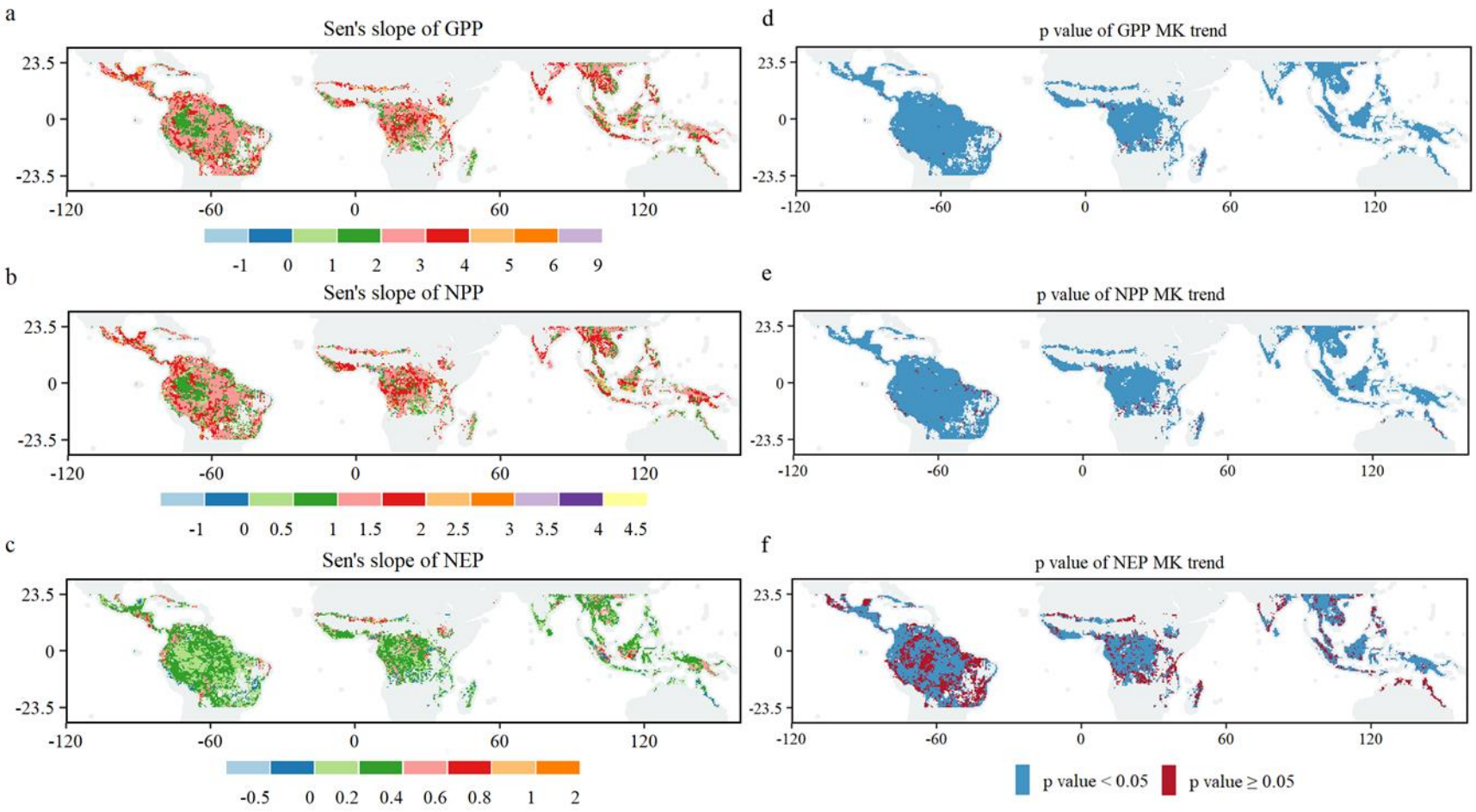

Figure 4- 8 Sen's slope of the tropical rainforests annual GPP (g C m^{-2} $year^{-1}$, a), NPP (g C m^{-2} $year^{-1}$, b), and NEP (g C m^{-2} $year^{-1}$, c) during 1860-2018. And area of the tropical forests with significant and insignificant trends in annual GPP (d), NPP (e), and NEP (f). The significance of the trend is estimated through the MK trend test, and p-values less than 0.05 are significant.

3.4. Various factors' impacts with the CO_2 fertilization effect in the tropical rainforests

We investigated different environmental factors' contribution to GPP and NPP comparing with the CO_2 fertilization effect during the period 1860-2018 (Figure 4-9). The CO_2 fertilization effect and deforestation were found to be the two most significant factors that influenced the long-term GPP and NPP trends. The combined effects of climate variability, atmospheric CO_2, N deposition, and deforestation resulted in decreased tropical rainforest GPP and NPP with varying degrees. Before the 1910s, the negative deforestation impacts offset the positive CO_2 fertilization effect, resulting in a slight GPP reduction of 0.20 Pg C $year^{-1}$. Between the 1920s and the 1960s, deforestation was the dominating factor of the significantly declined GPP (0.83 Pg C $year^{-1}$). The largest GPP reduction (1.56 Pg C $year^{-1}$) occurred in the 1960s. After the 1960s, the CO_2 fertilization effect largely stimulated GPP increase, leading to the increased tropical rainforest GPP. During the1860s to the 1910s, NPP had a slight increase of 0.0019 Pg C $year^{-1}$ due to the combined effect of environmental factors. Then the NPP shows a similar pattern with GPP from the 1920s to the 2010s.

Compared with atmospheric CO_2 and deforestation, climate and N deposition had a small effect on the simulated GPP and NPP throughout the study period. Climate presented diverged impacts on GPP and NPP in some periods. For example, in the 1990s, 2000s, and 2010s, climate increased GPP by 0.13, 0.44, and 0.59 Pg C $year^{-1}$ but reduced NPP by 0.15, 0.06, and 0.09 Pg C $year^{-1}$. The GPP and NPP increase by N deposition was relatively stable after the 2000s as a result of a relatively stable level in the N deposition input (Figure S2-3).

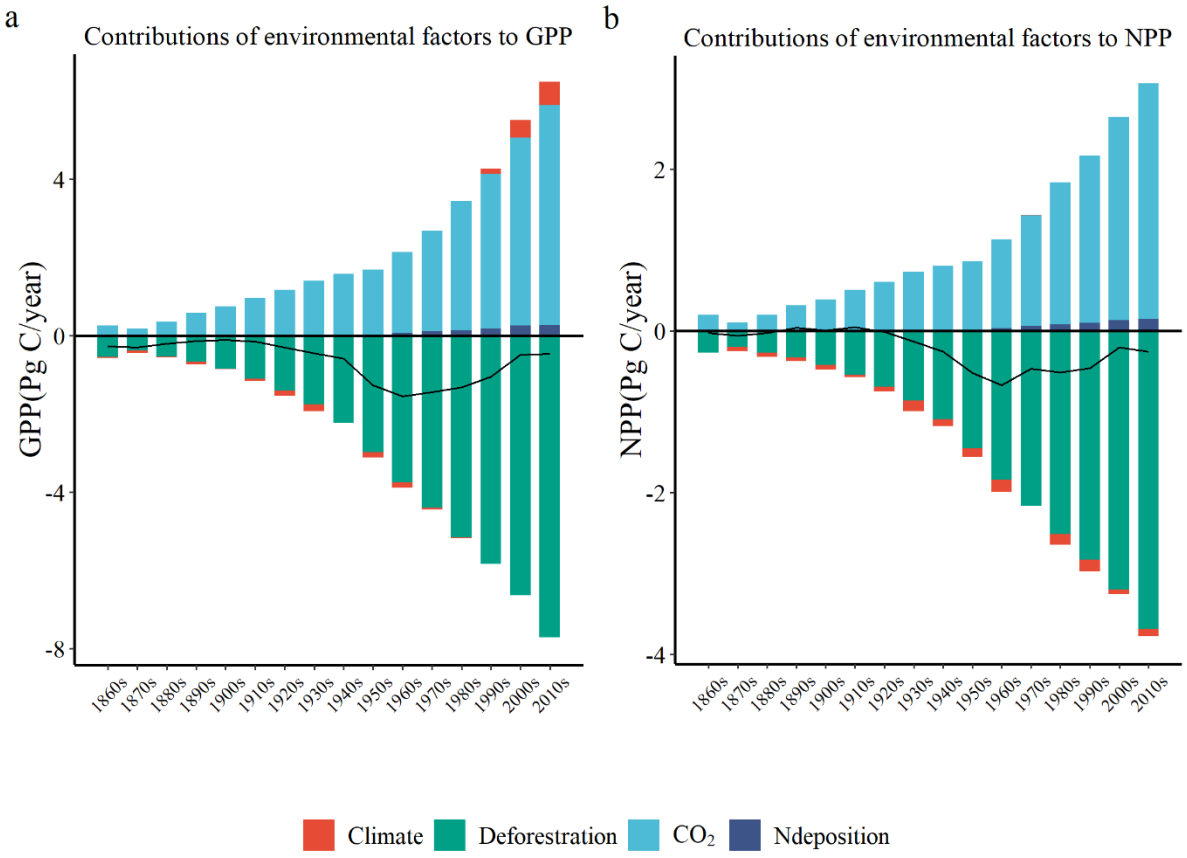

Figure 4- 9 Changes in tropical rainforests decadal GPP (a) and NPP (b) contributed by multiple environmental factors, including climate variability (Climate), atmospheric CO_2 (CO_2), atmospheric N deposition (N deposition), and deforestation during 1860–2018 simulated by the DLEM-CNP. Contributions of environmental factors were estimated by the difference between simulation scenarios (Table 4-1). Black lines represent the combined effects of all the driving factors(S1-S0).

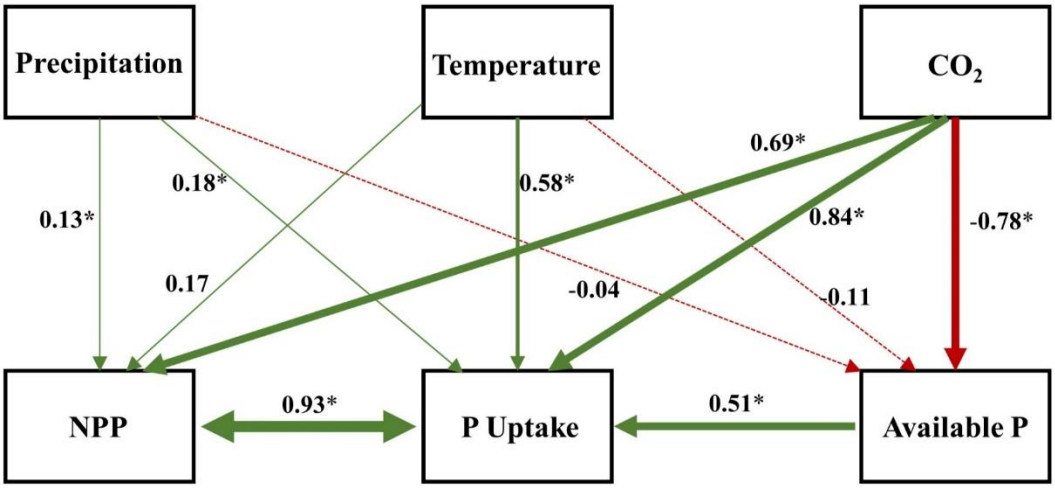

Figure 4- 10 Structural equation model of NPP interactions with P uptake, available P, precipitation, temperature, and CO_2. Numbers adjacent to arrows in the diagram are standardized path coefficients indicating the magnitude of the influence between factors, and the significance level is indicated by * ($p < 0.05$). The width of arrows is proportional to the strength of standardized path coefficients, and the green and red colors indicate positive and negative effects, respectively.

PAM was used to quantify the direct and indirect effects of CO_2 and climate with NPP, P uptake, and available P. As shown in Figure 4-10, annual mean precipitation and temperature had a small positive effect on NPP, while the CO_2 concentration had a major influence on NPP increase, with a direct effect of 0.69, indicating that the CO_2 fertilization effect is the most significant factor enhancing tropical rainforests NPP. The NPP showed a significantly positive correlation with plant P uptake, with a correlation coefficient of 0.93, suggesting that an increase in NPP was accompanied by increasing plant P uptake as more P is needed for plants to support C fixation. Meanwhile, the available P in soil also significantly promoted plant P uptake, with a direct positive effect of 0.51. However, the CO_2 concentration showed a significantly negative effect on the available P in the soil, with a direct effect of -0.78, indicating that under the increased CO_2 condition, soil available P may damp the CO_2 fertilization effect. In addition, precipitation and temperature have negative effects on available P, but not significantly.

4. Discussion

4.1 Spatial heterogeneity of the simulated GPP and NPP

Simulations of the DLEM-CNP showed considerable spatial variations in annual GPP and NPP compared to the simulations of the DLEM-C and had a different spatial pattern compared to the DLEM-CN (Figure 4-5). The GPP and NPP simulated by the DLEM-CNP showed a decreasing gradient from west to east across the Amazonia (Figure 4-5), which is consistent with field observations. In the Amazon basin, field observations have demonstrated the spatial variation of forest aboveground wood productivity (Malhi et al., 2004) and NPP (Aragão et al., 2009; Malhi et al., 2009). These studies showed that Amazon forests in the west tend to have higher productivity, while those in the east and central Amazon are slower growing with lower NPP (Baker et al., 2004; Malhi et al., 2004; Quesada et al., 2012). A number of mechanisms have been discussed in the existing literature about the productivity gradient in the Amazon region, such as climate, soil physical and chemical properties, soil nutrient limitations, and species composition (Castanho et al., 2013; Fauset et al., 2019; Fyllas et al., 2009; Malhi, 2012; Mercado et al., 2011; Quesada et al., 2012). However, the underlying mechanisms are still not well understood. In the DELM-CNP simulation, we showed that this productivity gradient in the Amazon region is related to P limitation and soil P availability.

Beyond the Amazon region, the DLEM-CNP simulated GPP and NPP do not show significant differences between different continents. Some field studies indicated that tropical rainforest productivity might vary between different continents (Banin et al., 2014; Lewis et al., 2013). However, there have been too few systematic cross-continental comparisons of tropical rainforest productivity to draw a clear conclusion, so more studies for cross-continental comparisons of tropical rainforests are still needed.

4.2 Phosphorus limitation on the CO_2 fertilization effect

Elevated CO_2 concentration increasing photosynthesis is undisputed (Lloyd & Farquhar, 1996), and aboveground biomass growth is perhaps the most obvious manifestation of the CO_2 fertilization effect on trees in many field experiments (Norby et al., 2005). However, questions have arisen concerning the CO_2 fertilization effect will be constrained by nutrient cycling. Nutrients, primarily N and P, control or limit the plant responses to the CO_2 fertilization effect has been long recognized (Norby et al., 2010; Terrer et al., 2019; Thornton et al., 2007; Wieder et al., 2015). Our results showed that P limitation reduced the CO_2 effects on GPP and NPP in the tropical rainforests (Figure 4-4 and 4-7), which was consistent with the simulation of the planned AmazonFACE experiment (Fleischer et al., 2019). Their simulation showed that NPP response to 15-year elevated CO_2 (+200 ppm) was 35%, 29%, 9% for the C, CN, and CNP models, respectively. Fleischer et al. (2019) showed that the CO_2 fertilization effect on GPP and NPP showed the fastest declined in the CNP models due to P limitation. Several modeling studies also demonstrated that coupling P dynamics into TBMs could reduce the CO_2 fertilization impacts on terrestrial C uptake in the Amazon basin and other tropical regions (Goll et al., 2012; Wang et al., 2010; Yang et al., 2019; Yang et al., 2016; Zhang et al., 2011). Additionally, McMurtrie et al. (2008) reported that plant growth at low nutrient availability consistently reduces the percentage growth response to elevated CO_2. This pattern was shown in field experiments of many tropical tree species (Cernusak et al., 2011; Winter et al., 2001; Winter et al., 2000). These results supported our findings that the GPP and NPP increase rates reduced when considering P limitation. In our results, from 1860 to 2018, the differences in GPP and NPP between DLEM-C, DLEM-CN, and DLEM-CNP increased over time, indicating that P limitation on CO_2 fertilization effect increased gradually.

The overall picture from the PAM also indicates that under the increased CO_2 condition, P becomes more limiting because more P is needed for plant growth, but soil available P may decrease and constrain the demanded P uptake. Despite the fact that total productivity increased under elevated CO_2, the increase is constrained by P availability in tropical forests where antecedent soil P availability is low (Terrer et al., 2019).

4.3 Comparison of DLEM-CNP simulated terrestrial C fluxes with other estimates

Bottom-up estimates of C stocks and fluxes in tropical forests based on inventory data and long-term field observations provide a good opportunity to compare with model results. Malhi (2010) estimated that the intact tropical rainforest represents a carbon sink of 0.82 ± 0.11 Pg C $year^{-1}$ during 1987 – 1997 based on the analysis of Lewis et al. (2009) and the forest areas in each continent. For the same period, our simulation of NEP was 0.60 ± 0.35 Pg C $year^{-1}$, which is comparable with Malhi's estimate. Hubau et al. (2020) suggested that the C sink in structurally intact old-growth tropical forests in the pan-tropics is between 0.16–1.52 Pg C $year^{-1}$ for 1980–1990, 0.88–1.63 Pg C $year^{-1}$for 1990–2000, 0.70–1.25 Pg C $year^{-1}$ for 2000–2010 and 0.25–1.18 Pg C $year^{-1}$ for 2010–2015. DLEM-CNP simulated NEP for the same periods are 0.60 ± 0.45, 0.64 ± 0.40, 0.77 ± 0.27 and 0.77 ± 0.30 Pg C $year^{-1}$, respectively. All the DLEM-CNP simulated values fall within the inventory-based statistic intervals.

4.4 Nutrient and drought effects on tropical rainforests under the rising CO_2

Our results showed that the NEP of the tropical rainforests has significant interannual variation related to ENSO cycles. In the El Niño years of 1998, 1987, 1983, 1969, 1958, 1941, 1931, 1926, 1871, the tropical rainforests had negative NEP (Figure 4-6f), implying that the tropical rainforests are a C source during most El Niño years. The tropical rainforest C sink declines during El Niño years, which has been recognized in previous studies. Tian et al. (1998)

suggested that El Niño events with hot and dry weather over much of the Amazon region drove a shift of Amazon forest carbon balance from a C sink towards a net C source. Bastos et al. (2018) investigated the 2015/2016 El Niño impacts on the terrestrial carbon cycle with TBMs simulations and reported that decreased vegetation productivity, rather than increased respiration, dominated the net biome productivity anomalies in response to ENSO throughout the tropics. Our findings are consistent with these studies (Figure S2-5). Furthermore, the interaction between drought and plant nutrient availability may intensify the decrease in productivity during a drought event by reducing soil nutrient availability. The reduced soil moisture content during droughts can limit available nutrients for plant to use by decreasing microbial activity (Lévesque et al., 2016; Schimel et al., 2007) and reducing nutrient diffusion and mass flow in the soil (Lambers et al., 2008). However, drought impact on nutrient uptake is species- and nutrient-dependent (Lévesque et al., 2016). Additionally, the low nutrient availability could change plant traits such as reduced shoot-to-root ratios in order to decrease the susceptibility to drought (Ewers et al., 2000) as well as alleviate soil drought as a result of P limitation reducing water consumption during wet periods (Goll et al., 2018).

Furthermore, increasing CO_2 concentration could enhance the resistance of tropical rainforests to drought. Plants could improve water use efficiency (WUE) with rising CO_2, thereby fixing more C through photosynthesis for a given amount of transpiration (Battipaglia et al., 2013). This could help maintain more soil water owing to reduced transpiration, which could prolong transpiration and, therefore, photosynthesis for a longer time between rain events (Holtum & Winter, 2010; Leuzinger & KÖRner, 2007). Such water savings mechanism could benefit microbial activity and nutrient provision and maintain turgor pressure in meristem tissues for cell expansion (Boyer, 1968; Eamus, 1991), and, thereby, promote plant growth.

4.5 Uncertainty and future work

Uncertainties in this study mainly come from TrEBF subdivision classification and model parameterization and simulation. First, although grouping TrEBF into four subdivisions and assigning different V_{cmax25} enhanced the model performance of GPP simulation at FLUXNET sites, this is an exploratory approach for improving the representation of biophysical parameters of tropical rainforests. With a small number (13) of tropical rainforest information sites, the k-mean cluster approach to cluster grids into 4 group centers may introduce bias, which could increase uncertainty to our subdivision classification. Thus, in the future, we need to expand the numbers of tropical rainforest sites with reliable data to help create a better TrEBF subdivision. Second, our simulations did not consider the fire effect, which is a critical factor in the tropical rainforest C cycle. Carbon emissions from tropical forest fires can have a large impact on C flux interannual variability (Cochrane, 2003). For instance, forest fires in Amazonia released an average of 454 Tg of CO_2 per year from 2003 to 2015, with large spikes during the dry years in 2005, 2007, and 2015 (Brando et al., 2019; Silva et al., 2018). During the 1997–1998 El Niño event, large areas of forests burned in Indonesia, releasing an estimated 0.81–2.57 Pg C to the atmosphere (Brando et al., 2019; Page et al., 2002). In addition, fires resulted in increased tree mortality, changed ecosystem productivity, and release large amounts of C to the atmosphere as dead trees decompose (Barlow et al., 2003). Third, the DLEM-CNP lacks detailed representations of the tree mortality events caused by wind and insects. Without accurately accounting for tree mortality, the C sink in tropical rainforests may be overestimated (Trumbore et al., 2015). Finally, while the current model includes a detailed treatment of many components of the terrestrial P cycle, it lacks details on the biochemical mineralization process, a process that plants and microbes can produce phosphatase enzymes to mineralize P in soil organic matter but without mineralizing C and N (Mcgill & Cole,

1981). This may result in an underestimation of the available P and cause stronger P limitation on plant productivity (Wang et al., 2007).

5. Conclusions

This study represents the first attempt to assess the long-term historical changes of GPP, NPP, and NEP with a fully coupled C-N-P ecosystem model for pantropical rainforests under elevated CO_2, using a TrEBF subdivision classification scheme. The simulations with subdivided TrEBF and different V_{cmax25} improved model accuracy. And results showed that the P limitation reduced the responses of GPP, NPP, and NEP in the tropical rainforests to the CO_2 fertilization effect. The combined effects of N and P limitation reduced the CO_2 fertilization effect on the GPP, NPP, and NEP by 45%, 46%, and 41%, respectively. Compared with the DLEM-CN, the DLEM-CNP lowered the GPP increase by 25%, the NPP increase by 25%, and the NEP increase 28% from 1860 to 2018. DLEM-CNP simulations showed large spatial variations of ecosystem GPP and NPP associated with the P limitation on photosynthesis. Using DLEM-CNP under historical environmental conditions during 1860-2018, we estimated that tropical rainforests GPP increased by 17 % from 2464 $\pm$ 9 g C m^{-2} $year^{-1}$ to 2881 $\pm$ 25 g C m^{-2} $year^{-1}$, NPP increased by 16 % from 1192 $\pm$ 10 g C m^{-2} $year^{-1}$ to 1383 $\pm$ 21 g C m^{-2} $year^{-1}$, and NEP increased by 121% from 29 $\pm$ 13 g C m^{-2} $year^{-1}$ to 65 $\pm$ 23 g C m^{-2} $year^{-1}$ from the 1860s to the 2010s. In the 2000s and 2010s, the NEP reached the highest amount of 0.82 $\pm$ 0.28 Pg C $year^{-1}$. The CO_2 fertilization effect was the most prominent factor in enhancing the GPP and NPP, while deforestation was the primary factor accounting for GPP and NPP reduction and offset the CO_2 fertilization effect by 147% and 135% from the 1860s to the 2010s. Our study implicated that the carbon sink potential of tropical rainforests is likely reduced due to the continuous increase in deforestation as well as the P-limitation and highlighted the importance of P limitation on the C cycle in tropical rainforests.

References

Aragão, L. E. O. C., Malhi, Y., Metcalfe, D. B., Silva-Espejo, J. E., Jiménez, E., Navarrete, D., et al. (2009). Above- and below-ground net primary productivity across ten Amazonian forests on contrasting soils. *Biogeosciences, 6*(12), 2759-2778. https://doi.org/10.5194/bg-6-2759-2009

Baker, T. R., Phillips, O. L., Malhi, Y., Almeida, S., Arroyo, L., Fiore, A. D., et al. (2004). Increasing biomass in Amazonian forest plots. *Philosophical Transactions of the Royal Society of London. Series B: Biological Sciences, 359*(1443), 353-365. https://doi.org/10.1098/rstb.2003.1422

Banin, L., Lewis, S. L., Lopez-Gonzalez, G., Baker, T. R., Quesada, C. A., Chao, K.-J., et al. (2014). Tropical forest wood production: a cross-continental comparison. *Journal of Ecology, 102*(4), 1025-1037. https://doi.org/10.1111/1365-2745.12263

Barlow, J., Peres, C. A., Lagan, B. O., & Haugaasen, T. (2003). Large tree mortality and the decline of forest biomass following Amazonian wildfires. *Ecology letters, 6*(1), 6-8. https://doi.org/10.1046/j.1461-0248.2003.00394.x

Bastos, A., Friedlingstein, P., Sitch, S., Chen, C., Mialon, A., Wigneron, J.-P., et al. (2018). Impact of the 2015/2016 El Niño on the terrestrial carbon cycle constrained by bottom-up and top-down approaches. *Philosophical Transactions of the Royal Society B: Biological Sciences, 373*(1760), 20170304. https://doi.org/10.1098/rstb.2017.0304

Batjes, N. H. (2009). *ISRIC-WISE - Global Soil Profile Data (ver. 3.1)*. Retrieved from: https://doi.org/10.1594/PANGAEA.858569

Battipaglia, G., Saurer, M., Cherubini, P., Calfapietra, C., McCarthy, H. R., Norby, R. J., & Francesca Cotrufo, M. (2013). Elevated CO2 increases tree-level intrinsic water use efficiency: insights from carbon and oxygen isotope analyses in tree rings across three forest FACE sites. *New Phytologist, 197*(2), 544-554. https://doi.org/https://doi.org/10.1111/nph.12044

Bonan, G. B., Oleson, K. W., Fisher, R. A., Lasslop, G., & Reichstein, M. (2012). Reconciling leaf physiological traits and canopy flux data: Use of the TRY and FLUXNET databases in the Community Land Model version 4. *Journal of Geophysical Research: Biogeosciences, 117*(G2). https://doi.org/10.1029/2011JG001913

Boyer, J. S. (1968). Relationship of Water Potential to Growth of Leaves. *Plant physiology, 43*(7), 1056-1062. https://doi.org/10.1104/pp.43.7.1056

Brando, P. M., Paolucci, L., Ummenhofer, C. C., Ordway, E. M., Hartmann, H., Cattau, M. E., et al. (2019). Droughts, Wildfires, and Forest Carbon Cycling: A Pantropical Synthesis. *Annual Review of Earth and Planetary Sciences, 47*(1), 555-581. https://doi.org/10.1146/annurev-earth-082517-010235

Castanho, A. D. A., Coe, M. T., Costa, M. H., Malhi, Y., Galbraith, D., & Quesada, C. A. (2013). Improving simulated Amazon forest biomass and productivity by including spatial variation in biophysical parameters. *Biogeosciences, 10*(4), 2255-2272. https://doi.org/10.5194/bg-10-2255-2013

Cernusak, L. A., Winter, K., Dalling, J. W., Holtum, J. A. M., Jaramillo, C., Körner, C., et al. (2013). Tropical forest responses to increasing atmospheric CO2: current knowledge and opportunities for future research. *Functional plant biology, 40*(6), 531-551. https://doi.org/https://doi.org/10.1071/FP12309

Cernusak, L. A., Winter, K., Martínez, C., Correa, E., Aranda, J., Garcia, M., et al. (2011). Responses of Legume Versus Nonlegume Tropical Tree Seedlings to Elevated CO₂ Concentration. *Plant physiology, 157*(1), 372-385. https://doi.org/10.1104/pp.111.182436

Ciais, P., Sabine, C., Bala, G., Bopp, L., Brovkin, V., Canadell, J., et al. (2013). Carbon and other biogeochemical cycles. Climate change 2013: the physical science basis. Contribution of Working Group I to the Fifth Assessment Report of the Intergovernmental Panel on Climate Change. *Comput. Geom, 18*, 95-123.

Clark, D. A., Brown, S., Kicklighter, D. W., Chambers, J. Q., Thomlinson, J. R., Ni, J., & Holland, E. A. (2001). Net primary production in tropical forests: an evaluation and synthesis of existing field data. *Ecological applications, 11*(2), 371-384.

Clark, D. A., Piper, S. C., Keeling, C. D., & Clark, D. B. (2003). Tropical rain forest tree growth and atmospheric carbon dynamics linked to interannual temperature variation during 1984–2000. *Proceedings of the National Academy of Sciences, 100*(10), 5852. https://doi.org/10.1073/pnas.0935903100

Cochrane, M. A. (2003). Fire science for rainforests. *Nature, 421*(6926), 913-919. https://doi.org/10.1038/nature01437

Cox, P. M., Pearson, D., Booth, B. B., Friedlingstein, P., Huntingford, C., Jones, C. D., & Luke, C. M. (2013). Sensitivity of tropical carbon to climate change constrained by carbon dioxide variability. *Nature, 494*, 341. https://doi.org/10.1038/nature11882

Davidson, E. A., Reis de Carvalho, C. J., Vieira, I. C. G., Figueiredo, R. d. O., Moutinho, P., Yoko Ishida, F., et al. (2004). NITROGEN AND PHOSPHORUS LIMITATION OF BIOMASS GROWTH IN A TROPICAL SECONDARY FOREST. *Ecological applications, 14*(sp4), 150-163. https://doi.org/10.1890/01-6006

De Kauwe, M. G., Keenan, T. F., Medlyn, B. E., Prentice, I. C., & Terrer, C. (2016). Satellite based estimates underestimate the effect of CO2 fertilization on net primary productivity. *Nature Climate Change, 6*(10), 892-893. https://doi.org/10.1038/nclimate3105

Eamus, D. (1991). The interaction of rising CO2 and temperatures with water use efficiency. *Plant, Cell & Environment, 14*(8), 843-852. https://doi.org/https://doi.org/10.1111/j.1365-3040.1991.tb01447.x

Ewers, B. E., Oren, R., & Sperry, J. S. (2000). Influence of nutrient versus water supply on hydraulic architecture and water balance in Pinus taeda. *Plant, Cell & Environment, 23*(10), 1055-1066. https://doi.org/10.1046/j.1365-3040.2000.00625.x

Farquhar, G. D., von Caemmerer, S., & Berry, J. A. J. P. (1980). A biochemical model of photosynthetic CO2 assimilation in leaves of C3 species. *149*(1), 78-90. journal article. https://doi.org/10.1007/bf00386231

Fauset, S., Gloor, M., Fyllas, N. M., Phillips, O. L., Asner, G. P., Baker, T. R., et al. (2019). Individual-Based Modeling of Amazon Forests Suggests That Climate Controls Productivity While Traits Control Demography. *7*(83). Original Research. https://doi.org/10.3389/feart.2019.00083

Field, C. B., Behrenfeld, M. J., Randerson, J. T., & Falkowski, P. (1998). Primary Production of the Biosphere: Integrating Terrestrial and Oceanic Components. *Science, 281*(5374), 237-240. https://doi.org/10.1126/science.281.5374.237

Fleischer, K., Rammig, A., De Kauwe, M. G., Walker, A. P., Domingues, T. F., Fuchslueger, L., et al. (2019). Amazon forest response to CO2 fertilization dependent on plant phosphorus acquisition. *Nature Geoscience*. https://doi.org/10.1038/s41561-019-0404-9

Friedlingstein, P., Jones, M. W., O'Sullivan, M., Andrew, R. M., Hauck, J., Peters, G. P., et al. (2019). Global Carbon Budget 2019. *Earth Syst. Sci. Data, 11*(4), 1783-1838. https://doi.org/10.5194/essd-11-1783-2019

Friend, A. D., Arneth, A., Kiang, N. Y., Lomas, M., OgÉE, J., RÖDenbeck, C., et al. (2007). FLUXNET and modelling the global carbon cycle. *Global Change Biology, 13*(3), 610-633. https://doi.org/10.1111/j.1365-2486.2006.01223.x

Fu, Z., Gerken, T., Bromley, G., Araújo, A., Bonal, D., Burban, B., et al. (2018). The surface-atmosphere exchange of carbon dioxide in tropical rainforests: Sensitivity to environmental drivers and flux measurement methodology. *Agricultural and Forest Meteorology, 263*, 292-307. https://doi.org/https://doi.org/10.1016/j.agrformet.2018.09.001

Fyllas, N. M., Patino, S., Baker, T., Bielefeld Nardoto, G., Martinelli, L., Quesada, C., et al. (2009). Basin-wide variations in foliar properties of Amazonian forest: phylogeny, soils and climate. *6*, 2677-2708.

Goll, D., Joetzjer, E., Huang, M., & Ciais, P. (2018). Low Phosphorus Availability Decreases Susceptibility of Tropical Primary Productivity to Droughts. *Geophysical Research Letters, 45*(16), 8231-8240.

Goll, D., Vuichard, N., Maignan, F., Jornet-Puig, A., Sardans, J., Violette, A., et al. (2017). A representation of the phosphorus cycle for ORCHIDEE (revision 4520). *Geoscientific Model Development Discussions, 10*(10), 3745-3770.

Goll, D. S., Brovkin, V., Parida, B. R., Reick, C. H., Kattge, J., Reich, P. B., et al. (2012). Nutrient limitation reduces land carbon uptake in simulations with a model of combined

carbon, nitrogen and phosphorus cycling. *Biogeosciences, 9*(9), 3547-3569. https://doi.org/10.5194/bg-9-3547-2012

He, L., Chen, J. M., Liu, J., Zheng, T., Wang, R., Joiner, J., et al. (2019). Diverse photosynthetic capacity of global ecosystems mapped by satellite chlorophyll fluorescence measurements. *Remote sensing of Environment, 232*, 111344. https://doi.org/https://doi.org/10.1016/j.rse.2019.111344

Hofhansl, F., Andersen, K. M., Fleischer, K., Fuchslueger, L., Rammig, A., Schaap, K. J., et al. (2016). Amazon Forest Ecosystem Responses to Elevated Atmospheric CO2 and Alterations in Nutrient Availability: Filling the Gaps with Model-Experiment Integration. *Frontiers in Earth Science, 4*(19). Perspective. https://doi.org/10.3389/feart.2016.00019

Holtum, J. A. M., & Winter, K. (2010). Elevated CO_2 and forest vegetation: more a water issue than a carbon issue? *Functional plant biology, 37*(8), 694-702. https://doi.org/https://doi.org/10.1071/FP10001

Hubau, W., Lewis, S. L., Phillips, O. L., Affum-Baffoe, K., Beeckman, H., Cuní-Sanchez, A., et al. (2020). Asynchronous carbon sink saturation in African and Amazonian tropical forests. *Nature, 579*(7797), 80-87. https://doi.org/10.1038/s41586-020-2035-0

Huntingford, C., Zelazowski, P., Galbraith, D., Mercado, L. M., Sitch, S., Fisher, R., et al. (2013). Simulated resilience of tropical rainforests to CO2-induced climate change. *Nature Geoscience, 6*(4), 268-273. https://doi.org/10.1038/ngeo1741

Jiang, M., Medlyn, B. E., Drake, J. E., Duursma, R. A., Anderson, I. C., Barton, C. V. M., et al. (2020). The fate of carbon in a mature forest under carbon dioxide enrichment. *Nature, 580*(7802), 227-231. https://doi.org/10.1038/s41586-020-2128-9

Jung, M., Henkel, K., Herold, M., & Churkina, G. (2006). Exploiting synergies of global land cover products for carbon cycle modeling. *Remote sensing of Environment, 101*(4), 534-553. https://doi.org/10.1016/j.rse.2006.01.020

Kattge, J., Knorr, W., Raddatz, T., & Wirth, C. (2009). Quantifying photosynthetic capacity and its relationship to leaf nitrogen content for global-scale terrestrial biosphere models. *Global Change Biology, 15*(4), 976-991. https://doi.org/10.1111/j.1365-2486.2008.01744.x

Kolby Smith, W., Reed, S. C., Cleveland, C. C., Ballantyne, A. P., Anderegg, W. R. L., Wieder, W. R., et al. (2016). Large divergence of satellite and Earth system model estimates of global terrestrial CO2 fertilization. *Nature Climate Change, 6*(3), 306-310. https://doi.org/10.1038/nclimate2879

Lambers, H., Chapin III, F. S., & Pons, T. L. (2008). *Plant physiological ecology*: Springer Science & Business Media.

Leuzinger, S., & KÖRner, C. (2007). Water savings in mature deciduous forest trees under elevated CO2. *Global Change Biology, 13*(12), 2498-2508. https://doi.org/https://doi.org/10.1111/j.1365-2486.2007.01467.x

Lévesque, M., Walthert, L., & Weber, P. (2016). Soil nutrients influence growth response of temperate tree species to drought. *Journal of Ecology, 104*(2), 377-387. https://doi.org/10.1111/1365-2745.12519

Lewis, S. L., Lopez-Gonzalez, G., Sonké, B., Affum-Baffoe, K., Baker, T. R., Ojo, L. O., et al. (2009). Increasing carbon storage in intact African tropical forests. *Nature, 457*(7232), 1003-1006. https://doi.org/10.1038/nature07771

Lewis, S. L., Sonké, B., Sunderland, T., Begne, S. K., Lopez-Gonzalez, G., Heijden, G. M. F. v. d., et al. (2013). Above-ground biomass and structure of 260 African tropical forests. *Philosophical Transactions of the Royal Society B: Biological Sciences, 368*(1625), 20120295. https://doi.org/doi:10.1098/rstb.2012.0295

Liu, J., Bowman, K. W., Schimel, D. S., Parazoo, N. C., Jiang, Z., Lee, M., et al. (2017). Contrasting carbon cycle responses of the tropical continents to the 2015–2016 El Niño. *Science, 358*(6360), eaam5690. https://doi.org/10.1126/science.aam5690

Liu, Y., Piao, S., Gasser, T., Ciais, P., Yang, H., Wang, H., et al. (2019). Field-experiment constraints on the enhancement of the terrestrial carbon sink by CO2 fertilization. *Nature Geoscience*. https://doi.org/10.1038/s41561-019-0436-1

Lloyd, J. (1999). The CO2 dependence of photosynthesis, plant growth responses to elevated CO2 concentrations and their interaction with soil nutrient status, II. Temperate and boreal forest productivity and the combined effects of increasing CO2 concentrations and increased nitrogen deposition at a global scale. *Functional Ecology, 13*(4), 439-459. https://doi.org/10.1046/j.1365-2435.1999.00350.x

Lloyd, J., & Farquhar, G. D. (1996). The CO_2 Dependence of Photosynthesis, Plant Growth Responses to Elevated Atmospheric CO₂ Concentrations and Their Interaction with Soil Nutrient Status. I. General Principles and Forest Ecosystems. *Functional Ecology, 10*(1), 4-32. https://doi.org/10.2307/2390258

Lovett, G. M., Cole, J. J., & Pace, M. L. (2006). Is Net Ecosystem Production Equal to Ecosystem Carbon Accumulation? *Ecosystems, 9*(1), 152-155. https://doi.org/10.1007/s10021-005-0036-3

MacQueen, J. (1967, 1967). *Some methods for classification and analysis of multivariate observations.* Paper presented at the Proceedings of the Fifth Berkeley Symposium on Mathematical Statistics and Probability, Volume 1: Statistics, Berkeley, Calif.

Malhi, Y. (2010). The carbon balance of tropical forest regions, 1990–2005. *Current Opinion in Environmental Sustainability, 2*(4), 237-244. https://doi.org/https://doi.org/10.1016/j.cosust.2010.08.002

Malhi, Y. (2012). The productivity, metabolism and carbon cycle of tropical forest vegetation. *Journal of Ecology, 100*(1), 65-75. https://doi.org/10.1111/j.1365-2745.2011.01916.x. https://doi.org/https://doi.org/10.1111/j.1365-2745.2011.01916.x

Malhi, Y., AragÃO, L. E. O. C., Metcalfe, D. B., Paiva, R., Quesada, C. A., Almeida, S., et al. (2009). Comprehensive assessment of carbon productivity, allocation and storage in three Amazonian forests. *Global Change Biology, 15*(5), 1255-1274. https://doi.org/10.1111/j.1365-2486.2008.01780.x

Malhi, Y., Baker, T. R., Phillips, O. L., Almeida, S., Alvarez, E., Arroyo, L., et al. (2004). The above-ground coarse wood productivity of 104 Neotropical forest plots. *Global Change Biology, 10*(5), 563-591. https://doi.org/10.1111/j.1529-8817.2003.00778.x

Mcgill, W. B., & Cole, C. V. (1981). Comparative Aspects of Cycling of Organic C, N, S and P through Soil Organic-Matter. *Geoderma, 26*(4), 267-286. https://doi.org/Doi 10.1016/0016-7061(81)90024-0

McMurtrie, R. E., Norby, R. J., Medlyn, B. E., Dewar, R. C., Pepper, D. A., Reich, P. B., & Barton, C. V. M. (2008). Why is plant-growth response to elevated CO2 amplified when water is limiting, but reduced when nitrogen is limiting? A growth-optimisation hypothesis. *Functional plant biology, 35*(6), 521-534. https://doi.org/https://doi.org/10.1071/FP08128

Mercado, L. M., Patiño, S., Domingues, T. F., Fyllas, N. M., Weedon, G. P., Sitch, S., et al. (2011). Variations in Amazon forest productivity correlated with foliar nutrients and modelled rates of photosynthetic carbon supply. *Philosophical transactions of the Royal Society of London. Series B, Biological sciences, 366*(1582), 3316-3329. https://doi.org/10.1098/rstb.2011.0045

Mitchard, E. T. A. (2018). The tropical forest carbon cycle and climate change. *Nature, 559*(7715), 527-534. https://doi.org/10.1038/s41586-018-0300-2

Norby, R. J., DeLucia, E. H., Gielen, B., Calfapietra, C., Giardina, C. P., King, J. S., et al. (2005). Forest response to elevated CO_2 is conserved across a broad range of productivity. *Proceedings of the National Academy of Sciences of the United States of America, 102*(50), 18052-18056. https://doi.org/10.1073/pnas.0509478102

Norby, R. J., Warren, J. M., Iversen, C. M., Medlyn, B. E., & McMurtrie, R. E. (2010). CO_2 enhancement of forest productivity constrained by limited nitrogen availability. *Proceedings of the National Academy of Sciences, 107*(45), 19368-19373. https://doi.org/10.1073/pnas.1006463107

Norby, R. J., Wullschleger, S. D., Gunderson, C. A., Johnson, D. W., & Ceulemans, R. (1999). Tree responses to rising CO2 in field experiments: implications for the future forest. *Plant, Cell & Environment, 22*(6), 683-714. https://doi.org/10.1046/j.1365-3040.1999.00391.x. https://doi.org/https://doi.org/10.1046/j.1365-3040.1999.00391.x

Norby, R. J., & Zak, D. R. (2011). Ecological Lessons from Free-Air CO2 Enrichment (FACE) Experiments. *Annual Review of Ecology, Evolution, and Systematics, 42*(1), 181-203. https://doi.org/10.1146/annurev-ecolsys-102209-144647

Page, S. E., Siegert, F., Rieley, J. O., Boehm, H.-D. V., Jaya, A., & Limin, S. (2002). The amount of carbon released from peat and forest fires in Indonesia during 1997. *Nature, 420*(6911), 61-65. https://doi.org/10.1038/nature01131

Pan, S., Tian, H., Dangal, S. R., Ouyang, Z., Tao, B., Ren, W., et al. (2014). Modeling and monitoring terrestrial primary production in a changing global environment: toward a multiscale synthesis of observation and simulation. *Advances in Meteorology, 2014*.

Pan, Y., Birdsey, R. A., Fang, J., Houghton, R., Kauppi, P. E., Kurz, W. A., et al. (2011). A Large and Persistent Carbon Sink in the World's Forests. *Science, 333*(6045), 988. https://doi.org/10.1126/science.1201609

Pastorello, G., Trotta, C., Canfora, E., Chu, H., Christianson, D., Cheah, Y.-W., et al. (2020). The FLUXNET2015 dataset and the ONEFlux processing pipeline for eddy covariance data. *Scientific Data, 7*(1), 225. https://doi.org/10.1038/s41597-020-0534-3

Quesada, C. A., Lloyd, J., Schwarz, M., Patiño, S., Baker, T. R., Czimczik, C., et al. (2010). Variations in chemical and physical properties of Amazon forest soils in relation to their genesis. *Biogeosciences, 7*(5), 1515-1541. https://doi.org/10.5194/bg-7-1515-2010

Quesada, C. A., Phillips, O. L., Schwarz, M., Czimczik, C. I., Baker, T. R., Patiño, S., et al. (2012). Basin-wide variations in Amazon forest structure and function are mediated by both soils and climate. *Biogeosciences, 9*(6), 2203-2246. https://doi.org/10.5194/bg-9-2203-2012

Schimel, D., Stephens, B. B., & Fisher, J. B. (2015). Effect of increasing CO_2 on the terrestrial carbon cycle. *Proceedings of the National Academy of Sciences, 112*(2), 436-441. https://doi.org/10.1073/pnas.1407302112

Schimel, J., Balser, T. C., & Wallenstein, M. (2007). MICROBIAL STRESS-RESPONSE PHYSIOLOGY AND ITS IMPLICATIONS FOR ECOSYSTEM FUNCTION. *Ecology, 88*(6), 1386-1394. https://doi.org/10.1890/06-0219

Silva, C. V. J., Aragão, L. E. O. C., Barlow, J., Espirito-Santo, F., Young, P. J., Anderson, L. O., et al. (2018). Drought-induced Amazonian wildfires instigate a decadal-scale disruption of forest carbon dynamics. *Philosophical Transactions of the Royal Society B: Biological Sciences, 373*(1760), 20180043. https://doi.org/10.1098/rstb.2018.0043

Tanner, E. V. J., Vitousek, P. M., & Cuevas, E. (1998). EXPERIMENTAL INVESTIGATION OF NUTRIENT LIMITATION OF FOREST GROWTH ON WET TROPICAL MOUNTAINS. *Ecology, 79*(1), 10-22. https://doi.org/10.1890/0012-9658(1998)079[0010:EIONLO]2.0.CO;2

Terrer, C., Jackson, R. B., Prentice, I. C., Keenan, T. F., Kaiser, C., Vicca, S., et al. (2019). Nitrogen and phosphorus constrain the CO2 fertilization of global plant biomass. *Nature Climate Change, 9*(9), 684-689. https://doi.org/10.1038/s41558-019-0545-2

Thornton, P. E., Lamarque, J.-F., Rosenbloom, N. A., & Mahowald, N. M. (2007). Influence of carbon-nitrogen cycle coupling on land model response to CO2 fertilization and climate variability. *Global Biogeochemical Cycles, 21*(4). https://doi.org/10.1029/2006GB002868

Tian, H., Melillo, J. M., Kicklighter, D. W., McGuire, A. D., Helfrich, J. V. K., Moore, B., & Vörösmarty, C. J. (1998). Effect of interannual climate variability on carbon storage in Amazonian ecosystems. *Nature, 396*(6712), 664-667. https://doi.org/10.1038/25328

Tian, H., Yang, J., Lu, C., Xu, R., Canadell, J. G., Jackson, R. B., et al. (2018). The Global N2O Model Intercomparison Project. *Bulletin of the American Meteorological Society, 99*(6), 1231-1251. https://doi.org/10.1175/BAMS-D-17-0212.1

Trumbore, S., Brando, P., & Hartmann, H. (2015). Forest health and global change. *Science, 349*(6250), 814-818. https://doi.org/10.1126/science.aac6759

Turner, B. L., Brenes-Arguedas, T., & Condit, R. (2018). Pervasive phosphorus limitation of tree species but not communities in tropical forests. *Nature, 555*, 367. https://doi.org/10.1038/nature25789

Vitousek, P. M. (2004). *Nutrient cycling and limitation: Hawai'i as a model system*: Princeton University Press.

Vitousek, P. M., Porder, S., Houlton, B. Z., & Chadwick, O. A. (2010). Terrestrial phosphorus limitation: mechanisms, implications, and nitrogen–phosphorus interactions. *Ecological applications, 20*(1), 5-15.

Walker, A. P., Beckerman, A. P., Gu, L., Kattge, J., Cernusak, L. A., Domingues, T. F., et al. (2014). The relationship of leaf photosynthetic traits – Vcmax and Jmax – to leaf nitrogen, leaf phosphorus, and specific leaf area: a meta-analysis and modeling study. *Ecology and Evolution, 4*(16), 3218-3235. https://doi.org/10.1002/ece3.1173

Walker, T., & Syers, J. K. (1976). The fate of phosphorus during pedogenesis. *Geoderma, 15*(1), 1-19.

Wang, S., Zhang, Y., Ju, W., Chen, J. M., Ciais, P., Cescatti, A., et al. (2020a). Recent global decline of CO_2 fertilization effects on vegetation photosynthesis. *Science, 370*(6522), 1295-1300. https://doi.org/10.1126/science.abb7772

Wang, S., Zhang, Y., Ju, W., Chen, J. M., Ciais, P., Cescatti, A., et al. (2020b). Recent global decline of CO₂ fertilization effects on vegetation photosynthesis. *Science, 370*(6522), 1295-1300. https://doi.org/10.1126/science.abb7772

Wang, Y. P., Houlton, B. Z., & Field, C. B. (2007). A model of biogeochemical cycles of carbon, nitrogen, and phosphorus including symbiotic nitrogen fixation and phosphatase production. *Global Biogeochemical Cycles, 21*(1). https://doi.org/10.1029/2006GB002797

Wang, Y. P., Law, R., & Pak, B. (2010). A global model of carbon, nitrogen and phosphorus cycles for the terrestrial biosphere. *Biogeosciences, 7*(7), 2261-2282.

Wang, Z., Tian, H., Yang, J., Shi, H., Pan, S., Yao, Y., et al. (2020c). Coupling of Phosphorus Processes with Carbon and Nitrogen Cycles in the Dynamic Land Ecosystem Model: Model Structure, Parameterization and Evaluation in Tropical Forests. *Journal of Advances in Modeling Earth Systems, n/a*(n/a), e2020MS002123. https://doi.org/10.1029/2020MS002123

Wieder, W. (2014). Regridded Harmonized World Soil Database v1.2. In: ORNL Distributed Active Archive Center.

Wieder, W. R., Cleveland, C. C., Smith, W. K., & Todd-Brown, K. (2015). Future productivity and carbon storage limited by terrestrial nutrient availability. *Nature Geoscience, 8*, 441. https://doi.org/10.1038/ngeo2413

Winter, K., Aranda, J., Garcia, M., Virgo, A., & Paton, S. R. (2001). Effect of elevated CO2 and soil fertilization on whole-plant growth and water use in seedlings of a tropical pioneer tree, Ficus insipida Willd. *Flora, 196*(6), 458-464. https://doi.org/https://doi.org/10.1016/S0367-2530(17)30087-7

Winter, K., Garcia, M., Lovelock, C. E., Gottsberger, R., & Popp, M. (2000). Responses of model communities of two tropical tree species to elevated atmospheric CO2 : growth on unfertilized soil. *Flora, 195*(4), 289-302. https://doi.org/https://doi.org/10.1016/S0367-2530(17)30988-X

Yang, J., Tian, H., Pan, S., Chen, G., Zhang, B., & Dangal, S. (2018). Amazon drought and forest response: Largely reduced forest photosynthesis but slightly increased canopy greenness during the extreme drought of 2015/2016. *Glob Chang Biol, 24*(5), 1919-1934. https://doi.org/10.1111/gcb.14056

Yang, X., Post, W. M., Thornton, P. E., & Jain, A. K. (2014a). Global Gridded Soil Phosphorus Distribution Maps at 0.5-degree Resolution. In: ORNL Distributed Active Archive Center.

Yang, X., Ricciuto, D. M., Thornton, P. E., Shi, X., Xu, M., Hoffman, F., & Norby, R. J. (2019). The effects of phosphorus cycle dynamics on carbon sources and sinks in the Amazon region: a modeling study using ELM v1. *Journal of Geophysical Research: Biogeosciences, 0*(ja). https://doi.org/10.1029/2019JG005082

Yang, X., Thornton, P., Ricciuto, D., & Post, W. (2014b). The role of phosphorus dynamics in tropical forests–a modeling study using CLM-CNP. *Biogeosciences, 11*(6), 1667-1681.

Yang, X., Thornton, P. E., Ricciuto, D. M., & Hoffman, F. M. (2016). Phosphorus feedbacks constraining tropical ecosystem responses to changes in atmospheric CO2 and climate. *Geophysical Research Letters, 43*(13), 7205-7214. https://doi.org/10.1002/2016GL069241

Zaehle, S., & Friend, A. D. (2010). Carbon and nitrogen cycle dynamics in the O-CN land surface model: 1. Model description, site-scale evaluation, and sensitivity to parameter estimates. *Global Biogeochemical Cycles, 24*(1). https://doi.org/10.1029/2009GB003521

Zhang, Q., Wang, Y. P., Pitman, A. J., & Dai, Y. J. (2011). Limitations of nitrogen and phosphorous on the terrestrial carbon uptake in the 20th century. *Geophysical Research Letters, 38*(22). https://doi.org/10.1029/2011GL049244

Chapter 5 Future phosphorus availability and its effect on carbon sequestration in tropical regions

Abstract

Tropical terrestrial ecosystems play a significant role in the global carbon cycle because of the substantial amount of carbon assimilated through plant production. Using a C-N-P coupled terrestrial ecosystem model (DLEM-CNP), we investigate the potential effects of climate change and rising atmospheric CO_2 concentration on tropical terrestrial ecosystem gross primary production (GPP), net primary production (NPP), and carbon use efficiency (CUE) during 2020-2100. Results showed that the P limitation on the CO_2 fertilization effect reduced future tropical GPP and NPP. Under the SSP585 scenario, the CO_2 fertilization effect would reach plateaus and the tropical ecosystem's capability to respond to CO_2 increase would weaken after 2060. Under future environmental conditions during 2020-2100, DLEM-CNP estimated that under the SSP126 scenario, the tropical GPP, NPP, and CUE would slightly increase, with a substantially interannual variation. Under the SSP585 scenario, the tropical GPP and NPP would increase by 44% and 21% from 2020 to 2100, respectively, but the CUE would decrease 15% under the SSP585 scenario. The CO_2 fertilization effect is the dominant factor that would increase the future GPP and NPP in tropical ecosystems. The climate effect is the most significant factor that would decrease the CUE under both SSP126 and SSP585 scenarios.

1. Introduction

In the 21st century, the global atmospheric CO_2 concentration is predicted to keep increasing due to anthropogenic activities (IPCC, 2013). With a third of CO_2 emissions absorbed by global terrestrial ecosystems, the increase of atmospheric CO_2 is slowed down by terrestrial ecosystems (Friedlingstein et al., 2020). Among global terrestrial ecosystems, tropical forests and savannahs account for 60% gross primary production (GPP) (Beer et al., 2010). Therefore, tropical terrestrial ecosystems play a pivotal role in regulating the exchange of carbon (C) between land and the atmosphere. Yet, the magnitude and spatial pattern of the future tropical C sink at elevated CO_2 levels remain uncertain due to our limited knowledge on vegetation responses to increased CO_2 concentration and nutrient limitation.

The nutrient limitation on plant growth has been found to reduce the capacity of terrestrial ecosystem to absorb atmospheric CO_2. N limitation on productivity mostly occurs in temperate and boreal forests, whereas phosphorus (P) limitation was primarily observed in tropical forests (Hofhansl et al., 2016; Vitousek et al., 2010; Walker & Syers, 1976; Wang et al., 2020a). Free-air CO_2 enrichment (FACE) experiments in temperate areas indicated that soil nutrient availability, particularly nitrogen (N), limits the magnitude of forest productivity increase (Norby et al., 2010). However, FACE experiments have not been conducted in tropical forests so far (Cernusak et al., 2013; Hofhansl et al., 2016; Jiang et al., 2020b). Some studies based on model and remote sensing indicate that tropical low phosphorus supply constrains plant responses to elevated CO_2 (Fleischer et al., 2019; Wang et al., 2020a; Wieder et al., 2015; Yang et al., 2016). Due to the importance of the P cycle, TBMs have started to include the P dynamics and impacts on vegetation growth (Thornton et al., 2007; Zaehle & Friend, 2010). Recent progress in developing the quantitative frameworks in TBMs to represent the P cycle including the Community Land Model (CLM -CNP)

(Yang et al., 2014b), CABLE-CNP (Wang et al., 2007), Organizing Carbon and Hydrology In Dynamic Ecosystems (ORCHIDEE) (Goll et al., 2017), and DLEM-CNP (Wang et al., 2020b).

Carbon use efficiency (CUE, net primary production (NPP)/gross primary production (GPP) ratio) is an indicator related to the allocation of photosynthesized products by plants. The carbon use efficiency indicates the fraction of total assimilated carbon being incorporated into new tissues and represents the efficiency with which ecosystems sequester carbon from the atmosphere in terrestrial biomass (DeLucia et al., 2007; Valentini et al., 2000). The CUE is a critical ecosystem property for C cycle research because it is often used to calculated GPP from NPP, or likewise to estimate autotrophic respiration (Ra) as the difference between GPP and NPP (Waring et al., 1998; Zhang et al., 2009). Several studies have evaluated the effects of climate variables on the ecosystem CUE at multiple scales (Rowland et al., 2014; Zhang et al., 2014). Knowledge has advanced since the development of remote sensing and numerical modeling technology with respect to the potential effects of climate change and other drivers on the C cycle at large scales. Under future climate change and elevated CO_2 conditions, with C-N-P interaction, to evaluate tropical region C fluxes and CUE are not well explored.

Numerical modeling has played an important role in simulating the terrestrial C cycle since the 1970s (Alton et al., 2009; Berner & Lasaga, 1989; Liu et al., 2008). Model simulation experiments provide a possible solution for quantifying the contributions of different environmental factors on the C cycle. In this study, we used the DLEM-CNP to estimate the tropical terrestrial C fluxes and CUE patterns in the 21st century in response to climate change, increasing atmospheric CO_2, N deposition and land use/land cover change. The purpose of this study is to: (1) investigate nutrient limitation on the GPP, NPP, and CUE during the 21st century in tropical regions; (2) provide the estimate of tropical terrestrial GPP, NPP, and CUE during the

21st century; (3) evaluate climate, CO_2, N deposition and land use/land cover change impacts on tropical terrestrial GPP, NPP, CUE during 2020-2100.

2. Methods

2.1. Model Description

The Dynamic Land Ecosystem Model-CNP (DLEM-CNP) is a highly integrated process-based terrestrial biosphere model, includes N and P controls on vegetation and soil biogeochemical processes (Wang et al., 2020b) (Figure 2-2).

2.2. Input Data

All the climate forcing is from CMIP6 models the IPSL-CM6A-LR and is bias-corrected and down-scaled to a spatial resolution of 0.5° to keep consistent with historical data. Future climate data during 2020-2100 include two different scenarios: SSP1-2.6 and SSP5-8.5. In the lead up to the IPCC AR6, the energy modeling community has developed a new set of emissions scenarios driven by different socioeconomic assumptions, these are the "Shared Socioeconomic Pathways" (SSPs). The IPCC AR5 featured four Representative Concentration Pathways (RCPs), these scenarios – RCP2.6 and RCP8.5 – have new versions in CMIP6. These updated scenarios are called SSP1-2.6 and SSP5-8.5, each of which results in similar 2100 radiative forcing levels as their predecessor in AR5. The RCP2.6 emission and concentration pathway are representative of the literature on mitigation scenarios aiming to limit the increase of global mean temperature to 2°C. These scenarios form the low end of the scenario literature in terms of emissions and radiative forcing. They often show negative emissions from energy use in the second half of the 21st century (van Vuuren et al., 2011). The RCP8.5 combines assumptions about high population and relatively slow income growth with modest rates of technological change and energy intensity improvements, leading in the long term to high energy demand and GHG emissions in the absence of climate

change policies. Compared to the total set of RCPs, RCP8.5 thus corresponds to the pathway with the highest greenhouse gas emissions (Riahi et al., 2011).

Annual CO_2 concentration during 2020-2100 under different SPP scenarios was achieved from Meinshausen et al. (2020), which were generated using the reduced complexity climate-carbon cycle model MAGICC7.0. Land use/land cover change data and monthly gridded N deposition during 2020-2100 under different SPP scenarios were from the IMAGE model.

Soil physical properties were taken from ISRIC-WISE Harmonized Global Soil Profile Data Set (Batjes, 2009). Parent P content data was obtained from Global Gridded Soil Phosphorus Distribution Maps (Yang et al., 2014a). The elevation, slope, and aspect were derived from the Global 30 Arc-Second Elevation product (GTOPO30; https://lta.cr.usgs.gov/GTOPO30).

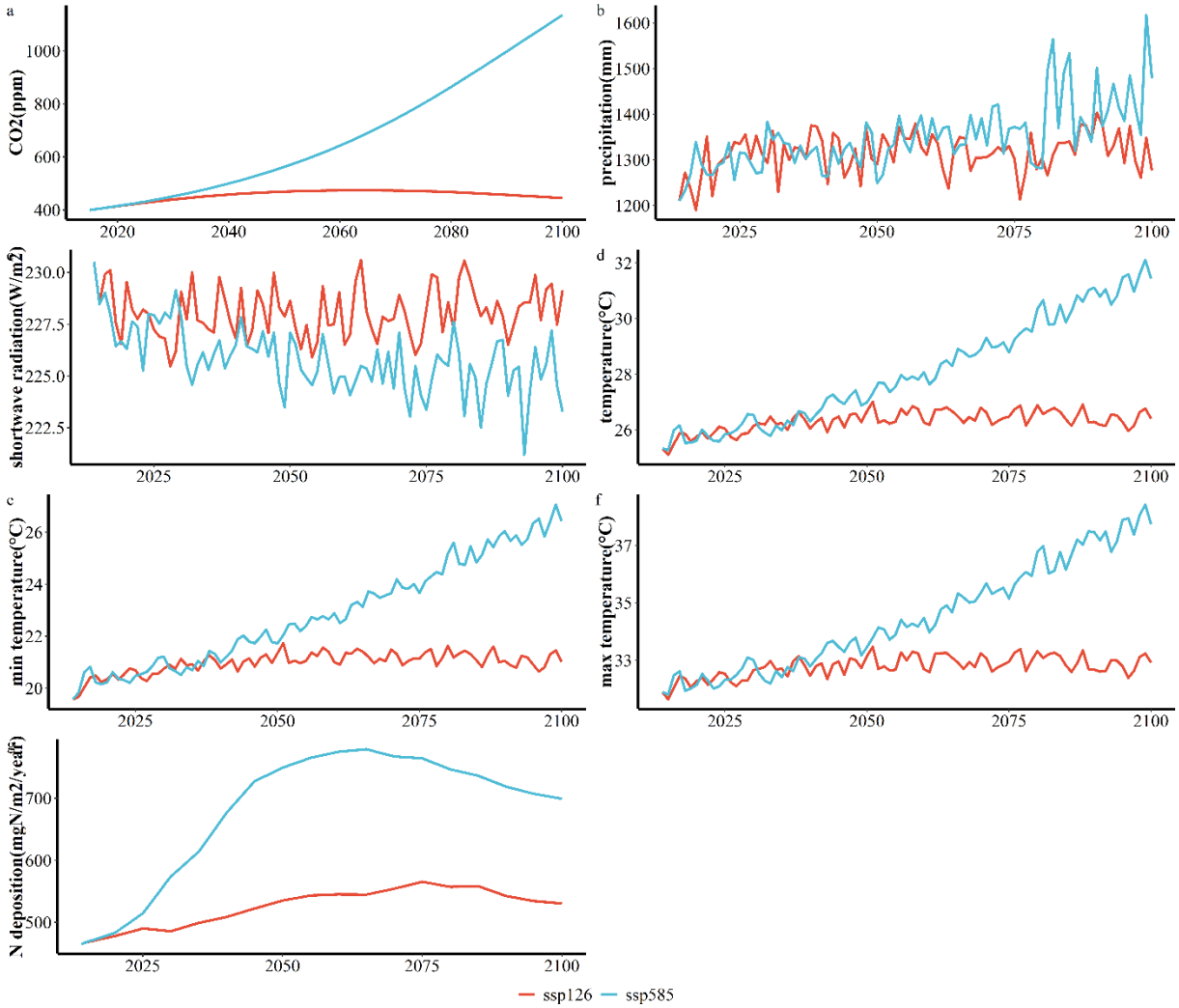

Figure 5- 1 Climate data under SSP1-2.6 (red) and SSP5-8.5 (blue) in tropical region: (a) atmosphere CO_2 concentration, (b) annual precipitation, (c) average shortwave radiation, (d) average annual temperature, (e) average minimum temperature, (f) average maximum temperature (g) annual total N deposition.

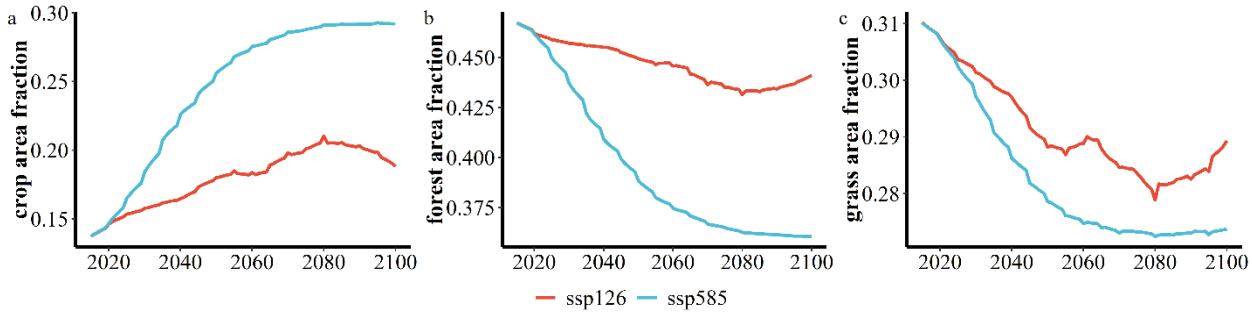

Figure 5- 2 Future vegetation cover fraction change (a) crop area fraction (b) forest area fraction (c) grassland area fraction under SSP1-2.6 (red) and SSP5-8.5 (blue).

2.3 Data for Model evaluation

FLUXNET data is a standard TBMs benchmark (Friend et al., 2007). We selected FLUXNET sites in tropical areas with different vegetation types (Figure 5-3) for model validation and performance evaluation. Annual mean gross primary production (GPP) was used to evaluate DLEM-CNP performance.

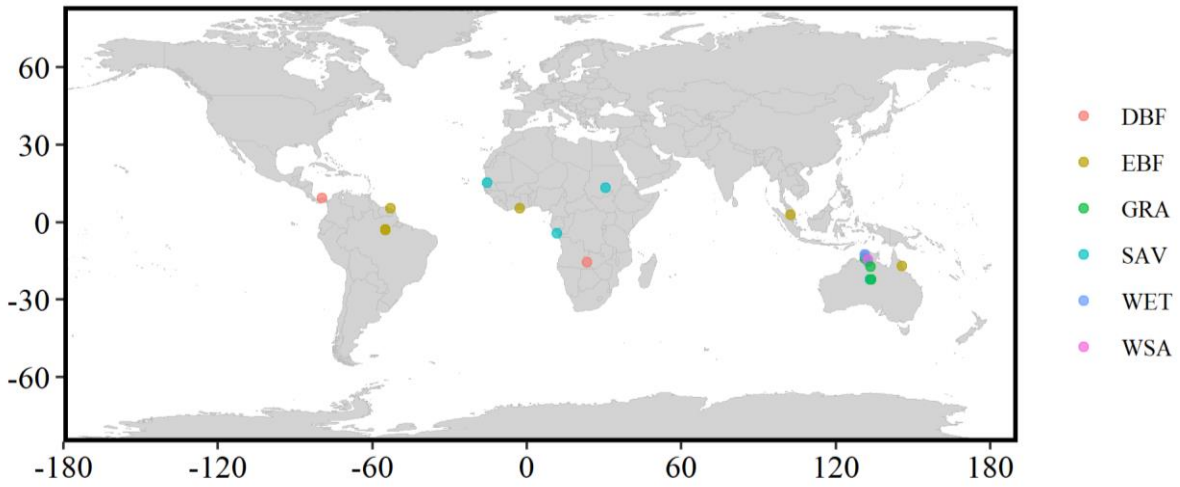

Figure 5- 3 Selected FLUXNET sites location.

The improved global MODIS primary production products have been widely used to monitor ecological conditions, natural resources, and environmental changes (Zhao et al., 2005; Zhao et al., 2006). The MODIS GPP values are calculated as follows:

$$GPP = \varepsilon_{max} \times 0.45 \times SW_{rad} \times FPAR \times fVPD \times fT_{min}$$

where ε_{max} is the maximum light use efficiency under optimal conditions; SW_{rad} is the incoming short-wave solar radiation, of which 45% is Photosynthetically Active Radiation (PAR); FPAR is the fraction of PAR absorbed by the plant canopy; fVPD is vapor pressure deficits scalar, and fT_{min} is the daily minimum temperature (T_{min},◦C) scalar.

The MODIS NPP is defined as the difference between GPP and respiration, including maintenance and growth components. The newly developed NPP is calculated as follows:

$$NPP = \sum_{1}^{365} GPP - R_{m\_lr} - R_{m\_w} - R_g$$

where R_{m_lr} is the maintenance respiration from living leaves and fine roots, and R_{m_w} is the annual maintenance respiration from living wood, R_g is annual growth respiration. More detailed descriptions for modeling MODIS GPP and NPP can be found in related publications (Zhao & Running, 2010; Zhao et al., 2006). Tropical CUE for each grid cell was calculated as the ratio of annual NPP to GPP from 2000 to 2014.

2.4 Model simulation experiments

First, the DLEM-C (without N and P limitations, which was executed with the same model code without N and P limitations on photosynthesis or decomposition), DLEM-CN (without P limitation, assuming P saturation), DLEM-CNP (with N and P limitations) were driven by CO_2 from 1900-2100 to examine the effects of nutrient limitation on the CO_2 fertilization effect.

To simulate the effects of individual environmental factors on GPP, NPP, and CUE, we use DLEM-CNP to implement five numerical experiments (S1 to S5, Table 5-1). The S1 experiment included the variations of all time-varying driving forces and represent the model's "near-reality" of ecosystem dynamics. The individual effects of land use/land cover change (LULC), atmospheric CO_2 (CO_2), N deposition (NDEP), and climate (CLIM) were calculated as S1 - S2, S1 - S3, S1 - S4, and S1- S5, respectively

Table 5- 1 Simulation protocol with the Dynamic Land Ecosystem Model

Experiments	CLIM	CO_2	NDEP	LULC
DLEM-C	1900	1900-2100	1900	1900
DLEM-CN	1900	1900-2100	1900	1900
DLEM-CNP	1900	1900-2100	1900	1900
S1	2020-2100	2020-2100	2020-2100	2020-2100
S2	2020-2100	2020-2100	2020-2100	2020
S3	2020-2100	2020	2020-2100	2020-2100
S4	2020-2100	2020-2100	2020	2020-2100
S5	2020	2020-2100	2020-2100	2020-2100

Note: CLIM is climate; NDEP is N deposition; CO_2 is atmospheric CO_2; LULC is land use/land cover change.

3. Results

3.1. Model validation results

The FLUXNET site mainly includes deciduous broadleaf forests, evergreen broadleaf forests, grasslands, savannas, and woody savannas. The capacity of the DLEM-CNP to reproduce the observed annual GPP of different plant types in tropical region FLUXNET sites was demonstrated in Figure 5-4. Generally, the DLEM-CNP performed well for all sites with $R^2 = 0.88$. During 2000-2014, from MODIS products, we calculated the pan-tropical mean CUE is 0.42 ± 0.13; the DLEM-CNP estimated CUE is 0.45 ± 0.06.

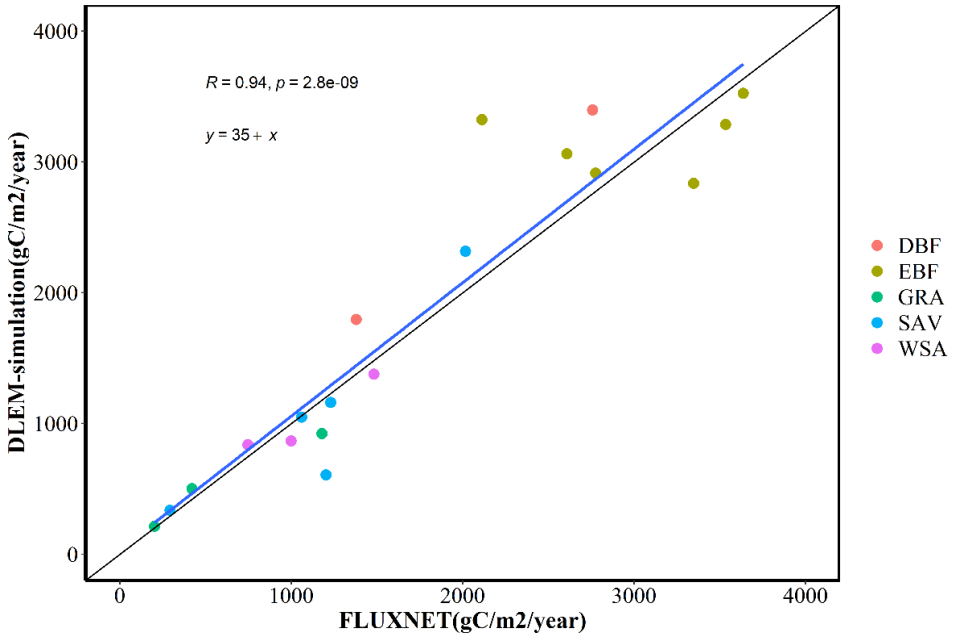

DBF: Deciduous Broadleaf Forests; EBF: Evergreen Broadleaf Forests; GRA: Grasslands; SAV: Savannas; WSA: Woody Savannas.

Figure 5- 4 Multiple-year mean GPP of DLEM-simulation vs. FLUXNET observation.

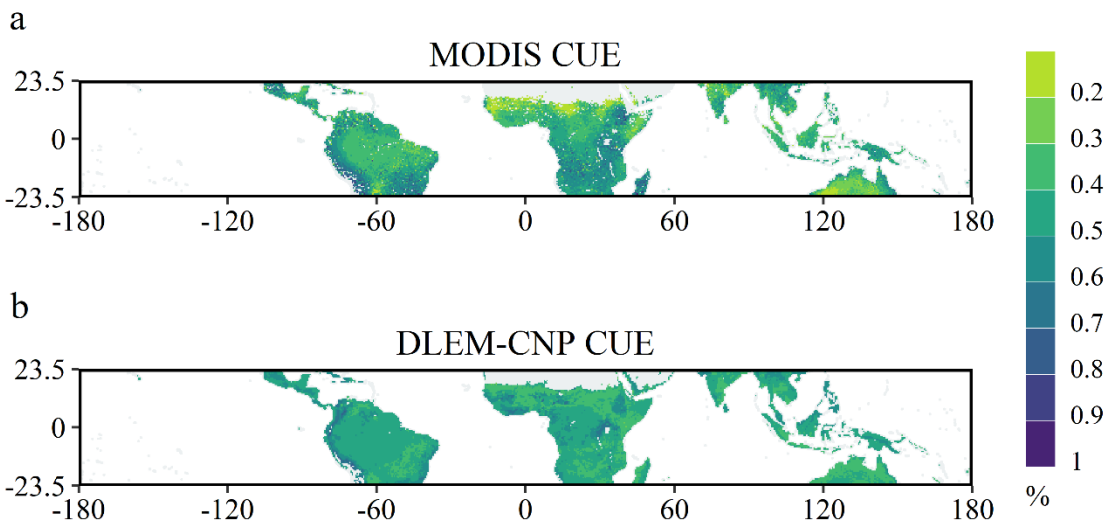

Figure 5- 5 Mean annual CUE from 2000 to 2014 estimated by (a)MODIS (b) DLEM-CNP.

3.2 Nutrient limitation on future CO_2 fertilization effect

Under the SSP126 scenario, CO_2 concentration is projected to increase from 414 ppm in 2020 to 474 ppm in 2063 with a rate of 1.38 ppm/year and then start to decrease to 445 ppm in 2100 by 0.84 ppm/year. Under the SSP585 scenario, the CO_2 concentration would increase from 414 ppm in 2020 to 1135 ppm in 2100 by 9.07 ppm/year. Model simulations show that increasing CO_2 would lead to a sustained increase of GPP and NPP in tropical regions due to the CO_2 fertilization effect in all DLEM-C, DLEM-CN, and DLEM-CNP simulations (Figure 5-6). Under the SSP126, the low end of the scenario in terms of emissions, for DLEM-C, DLEM-CN, and DLEM-CNP, the GPP would increase by 3%, 9%, 6%, and NPP would increase by 2%, 7%, 4%, respectively, from 2020 to 2100. At the end of the 21st century, DLEM-CNP indicates the tropical GPP would decrease by 40% and 21% comparing to those of DLEM-C and DLEM-CN, respectively; the NPP decrease by 40% and 23% comparing to those of DLEM-C and DLEM-CN, respectively. Under the SSP585 scenario, for DLEM-C, DLEM-CN, and DLEM-CNP, the GPP would increase by 31%, 43%, 32%, and NPP would increase by 29%, 42%, 31%, respectively, from 2020 to 2100. At the end of the 21st century, DLEM-CNP indicates the tropical GPP would decrease by 41% and 25% comparing to those of DLEM-C and DLEM-CN; the NPP would decrease by 40% and 27% comparing to DLEM-C and DLEM-CN, respectively. Under the SSP126 scenario, DLEM-CNP indicates the tropical CUE would increase by 1.6% relative to that of DLEM-C, but slightly decrease 0.2% relative to DLEM-CN. Under the SSP585 scenario, DLEM-CNP shows the tropical CUE increase by 2% relative to DLEM-C and decrease 0.2% relative to DLEM-CN.

We analyzed the GPP and NPP growth rates of five-year running mean with CO_2 changing rate (Figure 5-7). Under the SSP126 scenario, the growth rate of CO_2 concentration would keep

decreasing, resulting in the tropical GPP and NPP growth rates decreasing. Under the SSP585 scenario, the CO_2 concentration growth rate would increase and reach a peak in the 2080s and then start to decrease. However, the tropical GPP and NPP growth rate peak in the 2060, earlier than the peak of CO_2 concentration growth rate. Moreover, considering N and P limitations, the model shows a delayed peak than DLEM-C. DLEM-CN and DLEM-CNP show a stronger increase rate and increasing inter-annual variation with respect to GPP and NPP than DLEM-C.

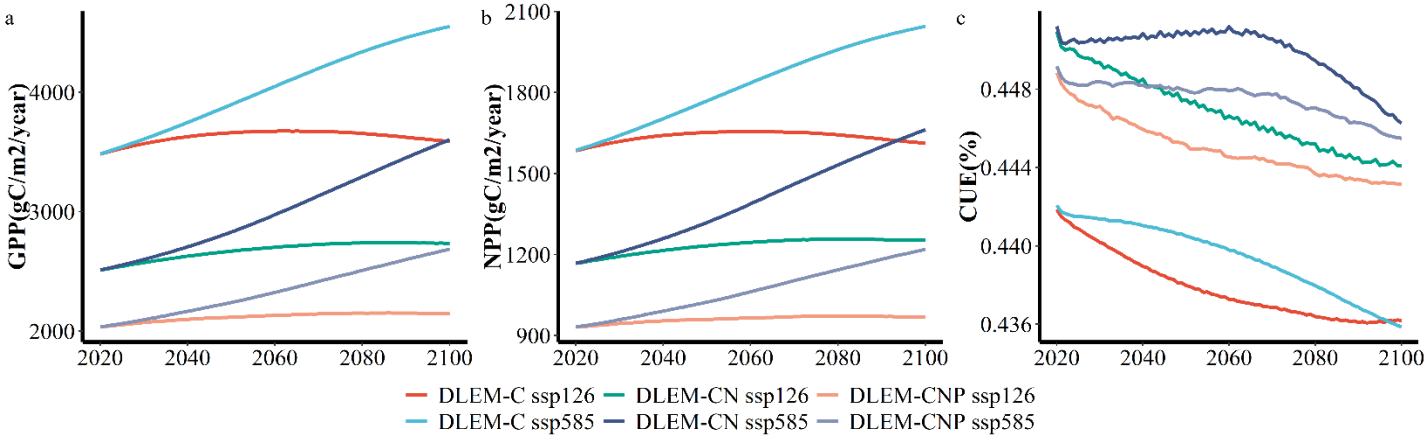

Figure 5- 6 DLEM-C, DLEM-CN, DLEM-CNP simulated (a)GPP, (b) NPP, (c) CUE, with only CO_2 changing from 2020 to 2100.

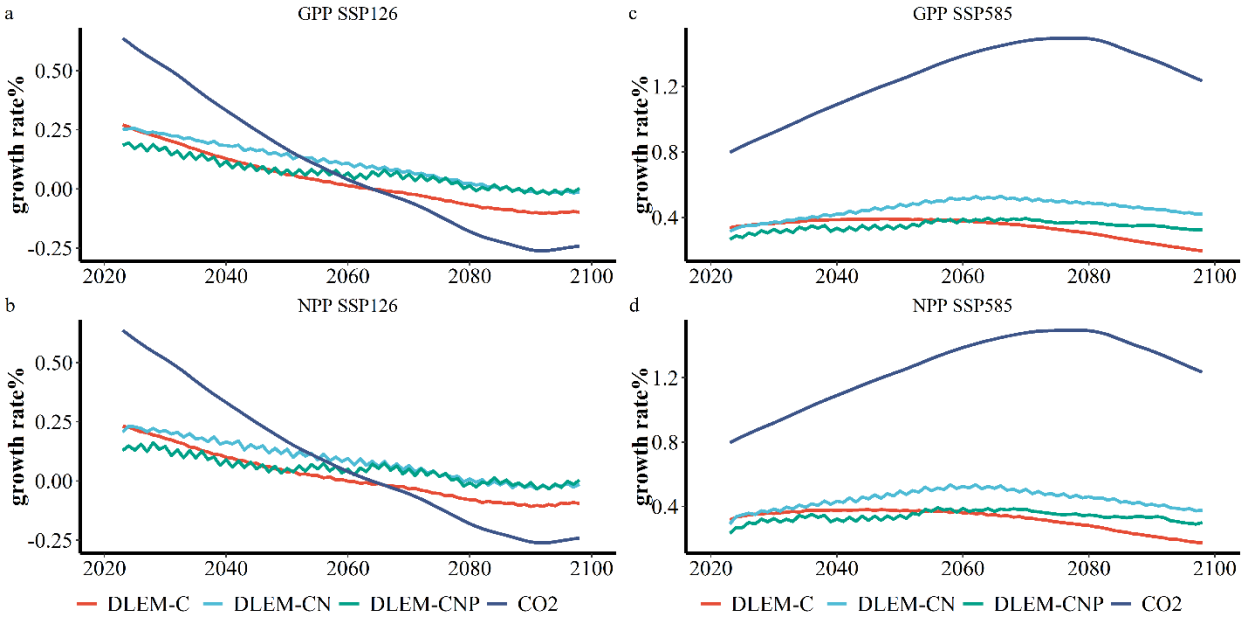

Figure 5- 7 DLEM-C, DLEM-CN, DLEM-CNP simulated growth rate of (a) GPP, (b) NPP under the SSP126 CO_2 concentration scenario; and (c) GPP, (d) NPP under the SSP585 CO_2 concentration scenario.

3.3 DLEM-CNP future projection

DLEM-CNP was driven by all time-varying driving forces, including land use/land cover change, atmospheric CO_2, N deposition, and climate from 2020 to 2100, to estimate the future tropical ecosystem C dynamics. Under the future SSP126 scenario, the tropical GPP, NPP, CUE would slightly increase, with a clear interannual variation. While, under the SSP585 scenario, the tropical GPP would increase by 44% from 2020 to 2100; the NPP would increase by 21%. The CUE shows a 15% decrease under the SSP585 scenario (Figure 5-8). Because forests and grassland have different plant traits, we further separated the tropical forests and grasslands to evaluate their response under different SSP scenarios. Figure 5-9, results indicated that forests and grasslands would have similar GPP and NPP increase trends. Both forests and grasslands show decrease trends of CUE under the SSP585 scenario, and forests have higher CUE than grassland.

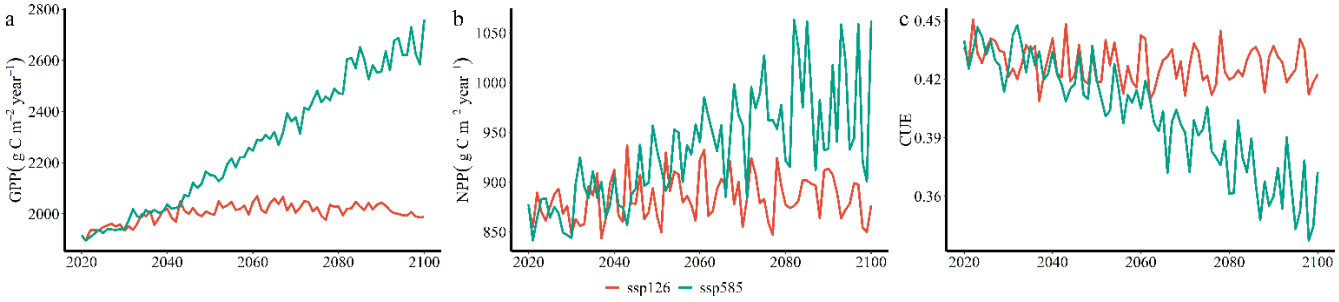

Figure 5- 8 DLEM-CNP under all time-varying driving forces, including land use/land cover change, atmospheric CO_2, N deposition, and climate from 2020 to 2100. (a) GPP, (b) NPP, (c) CUE.

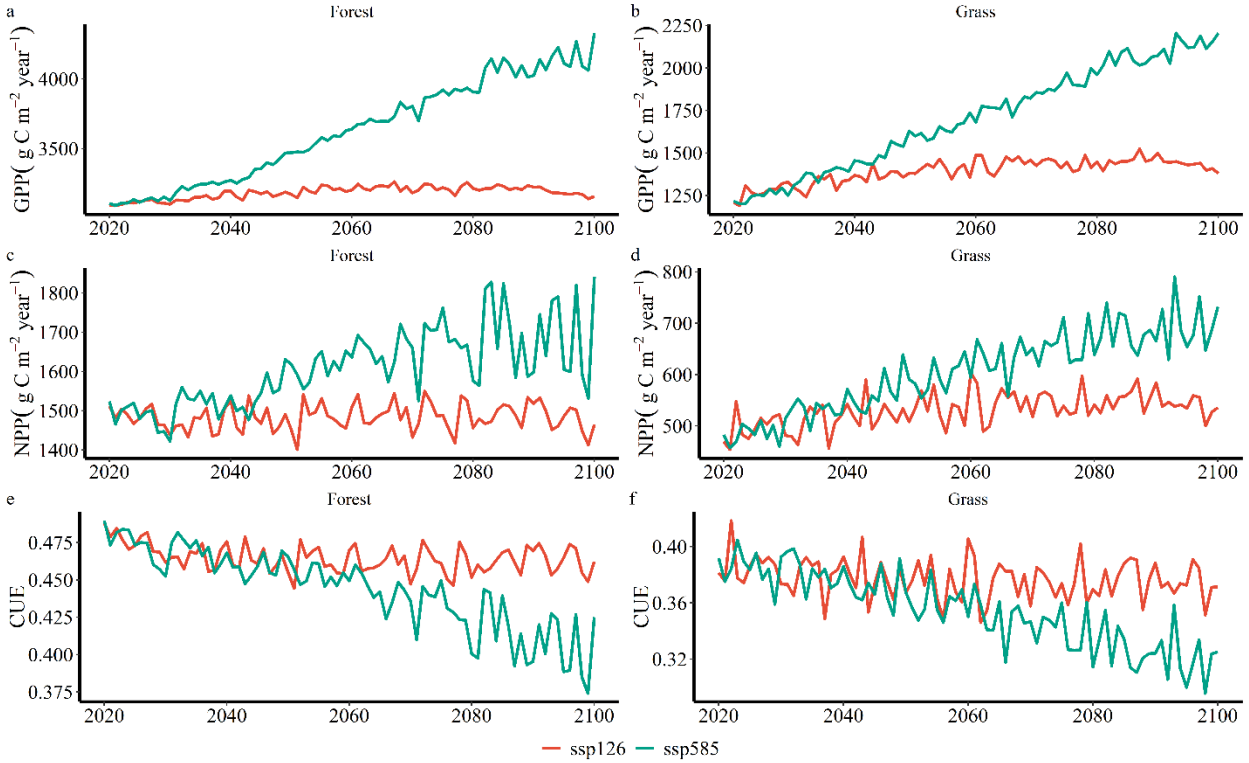

Figure 5- 9 DLEM-CNP for forests and grass, under all time-varying driving forces, including land use/land cover change, atmospheric CO_2, N deposition, and climate from 2020 to 2100.

3.4 Environmental factors' contribution to GPP, NPP, and CUE

We investigated different environmental factors' contribution to GPP, NPP, and CUE under SSP126 and SSP585 scenarios during the period 2020-2100 (Figure 5-10). The CO_2 fertilization effect is the dominant factor that would increase the future GPP and NPP. The CO_2 fertilization effect would contribute to increases in GPP by 117 and 492 $gCm^{-2}year^{-1}$ and increases in NPP by 51 $gCm^{-2}year^{-1}$ and 192 $gCm^{-2}year^{-1}$ under SSP126 and SSP585 scenarios, respectively. The land use/land cover change would decrease GPP by 32 and 99 $gCm^{-2}year^{-1}$, and decrease NPP by 18 and 50 $gCm^{-2}year^{-1}$ under SSP126 and SSP585 scenarios, respectively, mainly because of deforestation. The climate effect presents diverged impacts on GPP and NPP in the future. Climate would promote tropical GPP and reduce NPP. The climate effect was found to be the most significant factor that would decrease the CUE under both SSP126 and SSP585 scenarios. The

combined effects of climate variability, atmospheric CO_2, N deposition, and land use/land cover change would result in a decreased tropical CUE with varying degrees. Before the 2040s, the CO_2 fertilization effect would have a slightly positive effect. The climate effect would cause a large decrease in CUE under SSP585 scenarios, especially during the 2070s to 2100s. Compared with atmospheric CO_2 and climate, land use/land cover change and N deposition would have a small effect on the simulated CUE throughout the study period.

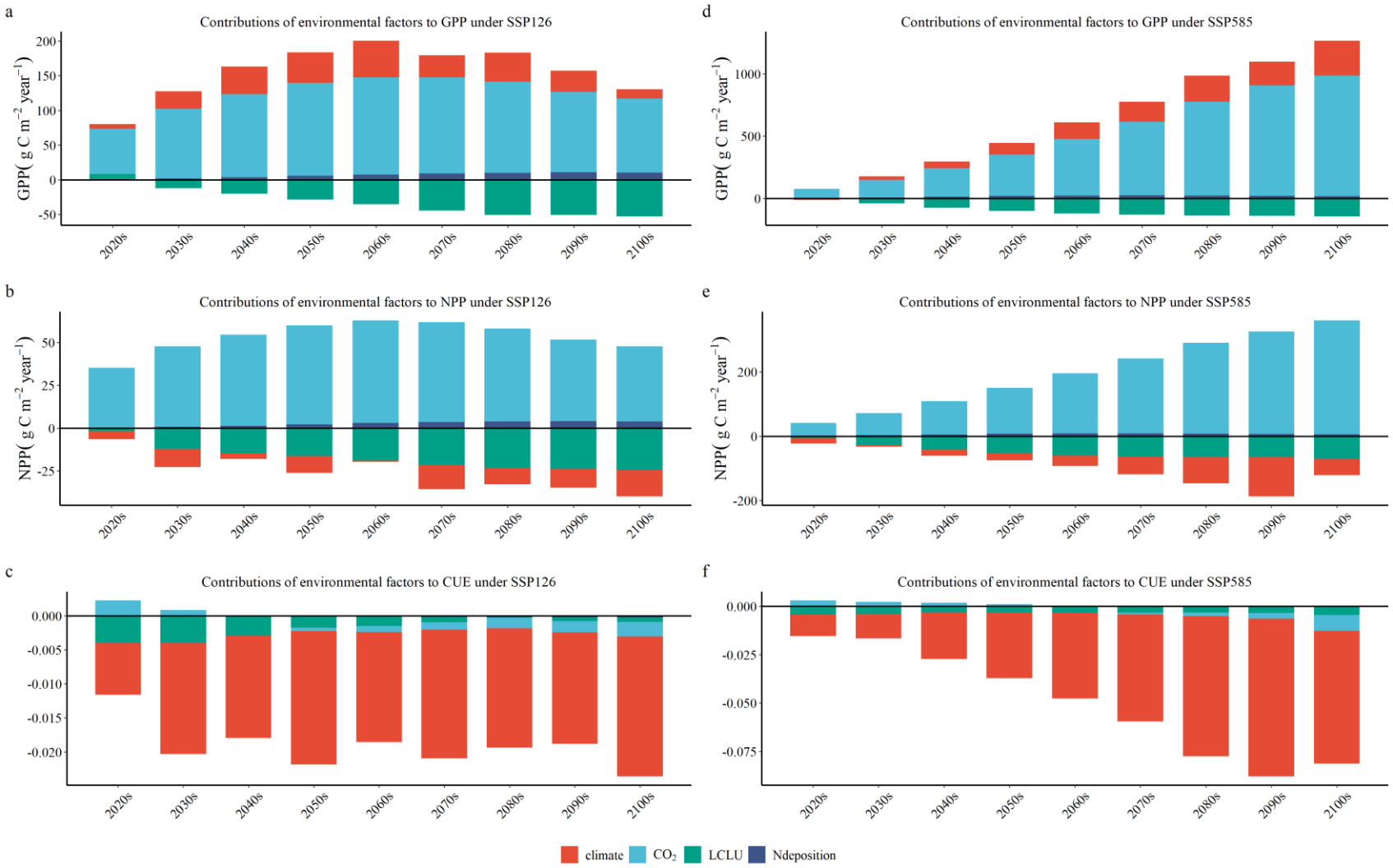

Figure 5- 10 Contributions of environmental factors (climate, CO_2, land use land cover change, and N deposition) to GPP, NPP, and CUE under SSP126 (a,b,c) and SSP585 (d,e,f).

4. Discussion

4.1 Nutrient effects on GPP, NPP, CUE

In the simulation of DLEM-C, DLEM-CN, DLEM-CNP driven by CO_2 from 1900-2100 under the SSP585 CO_2 concentration scenario, the tropical GPP and NPP growth rates show an earlier peak than the CO_2 growth rate in 2060. This phenomenon indicates that the CO_2 fertilization effect reaches plateaus and the tropical ecosystem's capability to respond to CO_2 increase weakens after 2060 under the SSP585 CO_2 concentration scenario. In a recent study using multiple long-term satellites and ground-based datasets, Wang et al. (2020a) also showed that the plant response to increasing CO_2 concentration has declined, correlating well with changing nutrient concentrations and availability of soil water. Besides, experimental evidence indicates that the percentage growth response to elevated CO_2 is amplified under water limitation but reduced under nitrogen limitation (Jiang et al., 2020a; McMurtrie et al., 2008). Including the nutrients cycle, the model showed more variation in year-to-year GPP and NPP growth rates, which is moderate in the DLEM-C. In our model, a large part of the N and P for plant uptake is from the decomposition process. When there is an increase of GPP introduced by increasing CO_2, the NP limitation occurs because there is not much available NP in soil for plant uptake. After more litterfall goes into decomposition process, there is an alleviation of NP limitation because mineralization releases more N and P, which can be uptaken by plant.

4.2 CUE response to environmental factors

A number of studies have found that the NPP/GPP ratio varies with ecosystem types, climate, soil nutrients and geographic locations (DeLucia et al., 2007; Maseyk et al., 2008; Xiao et al., 2003). A recent study found that forests in high-nutrient availability areas allocate more photosynthesis to plant biomass production than forests in low-nutrient availability areas (Vicca

et al., 2012). In our results, the climate has dominating impacts on CUE, which is consistent with other studies. Zhang et al. (2014), using remote sensing data, revealed a decreasing NPP/GPP ratio under increased precipitation and temperature at a global scale. The global terrestrial plant ecosystem exhibited a decreasing NPP/GPP ratio over time, driven primarily by decreases in ecosystems: evergreen and deciduous broadleaf forests and open and closed shrubs. Studies indicate that NPP/GPP ratio exhibited a globally positive correlation with precipitation and a negative correlation with temperature in most vegetated areas. However, in our study, we did not separate climate effect as precipitation and temperature.

4.3 Uncertainties and improvements needed

It is critical to recognize the limitations and uncertainties that are inherent in such a study regarding input data, parameters and models. We used climate projections from the IPSL-CM6A-LR model under the SSP126 and SSP585 scenarios. Discrepancies existing in different global climate models could lead to different estimations of GPP, NPP, and CUE responses as projected climate variables change. Further analysis is helpful to explore the uncertainty ranges by adopting climate inputs derived from multiple climate models. Besides, although parameters were well-calibrated based on existing field observation data, some processes such as responses of carbon assimilation/allocation and stomatal conductance to elevated temperature and CO_2 may be changed due to plant acclimatization and dynamic responses of phenology and growing season length, which have not been included in the current DLEM simulations. In future studies, it is important to consider the role of plant acclimatization in order to provide the best estimates of tropical GPP, NPP, and CUE under changing climatic conditions.

5. Conclusions

This study assesses the future changes of GPP, NPP, and CUE with a fully coupled C-N-P ecosystem model for pan-tropical ecosystems under SSP126 and SSP585 scenarios. Results showed that the P limitation on the CO_2 fertilization effect would reduce future tropical GPP and NPP. Under the SSP585 scenario with high CO_2 concentration, the tropical GPP and NPP growth rates reach a peak earlier than the peak of CO_2 concentration growth rate. The CO_2 fertilization effect would reach plateaus and the tropical ecosystem's capability to respond to CO_2 increase would weaken after 2060. Using the DLEM-CNP under future environmental conditions during 2020-2100, we estimated that under the SSP126 scenario, the tropical GPP, NPP, and CUE would slightly increase, with a clear interannual variation. Under the SSP585 scenario, the tropical GPP would increase by 44% from 2020 to 2100; the NPP would increase by 21%. However, The CUE would decrease by 15% under the SSP585 scenario. The CO_2 fertilization effect is the dominant factor that would increase the future GPP and NPP. The climate effect is found to be the most significant factor that would decrease the CUE under both SSP126 and SSP585 scenarios. Our study implicated that the CUE of the tropical region is changing under the future climate condition. Our study highlighted the importance of P limitation on the future C cycle in tropical areas. This study could improve the understanding of the future change patterns in GPP, NPP, CUE with C-N-P interaction and guide policymakers to put forward strategies for adapting to and mitigating the future impacts of changing climate and atmospheric composition.

reference

Alton, P., Fisher, R., Los, S., & Williams, M. (2009). Simulations of global evapotranspiration using semiempirical and mechanistic schemes of plant hydrology. *Global Biogeochemical Cycles, 23*(4). https://doi.org/10.1029/2009GB003540. https://doi.org/https://doi.org/10.1029/2009GB003540

Batjes, N. H. (2009). *ISRIC-WISE - Global Soil Profile Data (ver. 3.1)*. Retrieved from: https://doi.org/10.1594/PANGAEA.858569

Beer, C., Reichstein, M., Tomelleri, E., Ciais, P., Jung, M., Carvalhais, N., et al. (2010). Terrestrial Gross Carbon Dioxide Uptake: Global Distribution and Covariation with Climate. *Science, 329*(5993), 834-838. https://doi.org/10.1126/science.1184984

Berner, R. A., & Lasaga, A. C. (1989). Modeling the Geochemical Carbon Cycle. *Scientific American, 260*(3), 74-81.

Cernusak, L. A., Winter, K., Dalling, J. W., Holtum, J. A. M., Jaramillo, C., Körner, C., et al. (2013). Tropical forest responses to increasing atmospheric CO2: current knowledge and opportunities for future research. *Functional plant biology, 40*(6), 531-551. https://doi.org/https://doi.org/10.1071/FP12309

DeLucia, E. H., Drake, J. E., Thomas, R. B., & Gonzalez-Meler, M. (2007). Forest carbon use efficiency: is respiration a constant fraction of gross primary production? *Global Change Biology, 13*(6), 1157-1167. https://doi.org/10.1111/j.1365-2486.2007.01365.x

Fleischer, K., Rammig, A., De Kauwe, M. G., Walker, A. P., Domingues, T. F., Fuchslueger, L., et al. (2019). Amazon forest response to CO2 fertilization dependent on plant phosphorus acquisition. *Nature Geoscience*. https://doi.org/10.1038/s41561-019-0404-9

Friedlingstein, P., O'Sullivan, M., Jones, M. W., Andrew, R. M., Hauck, J., Olsen, A., et al. (2020). Global Carbon Budget 2020. *Earth Syst. Sci. Data, 12*(4), 3269-3340. https://doi.org/10.5194/essd-12-3269-2020

Friend, A. D., Arneth, A., Kiang, N. Y., Lomas, M., OgÉE, J., RÖDenbeck, C., et al. (2007). FLUXNET and modelling the global carbon cycle. *Global Change Biology, 13*(3), 610-633. https://doi.org/10.1111/j.1365-2486.2006.01223.x

Goll, D., Vuichard, N., Maignan, F., Jornet-Puig, A., Sardans, J., Violette, A., et al. (2017). A representation of the phosphorus cycle for ORCHIDEE (revision 4520). *Geoscientific Model Development Discussions, 10*(10), 3745-3770.

Hofhansl, F., Andersen, K. M., Fleischer, K., Fuchslueger, L., Rammig, A., Schaap, K. J., et al. (2016). Amazon Forest Ecosystem Responses to Elevated Atmospheric CO2 and Alterations in Nutrient Availability: Filling the Gaps with Model-Experiment Integration. *Frontiers in Earth Science, 4*(19). Perspective. https://doi.org/10.3389/feart.2016.00019

IPCC. (2013). *Climate Change 2013: The Physical Science Basis. Contribution of Working Group I to the Fifth Assessment Report of the Intergovernmental Panel on Climate Change* (T. F. Stocker, D. Qin, G.-K. Plattner, M. Tignor, S. K. Allen, J. Boschung, A. Nauels, Y. Xia, V. Bex, & P. M. Midgley Eds.). Cambridge, United Kingdom and New York, NY, USA: Cambridge University Press.

Jiang, M., Caldararu, S., Zhang, H., Fleischer, K., Crous, K. Y., Yang, J., et al. (2020a). Low phosphorus supply constrains plant responses to elevated CO2: A meta-analysis. *Global Change Biology, 26*(10), 5856-5873. https://doi.org/10.1111/gcb.15277. https://doi.org/https://doi.org/10.1111/gcb.15277

Jiang, M., Medlyn, B. E., Drake, J. E., Duursma, R. A., Anderson, I. C., Barton, C. V. M., et al. (2020b). The fate of carbon in a mature forest under carbon dioxide enrichment. *Nature, 580*(7802), 227-231. https://doi.org/10.1038/s41586-020-2128-9

Liu, M., Tian, H., Chen, G., Ren, W., Zhang, C., & Liu, J. (2008). Effects of Land-Use and Land-Cover Change on Evapotranspiration and Water Yield in China During 1900-20001. *JAWRA Journal of the American Water Resources Association, 44*(5), 1193-1207. https://doi.org/10.1111/j.1752-1688.2008.00243.x. https://doi.org/https://doi.org/10.1111/j.1752-1688.2008.00243.x

Maseyk, K., GrÜNzweig, J. M., Rotenberg, E., & Yakir, D. A. N. (2008). Respiration acclimation contributes to high carbon-use efficiency in a seasonally dry pine forest. *Global Change Biology, 14*(7), 1553-1567. https://doi.org/10.1111/j.1365-2486.2008.01604.x. https://doi.org/https://doi.org/10.1111/j.1365-2486.2008.01604.x

McMurtrie, R. E., Norby, R. J., Medlyn, B. E., Dewar, R. C., Pepper, D. A., Reich, P. B., & Barton, C. V. M. (2008). Why is plant-growth response to elevated CO2 amplified when water is limiting, but reduced when nitrogen is limiting? A growth-optimisation hypothesis. *Functional plant biology, 35*(6), 521-534. https://doi.org/https://doi.org/10.1071/FP08128

Meinshausen, M., Nicholls, Z. R. J., Lewis, J., Gidden, M. J., Vogel, E., Freund, M., et al. (2020). The shared socio-economic pathway (SSP) greenhouse gas concentrations and their extensions to 2500. *Geosci. Model Dev., 13*(8), 3571-3605. https://doi.org/10.5194/gmd-13-3571-2020

Norby, R. J., Warren, J. M., Iversen, C. M., Medlyn, B. E., & McMurtrie, R. E. (2010). CO_2 enhancement of forest productivity constrained by limited nitrogen availability. *Proceedings of the National Academy of Sciences, 107*(45), 19368-19373. https://doi.org/10.1073/pnas.1006463107

Riahi, K., Rao, S., Krey, V., Cho, C., Chirkov, V., Fischer, G., et al. (2011). RCP 8.5—A scenario of comparatively high greenhouse gas emissions. *Climatic Change, 109*(1), 33. https://doi.org/10.1007/s10584-011-0149-y

Rowland, L., Hill, T. C., Stahl, C., Siebicke, L., Burban, B., Zaragoza-Castells, J., et al. (2014). Evidence for strong seasonality in the carbon storage and carbon use efficiency of an

Amazonian forest. *Global Change Biology, 20*(3), 979-991. https://doi.org/10.1111/gcb.12375. https://doi.org/https://doi.org/10.1111/gcb.12375

Thornton, P. E., Lamarque, J.-F., Rosenbloom, N. A., & Mahowald, N. M. (2007). Influence of carbon-nitrogen cycle coupling on land model response to CO2 fertilization and climate variability. *Global Biogeochemical Cycles, 21*(4). https://doi.org/10.1029/2006GB002868

Valentini, R., Matteucci, G., Dolman, A. J., Schulze, E. D., Rebmann, C., Moors, E. J., et al. (2000). Respiration as the main determinant of carbon balance in European forests. *Nature, 404*(6780), 861-865. https://doi.org/10.1038/35009084

van Vuuren, D. P., Stehfest, E., den Elzen, M. G. J., Kram, T., van Vliet, J., Deetman, S., et al. (2011). RCP2.6: exploring the possibility to keep global mean temperature increase below 2°C. *Climatic Change, 109*(1), 95. https://doi.org/10.1007/s10584-011-0152-3

Vicca, S., Luyssaert, S., Peñuelas, J., Campioli, M., Chapin Iii, F. S., Ciais, P., et al. (2012). Fertile forests produce biomass more efficiently. *Ecology letters, 15*(6), 520-526. https://doi.org/10.1111/j.1461-0248.2012.01775.x. https://doi.org/https://doi.org/10.1111/j.1461-0248.2012.01775.x

Vitousek, P. M., Porder, S., Houlton, B. Z., & Chadwick, O. A. (2010). Terrestrial phosphorus limitation: mechanisms, implications, and nitrogen–phosphorus interactions. *Ecological applications, 20*(1), 5-15.

Walker, T., & Syers, J. K. (1976). The fate of phosphorus during pedogenesis. *Geoderma, 15*(1), 1-19.

Wang, S., Zhang, Y., Ju, W., Chen, J. M., Ciais, P., Cescatti, A., et al. (2020a). Recent global decline of CO_2 fertilization effects on vegetation photosynthesis. *Science, 370*(6522), 1295-1300. https://doi.org/10.1126/science.abb7772

Wang, Y. P., Houlton, B. Z., & Field, C. B. (2007). A model of biogeochemical cycles of carbon, nitrogen, and phosphorus including symbiotic nitrogen fixation and phosphatase production. *Global Biogeochemical Cycles, 21*(1). https://doi.org/10.1029/2006GB002797

Wang, Z., Tian, H., Yang, J., Shi, H., Pan, S., Yao, Y., et al. (2020b). Coupling of Phosphorus Processes with Carbon and Nitrogen Cycles in the Dynamic Land Ecosystem Model: Model Structure, Parameterization and Evaluation in Tropical Forests. *Journal of Advances in Modeling Earth Systems, n/a*(n/a), e2020MS002123. https://doi.org/10.1029/2020MS002123

Waring, R. H., Landsberg, J. J., & Williams, M. (1998). Net primary production of forests: a constant fraction of gross primary production? *Tree Physiology, 18*(2), 129-134. https://doi.org/10.1093/treephys/18.2.129

Wieder, W. R., Cleveland, C. C., Smith, W. K., & Todd-Brown, K. (2015). Future productivity and carbon storage limited by terrestrial nutrient availability. *Nature Geoscience, 8*, 441. https://doi.org/10.1038/ngeo2413

Xiao, C.-W., Yuste, J. C., Janssens, I. A., Roskams, P., Nachtergale, L., Carrara, A., et al. (2003). Above- and belowground biomass and net primary production in a 73-year-old Scots pine forest. *Tree Physiology, 23*(8), 505-516. https://doi.org/10.1093/treephys/23.8.505

Yang, X., Post, W. M., Thornton, P. E., & Jain, A. K. (2014a). Global Gridded Soil Phosphorus Distribution Maps at 0.5-degree Resolution. In: ORNL Distributed Active Archive Center.

Yang, X., Thornton, P., Ricciuto, D., & Post, W. (2014b). The role of phosphorus dynamics in tropical forests–a modeling study using CLM-CNP. *Biogeosciences, 11*(6), 1667-1681.

Yang, X., Thornton, P. E., Ricciuto, D. M., & Hoffman, F. M. (2016). Phosphorus feedbacks constraining tropical ecosystem responses to changes in atmospheric CO2 and climate. *Geophysical Research Letters, 43*(13), 7205-7214. https://doi.org/10.1002/2016GL069241

Zaehle, S., & Friend, A. D. (2010). Carbon and nitrogen cycle dynamics in the O-CN land surface model: 1. Model description, site-scale evaluation, and sensitivity to parameter estimates. *Global Biogeochemical Cycles, 24*(1). https://doi.org/10.1029/2009GB003521

Zhang, Y., Xu, M., Chen, H., & Adams, J. (2009). Global pattern of NPP to GPP ratio derived from MODIS data: effects of ecosystem type, geographical location and climate. *Global Ecology and Biogeography, 18*(3), 280-290. https://doi.org/10.1111/j.1466-8238.2008.00442.x. https://doi.org/https://doi.org/10.1111/j.1466-8238.2008.00442.x

Zhang, Y., Yu, G., Yang, J., Wimberly, M. C., Zhang, X., Tao, J., et al. (2014). Climate-driven global changes in carbon use efficiency. *Global Ecology and Biogeography, 23*(2), 144-155. https://doi.org/10.1111/geb.12086. https://doi.org/https://doi.org/10.1111/geb.12086

Zhao, M., Heinsch, F. A., Nemani, R. R., & Running, S. W. (2005). Improvements of the MODIS terrestrial gross and net primary production global data set. *Remote sensing of Environment, 95*(2), 164-176. https://doi.org/https://doi.org/10.1016/j.rse.2004.12.011

Zhao, M., & Running, S. W. (2010). Drought-Induced Reduction in Global Terrestrial Net Primary Production from 2000 Through 2009. *Science, 329*(5994), 940-943. https://doi.org/10.1126/science.1192666

Zhao, M., Running, S. W., & Nemani, R. R. (2006). Sensitivity of Moderate Resolution Imaging Spectroradiometer (MODIS) terrestrial primary production to the accuracy of meteorological reanalyses. *Journal of Geophysical Research: Biogeosciences, 111*(G1). https://doi.org/10.1029/2004JG000004.

Chapter 6 Summary and future research ideas

In this study, P impacts on C fluxes and the C-N-P interactions in the past and future were investigated at the site and tropical scales. A process-based fully coupled C-N-P model (DLEM-CNP) was developed on the platform of one existing terrestrial ecosystem model, and its performance was validated by benchmark datasets. We evaluated the N-P co-limitation effects by using DLEM-CNP to simulate the N, P fertilization addition experiment at Hawaii sites. We examined how P limitation has affected C fluxes of tropical rainforests during 1860-2018. Using historical environmental factors (such as climate change, land use/land cover change, atmospheric composition, etc.) to drive the DLEM-CNP, we examined tropical rainforests carbon fluxes and environmental factors' relative contributions to tropical rainforests carbon storage. Using future environmental and climate scenarios (SSP1-2.6 and SSP5-8.5), we examined pan-tropic GPP, NPP, and CUE changes in C-N-P coupled biogeochemical cycle. Meanwhile, underlying mechanisms of the changes and contributions from environmental factors were analyzed and quantified through numerical experiments by using the DLEM-CNP.

The major conclusions drawn from this study can be summarized as follows:

1) We developed a process-based P module on the platform of the Dynamic Land Ecosystem Model (DLEM) by considering P impacts on vegetation and soil biogeochemical processes, which upgraded the coupled CN model (DLEM-CN) into the coupled CNP model (DLEM-CNP). The DLEM-CNP fully incorporates CNP cycles in all pools (plant, litter, and soil organic/inorganic pools) and key biogeochemical processes.

2) The DLEM-CNP model had an outstanding innovation that it first time introduces the interactive co-limitation of N and P on vegetation C assimilation in the TBMs, overcoming the

shortcoming of using Liebig's law of the minimum. Validation results indicated a significant N and P impact on tropical forest C dynamics and highlighted the innovative improvements of introducing the N and P interactive co-limitation effect. Our results reveal interactions between C, N, P processes, indicating that the inclusion of the P cycle in the current TBMs is essential to better understand the impacts of global change on terrestrial ecosystems.

3) Consideration of the P cycle reduced the CO_2 fertilization effect on tropical rainforests gross primary production (GPP) by 25% and 45%, NPP by 25% and 46%, and net ecosystem production (NEP) by 28% and 41% relative to CN-only and C-only models, during 1860-2018.

4) During the period from the 1860s to the 2010s, the DLEM-CNP estimated that for per unit area, the tropical rainforest GPP increased by 17 %, Ra increased by 18%, NPP increased by 16 %, Rh increased by 13%, and NEP increased by 121%, respectively. Additionally, the enhanced GPP and NPP benefiting from the CO_2 fertilization effect had been offset by 147% and 135% due to deforestation from the 1860s to the 2010s.

5) The DLEM-CNP projected P limitation reduced the CO_2 fertilization effect on tropical ecosystem. Under the SSP126, at the end of the 21st century, DLEM-CNP indicates the tropical GPP would decrease by 40% and 21% comparing to those of DLEM-C and DLEM-CN; the NPP decrease by 40% and 23% comparing to those of DLEM-C and DLEM-CN, respectively. Under the SSP585 scenario, at the end of the 21st century, DLEM-CNP indicates the tropical GPP would decrease by 41% and 25% comparing to those of DLEM-C and DLEM-CN; the NPP would decrease by 40% and 27% relative to those of DLEM-C and DLEM-CN, respectively.

6) Under the future SSP126 scenario, the tropical GPP, NPP, CUE would slightly increase, with a clear interannual variation. While, under the SSP585 scenario, the tropical GPP would

increase by 44% from 2020 to 2100; the NPP would increase by 21%. The CUE would decrease by 15% under the SSP585 scenario. And forests have higher CUE than grassland.

7) The CO_2 fertilization effect was the dominant factor that increased the future GPP and NPP. Climate promoted tropical GPP and reduced NPP. The climate effect was found to be the most significant factor that decreased the CUE under both SSP126 and SSP585 scenarios.

To reduced uncertainties in this dissertation research, several future research needs have been identified. First, in the current DLEM version, we explicitly considered N and P limitation on C but neglected P effects on some N processes, such as the biological N fixation process. Several studies indicate that P availability may have impacts on N fixation. However, the mechanisms of P influence on N fixation have not yet been fully understood. Second, plants' adaptation to P limitation can change vegetation physiological characteristics. Plants evolve strategies for P acquisition and use in P-limiting environments, including decreased growth rate, increased growth per unit of P uptake, remobilization of internal P, modifications in carbon metabolism that bypass P-requiring steps, and alternative respiratory pathways. All these adaption strategies are supposed to lead to vegetation parameters change (e.g., V_{cmax}, minimum leaf C: N ratio, and minimum leaf C: P ratio). Third, a single PFT has a uniform set of parameters, which do not account for variations in space and, thus, inadequately represent its spatial heterogeneity. A more plant traits-based plant classification and parameterization algorithm are in need to be developed to improve model performance.

Nevertheless, this study is the first attempt for coupling the P cycle into the process-based DLEM model to investigate P limitation impacts and quantify the contributions of multiple environmental factors on C fluxes with the P cycle involved at tropical scales. These findings could

provide useful knowledge to design specific climate mitigation strategies. The P model developed in this study can be coupled into the earth system models and improve the accuracy of projections in future climate and global biogeochemical cycles.

Appendix 1. DLEM-CN structure of carbon allocation, nitrogen uptake and allocation, and decomposition

1. Allocation

The assimilated carbon deducted by growth respiration (GPP - Gr) is the carbon that is ready to be allocated to different tissue. The allocation strategy is first confined by the scarcest resource and then regulated by phenology.

1.1 Resource limited scalars

To estimate the relative allocation among leaf, stem and root pools, DLEM follows the relative allocation scheme developed by Friedlingstein et al. (1999). The relative allocation among different parts reflects the resource limitation on the plants. DLEM groups the resource limitations into two general types: aboveground limitation and belowground limitation. If the aboveground resources are limited, more available storage carbon will be allocated to sapwood and leaf so that the stem will grow taller and leaf will grow more. If the belowground resources are limited, more available storage carbon will be allocated to the roots to enhance plant's water/nutrients uptake capacity. In the current model, DLEM only considers the light limitation as aboveground stress. In order to give equal weight to aboveground (light) vs. belowground resources (water and nutrients), DLEM assumes that only the most limiting one of the two belowground resources drive the allocation pattern (i.e., the controlling resources are light and either water or nutrients). In summary, the model behaves as if one aboveground resource (light) directly controls the stem (sapwood) allocation of available storage carbon and one belowground resource (water or nitrogen) drives the root allocation of available storage carbon. Leaves get the residual:

$$\rho = r_0 \times \left\{ \frac{3 \times L}{[L + 2 \times \min(W, N)]} \right\} \quad (1)$$

$$\sigma = s_0 \times \left\{ \frac{3 \times \min(W, N)}{[\min(W, N) + 2L]} \right\} \quad (2)$$

$$\lambda = 1 - \rho - \sigma \quad (3)$$

where ρ and σ are the actual fractions of carbon allocated to root and sapwood, respectively; and r_0 and s_0 are the fractional carbon allocation to root and sapwood for non-limiting conditions, respectively. In normal conditions, both r_0 and s_0 is set to 0.3, giving a leaf allocation of 0.4 under conditions where resources are totally no limiting. L , W, and N are light, water and nutrients availability scalars, ranging from 0.01 (severely limited) to 1 (readily available).

DLEM uses the canopy leaf area index (LAI) to estimate L, the light availability scalar:

$$L = \exp(-k \times LAI) \quad (4)$$

where k is an extinction coefficient set to 0.5.

The water availability scalar, W, is determined by soil moisture factor β, ranging from 0 to 1:

$$W = \beta \quad (5)$$

The nutrients availability scalar, N, is determined based on the vegetation NP limitation factor:

$$N = \frac{2}{\frac{1}{f(N)} + \frac{1}{f(P)}} \quad (6)$$

$$f(N) = \frac{\sum_{i=1}^{5} n_i}{\sum_{i=1}^{5} \frac{c_i}{CN_{min,i}}} \quad (7)$$

$$f(P) = \frac{\sum_{i=1}^{5} p_i}{\sum_{i=1}^{5} \frac{c_i}{CP_{min,i}}} \quad (8)$$

where *i* represent leaf, sapwood, coarse root, fine root, and reproduction pool; n_i, p_i, and c_i are the amount of nitrogen, phosphorus, and carbon in each pool; $CN_{min,i}$, $CP_{min,i}$ is the minimum C:N and C: P ratio for each tissue.

1.2 Allocation according to phenology

The default fraction of carbon allocated to reproduction pool (f_{rep}) is a plant-dependent parameter. The default fraction of carbon allocated to leaf (f_{leaf}), sapwood (f_{sap}), coarse root (f_{cr}), fine root (f_{fr}) are,

$$f_{leaf} = \lambda \tag{9}$$

$$f_{sap} = \sigma \tag{10}$$

$$f_{cr} = \rho \times cr \tag{11}$$

$$f_{fr} = \rho \times fr \tag{12}$$

where cr and fr are the fractions of allocated carbon to coarse/fine root to allocated carbon to root. These default fractions are further adjusted according to phenology period and LAI. If the plant is in growing season and phenology stage is not reproduction stage, assimilated carbon is not allocated to reproduction pool. If LAI is greater than the maximum LAI (plant dependent parameter), no carbon is allocated to leaf. In growing season and LAI has not reached the maximum value, leaf growth is thought to be priority and carbon allocated to leaf is at its default fraction. The other tissues share the left carbon, while the fraction is decreased by a certain amount. In deciduous season and LAI is less than maximum value, the carbon allocated to reproduction pool is at default fraction, and other tissues share the left carbon.

The increment of each carbon pool is,

$$\Delta c_i = (GPP - GR) \times f_i \quad (13)$$

where *i* represent each tissue.

2. Nitrogen uptake and allocation

In DLEM, N processes are intimately coupled to the C processes by different biomass compartment specific C: N ratios. The N cycle is fully open, i.e., N inside the ecosystem can be exchanged with external sources and sinks through deposition, leaching, nitrous gas emissions, and so on. Combined with the inside mechanisms such as plant uptake and N mineralization, the open-N cycle provides a buffer to control the fluctuation of interior N (Rastetter et al., 1997). N flows follow mass balance principle, where change of ecosystem available N depends on the difference between N inputs (e.g., N deposition, fertilization, fixation) and N outputs (e.g., N leaching, N_2O, NO emission, NH_3 volatilization). The detailed information on DLEM, such as the model strategy related to N budget and N control on C cycling is accessible in other published papers (Liu et al., 2013; Lu & Tian, 2013; Lu et al., 2012; Ren et al., 2007; Tian et al., 2011; Yang et al., 2015). Here we primarily introduce the model strategy related to N uptake and allocation processes used in brief.

2.1 Nitrogen uptake

Nitrogen potential uptake (N_{up}, g N/m^2/day) is estimated as,

$$N_{up,pot} = N_{up,max} f(T_s) f(W, avn) \quad (14)$$

where $N_{up,max}$ is the maximum nitrogen uptake speed in optimum condition (g N/day), $f(T_s)$ is the temperature scalar,

$$f(T_s) = \frac{(T_s - Nup_{tmax})(T_s - Nup_{tmin})}{(T_s - Nup_{tmax})(T_s - Nup_{tmin}) - \left(T_s - Nup_{topt}\right)^2} \quad (15)$$

where T_s is soil temperature (°C); Nup_tmax, Nup_tmin, and Nup_topt are the maximum, minimum and optimum temperature for N uptake (°C). $f(W, avn)$ is the combined effect of water and available nitrogen,

$$f(W, avn) = \frac{f(w)avn}{f(w)avn + k_{up}} \tag{16}$$

where avn is the available nitrogen in soil, including inorganic ammonia and nitrate, k_{up} is the half-saturation coefficient for nitrogen uptake (g N/m^2, 1.0) $f(w)$ is the soil moisture factor,

$$f(w) = 0.9{\beta_t}^3 + 0.1 \tag{17}$$

The actual nitrogen uptake cannot exceed the maximum nitrogen deficit,

$$N_{up} = \min\left(N_{up,pot}, avn, \sum_{i=1}^{5} \frac{C_i}{CN_{min,i}} - \sum_{i=1}^{5} N_i\right) \tag{18}$$

where *i* represent leaf, sapwood, coarse root, fine root, and reproduction pool; N_i (g N/m^2) and C_i (g C/m^2) are the amount of N and C in each pool i; $CN_{min,i}$ is the minimum C to N ratio for each tissue (g C/m^2).

2.2 Nitrogen allocation

The nitrogen that is available for allocation (N_{alloc}) is,

$$N_{alloc} = \sum_{i=1}^{5} N_i + N_{up} \tag{19}$$

Nitrogen content (g N/m^2) in each tissue is updated as,

$$N_i = N_{alloc} \times \frac{\frac{C_i}{CN_{min,i}}}{\sum_{i=1}^{5} \frac{C_i}{CN_{min,i}}} \quad (20)$$

DLEM assumes nitrogen concentrations of sunlit leaf and shade leaf are different. Leaf nitrogen is further separated into sunlit leaf nitrogen concentration ($Ncon_{sun}$, g N/g biomass) and shade leaf nitrogen concentration ($Ncon_{shade}$, g N/g biomass) according to an extinction factor (k, 0.65), the leaf area index (LAI), and the LAI of sunlit and shaded leaves,

$$Ncon_{sun} = \frac{\frac{0.45 \times N_{leaf}}{C_{leaf}}}{\frac{LAI_{sun}}{LAI} + \frac{LAI_{shade} e^{-0.5k}}{LAI}} \quad (21)$$

$$Ncon_{shade} = Ncon_{sun} \times e^{-0.5k} \quad (22)$$

where N_{leaf} (g N/m^2) and C_{leaf} (g C/m^2) are actual leaf nitrogen and carbon concentration, respectively. The CN ratio of sunlit leaf and shade leaf is calculated as,

$$CN_{sun} = \frac{0.45}{Ncon_{sun}} \quad (23)$$

$$CN_{shade} = \frac{0.45}{Ncon_{shade}} \quad (24)$$

3. Decomposition

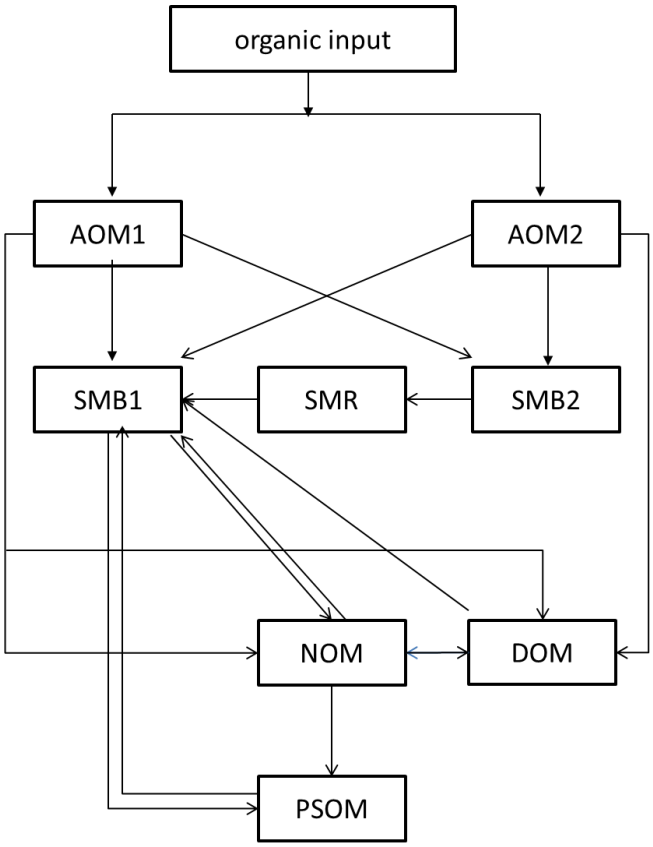

Figure S1- 1 Structure of DLEM soil organic pools.

Note: AOM: Added organic matter, i.e. litter. AOM1 and AOM2 have different residence time. SMB: soil microbial biomass, SMB1 is the autochthonous microbial, SMB2 is the zymogenous microbial; SMR: soil microbial residues; NOM: native organic matter; PSOM: passive soil organic matter.

DLEM estimates soil and litter decomposition with first-order decay rate constants (K_{Cpool}), which are adopted from the models of CENTURY (Parton et al., 1988). The decomposition rate of each soil organic carbon pool is influenced by soil temperature, soil water content, nutrient availability, and soil texture:

$$K_{Cpool} = \frac{K_{max}}{365} \times f(T) \times f(W) \times f(NP) f(clay) \quad (25)$$

$$f(T) = 4.89 \times e^{-3.432+0.1\times T\times\left(1-0.5\times\frac{T}{36.9}\right)} \tag{26}$$

$f(W)$ is the soil moisture scalar,

$$f(W) = \begin{cases} \dfrac{1-e^{-\frac{\theta}{\theta_{sat}}}}{1-e^{-\frac{\theta_{fc}}{\theta_{sat}}}} & \theta \le \theta_{fc} \\ 1.0044 - \dfrac{0.0044}{e^{-5\frac{\frac{\theta}{\theta_{sat}}-\frac{\theta_{fc}}{\theta_{sat}}}{1-\frac{\theta_{fc}}{\theta_{sat}}}}} & \theta > \theta_{fc} \end{cases} \tag{27}$$

$f(NP)$ is the nutrient scalar which is controlled by N limitation and P limitation:

$$f(NP) = \frac{2}{\frac{1}{f(N)} + \frac{1}{f(P)}} \tag{28}$$

$$f(NI) = 0.8 + 0.2 \times \frac{avn}{N_{imm}} \tag{29}$$

$$f(NM) = \begin{cases} 1 - \dfrac{avn - avn_{opt}}{avp_{opt}} & avn > avn_{opt} \\ 1 & \dfrac{avn_{opt}}{2} \le avn \le avn_{opt} \\ 1 + \dfrac{0.5avn_{opt} - avn}{avn_{opt}} & avn \le \dfrac{avn_{opt}}{2} \end{cases} \tag{30}$$

where K_{max} is the maximum decay rate (day^{-1}); $f(T)$ is the average soil temperature scalar; $f(clay)$ is the fraction of clay in soil (%); T is air temperature (°C); θ is soil water content (mm); θ_{sat} is soil water content at field capacity (mm); θ_{fc} is soil water content at field capacity at wilting point (mm); $f(NM)$ and $f(NI)$ are N scalars in mobilization and immobilization, respectively: N_{imm} is the potential N immobilization rate; avn is the available soil available N (g N m^{-2}); and avn_{opt} is the optimum available soil N (g N m^{-2}) (Banger et al., 2015).

Reference:

Banger, K., Tian, H., Tao, B., Lu, C., Ren, W., & Yang, J. (2015). Magnitude, Spatiotemporal Patterns, and Controls for Soil Organic Carbon Stocks in India during 1901–2010. *Soil Science Society of America Journal, 79*(3), 864-875. https://doi.org/10.2136/sssaj2014.11.0456

Bernhard-Reversat, F., C. Huttel, and G. Leme´e. (1978). *Structure and functioning of evergreen rain forest ecosystems of the Ivory Coast.* Retrieved from Paris, France.:

Cleveland, C. C., & Liptzin, D. (2007). C: N: P stoichiometry in soil: is there a "Redfield ratio" for the microbial biomass? *Biogeochemistry, 85*(3), 235-252.

Ducnuigeen, J., Williard, K., & Steiner, R. C. (1997). *Relative nutrient requirements of plants suitable for riparian vegetated buffer strips*: Interstate Commission on the Potomac River Basin Rockville, Maryland.

Folster, A., G. de las Salas, and P. Khanna. (1976). A tropical evergreen forest site with perched water table magdalena valley colombia biomass and bio element inventory of primary and secondary vegetation. *Oecologia Plantarum, 11*(4), 297-320.

Friedlingstein, P., Joel, G., Field, C. B., & Fung, I. Y. (1999). Toward an allocation scheme for global terrestrial carbon models. *Global Change Biology, 5*(7), 755-770. https://doi.org/10.1046/j.1365-2486.1999.00269.x

Goll, D. S., Brovkin, V., Parida, B. R., Reick, C. H., Kattge, J., Reich, P. B., et al. (2012). Nutrient limitation reduces land carbon uptake in simulations with a model of combined carbon, nitrogen and phosphorus cycling. *Biogeosciences, 9*(9), 3547-3569. https://doi.org/10.5194/bg-9-3547-2012

Kelly, J. M., Kovar, J. L., Sokolowsky, R., & Moorman, T. B. (2007). Phosphorus uptake during four years by different vegetative cover types in a riparian buffer. *Nutrient Cycling in Agroecosystems, 78*(3), 239-251. https://doi.org/10.1007/s10705-007-9088-4

Lescure, J.-P., Puig, H., Riera, B., Leclerc, D., Beekman, A., & Beneteau, A. (1983). La phytomasse épigée d'une forêt dense en Guyane française. *Acta Oecol, 4*, 237-251.

Liu, M., Tian, H., Yang, Q., Yang, J., Song, X., Lohrenz, S. E., & Cai, W. J. (2013). Long‐term trends in evapotranspiration and runoff over the drainage basins of the Gulf of Mexico during 1901–2008. *Water Resources Research, 49*(4), 1988-2012.

Lu, C., & Tian, H. (2013). Net greenhouse gas balance in response to nitrogen enrichment: perspectives from a coupled biogeochemical model. *Global Change Biology, 19*(2), 571-588. https://doi.org/10.1111/gcb.12049

Lu, C., Tian, H., Liu, M., Ren, W., Xu, X., Chen, G., & Zhang, C. (2012). Effect of nitrogen deposition on China's terrestrial carbon uptake in the context of multifactor environmental changes. *Ecological applications, 22*(1), 53-75.

McGroddy, M. E., Daufresne, T., & Hedin, L. O. (2004). Scaling of C: N: P stoichiometry in forests worldwide: implications of terrestrial redfield‐type ratios. *Ecology, 85*(9), 2390-2401.

Pan, S., Tian, H., Dangal, S. R., Ouyang, Z., Lu, C., Yang, J., et al. (2015). Impacts of climate variability and extremes on global net primary production in the first decade of the 21st century. *Journal of Geographical Sciences, 25*(9), 1027-1044.

Pan, S., Tian, H., Dangal, S. R., Ouyang, Z., Tao, B., Ren, W., et al. (2014). Modeling and monitoring terrestrial primary production in a changing global environment: toward a multiscale synthesis of observation and simulation. *Advances in Meteorology, 2014*.

Parton, W. J., Stewart, J. W. B., & Cole, C. V. (1988). Dynamics of C, N, P and S in grassland soils: a model. *Biogeochemistry, 5*(1), 109-131. https://doi.org/10.1007/BF02180320

Pellet, D., & El-Sharkawy, M. A. (1993). Cassava varietal response to phosphorus fertilization. II. Phosphorus uptake and use efficiency. *Field crops research, 35*(1), 13-20. https://doi.org/https://doi.org/10.1016/0378-4290(93)90132-7

Rai, S. N., & Proctor, J. (1986a). Ecological Studies on Four Rainforests in Karnataka, India: I. Environment, Structure, Floristics and Biomass. *Journal of Ecology, 74*(2), 439-454. https://doi.org/10.2307/2260266

Rai, S. N., & Proctor, J. (1986b). Ecological Studies on Four Rainforests in Karnataka, India: II. Litterfall. *Journal of Ecology, 74*(2), 455-463. https://doi.org/10.2307/2260267

Rastetter, E. B., Ågren, G. I., & Shaver, G. R. (1997). RESPONSES OF N-LIMITED ECOSYSTEMS TO INCREASED CO2: A BALANCED-NUTRITION, COUPLED-ELEMENT-CYCLES MODEL. *Ecological applications, 7*(2), 444-460. https://doi.org/10.1890/1051-0761(1997)007[0444:RONLET]2.0.CO;2

Ren, W., Tian, H., Liu, M., Zhang, C., Chen, G., Pan, S., et al. (2007). Effects of tropospheric ozone pollution on net primary productivity and carbon storage in terrestrial ecosystems of China. *Journal of Geophysical Research: Atmospheres, 112*(D22).

Tian, H., Xu, X., Lu, C., Liu, M., Ren, W., Chen, G., et al. (2011). Net exchanges of CO2, CH4, and N2O between China's terrestrial ecosystems and the atmosphere and their contributions to global climate warming. *Journal of Geophysical Research: Biogeosciences, 116*(G2). https://doi.org/10.1029/2010JG001393

Wang, R., Goll, D., Balkanski, Y., Hauglustaine, D., Boucher, O., Ciais, P., et al. (2017). Global forest carbon uptake due to nitrogen and phosphorus deposition from 1850 to 2100. *Global Change Biology, 23*(11), 4854-4872.

Yang, Q., Tian, H., Friedrichs, M. A., Hopkinson, C. S., Lu, C., & Najjar, R. G. (2015). Increased nitrogen export from eastern North America to the Atlantic Ocean due to climatic and anthropogenic changes during 1901–2008. *Journal of Geophysical Research: Biogeosciences, 120*(6), 1046-1068.

Appendix 2

Table S2- 1 Coordinates, climate data, and soil for the 13 tropical rainforest sites from Clark et al. (2001)

Abbreviations: annual prec, annual precipitation; prec sd, precipitation standard deviation in a year; Swrd, short wave radiation; Tmean, mean daily temperature; tmax, maximum temperature; tmin, minimum temperature; Sand, sand content in soil texture; Parent P, parent phosphorus in soil.

Site	longitude	latitude	annual prec (mm)	prec sd (mm)	Swrd ($Wm^{-2}d^{-1}$)	Tmean (℃)	tmax(℃)	tmin(℃)	Elevation(m)	Sand (%)	Parent P (gPm^{-2})
Brazil:Fazenda Dimona	-60	-2.5	2551.5	11.3	206.4	26.8	31.5	22.2	76.0	34.5	4
Brazil: Paragominas	-47.52	-2.98	1889.6	9.3	218.3	26.4	31.6	21.2	115.0	74.5	1
Colombia:Magdalena	-73.8	6.5	2613.0	9.9	253.3	26.1	32.7	19.6	1087.1	41.5	47
French Guiana	-55.75	5.25	1886.3	6.7	214.8	26.0	31.0	21.1	93.0	98	170
India: Bannadpare	75.7	12.08	4395.8	17.8	198.4	24.6	29.5	19.6	355.1	41.5	47
India: Agumbe	75.1	13.5	3561.1	15.2	177.4	23.0	28.8	17.1	577.1	41.5	47
Ivory Coast	-4.03	5.28	2404.0	7.7	213.6	26.1	29.2	23.1	76.7	89	47
Jamaica	-77	18	3148.9	14.1	258.9	25.4	27.4	23.5	1600.0	5	4
Malaysia	102.3	2.98	4063.8	11.7	223.0	25.5	29.8	21.1	49.9	44.5	5
Mexico	-105.05	19.5	1200.4	8.7	250.5	25.1	31.3	19.0	245.1	73	127
Puerto Rico	-66	18.42	3071.6	11.1	258.2	25.2	28.0	22.5	150.7	29	47
Venezuela	-67.05	1.9	3967.3	15.3	209.2	25.5	29.6	21.4	52.0	59.5	1
Papua New Guinea	145.18	-6	3848.2	16.8	255.9	20.3	23.7	16.9	1818.4	43	47

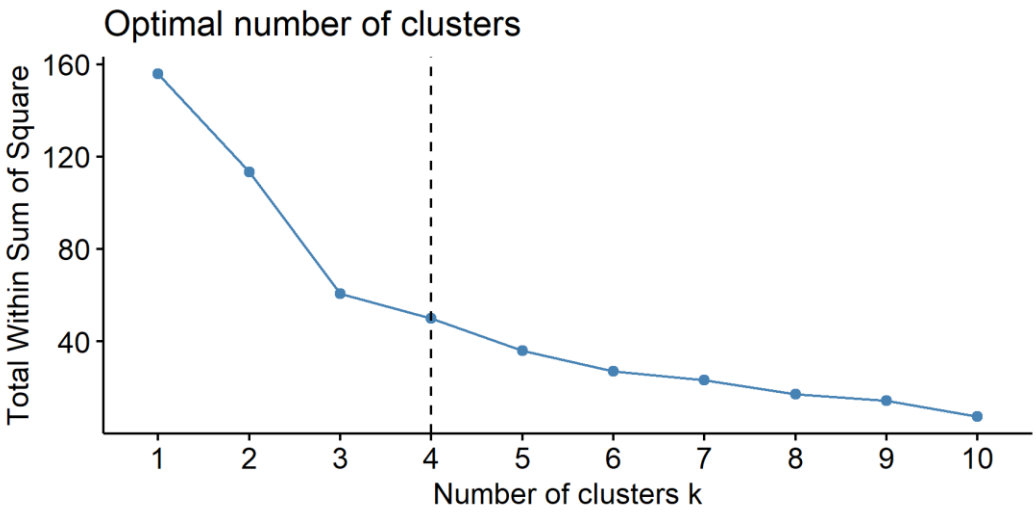

Figure S2- 1 The optimal number of clusters.

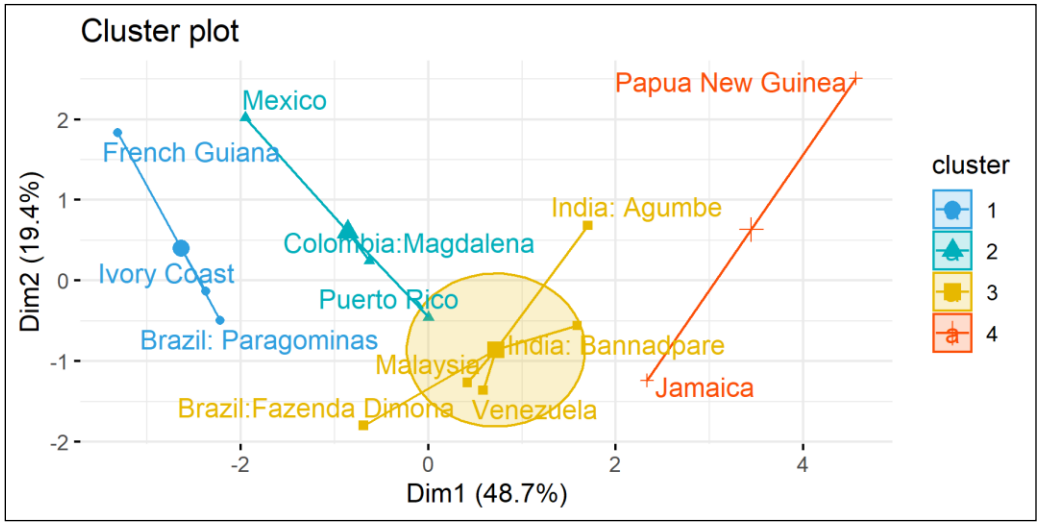

Figure S2- 2 K-means clustering cluster plot.

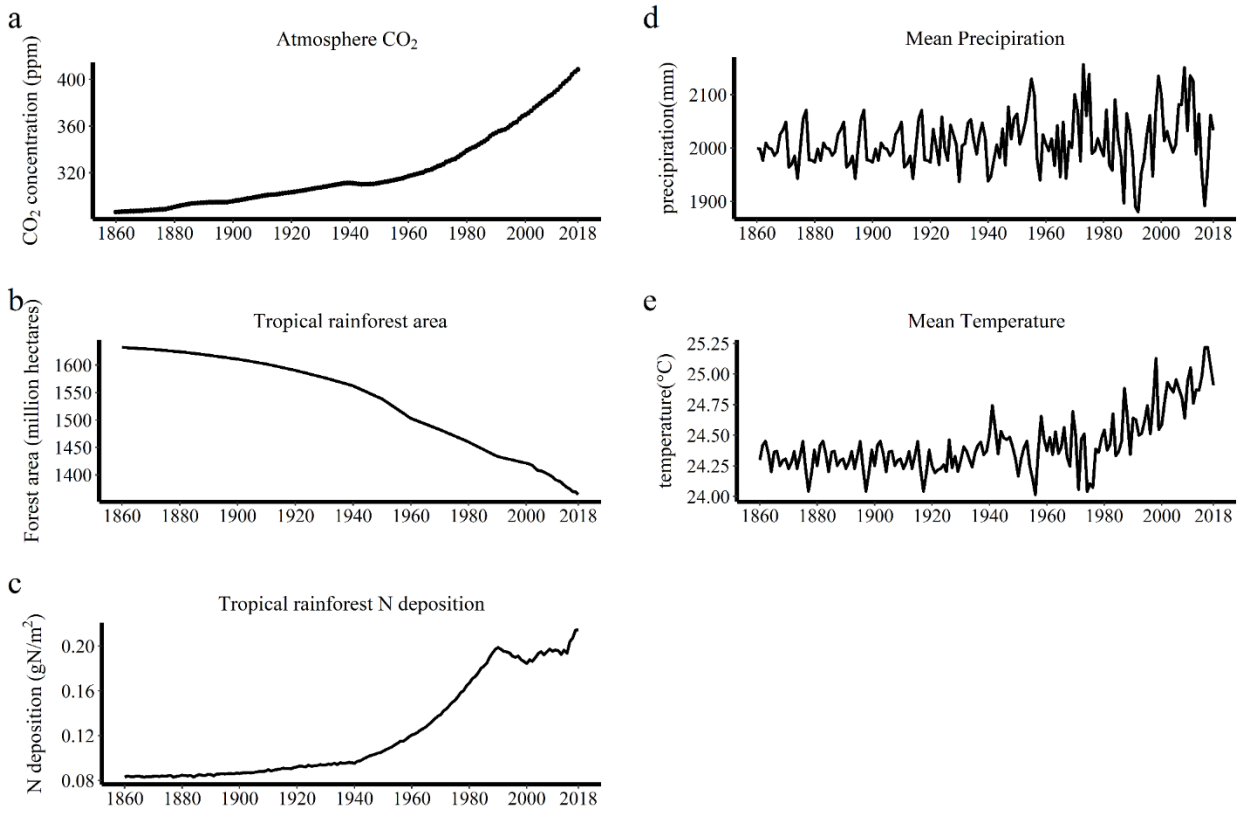

Figure S2- 3 The input data of the DLEM-CNP. (a) Atmospheric CO_2 concentration; (b) Intact tropical forest areas; (c) Average N deposition across tropical forest areas; (d) Annual precipitation across tropical forest areas; (e) Average temperature across tropical forest areas.

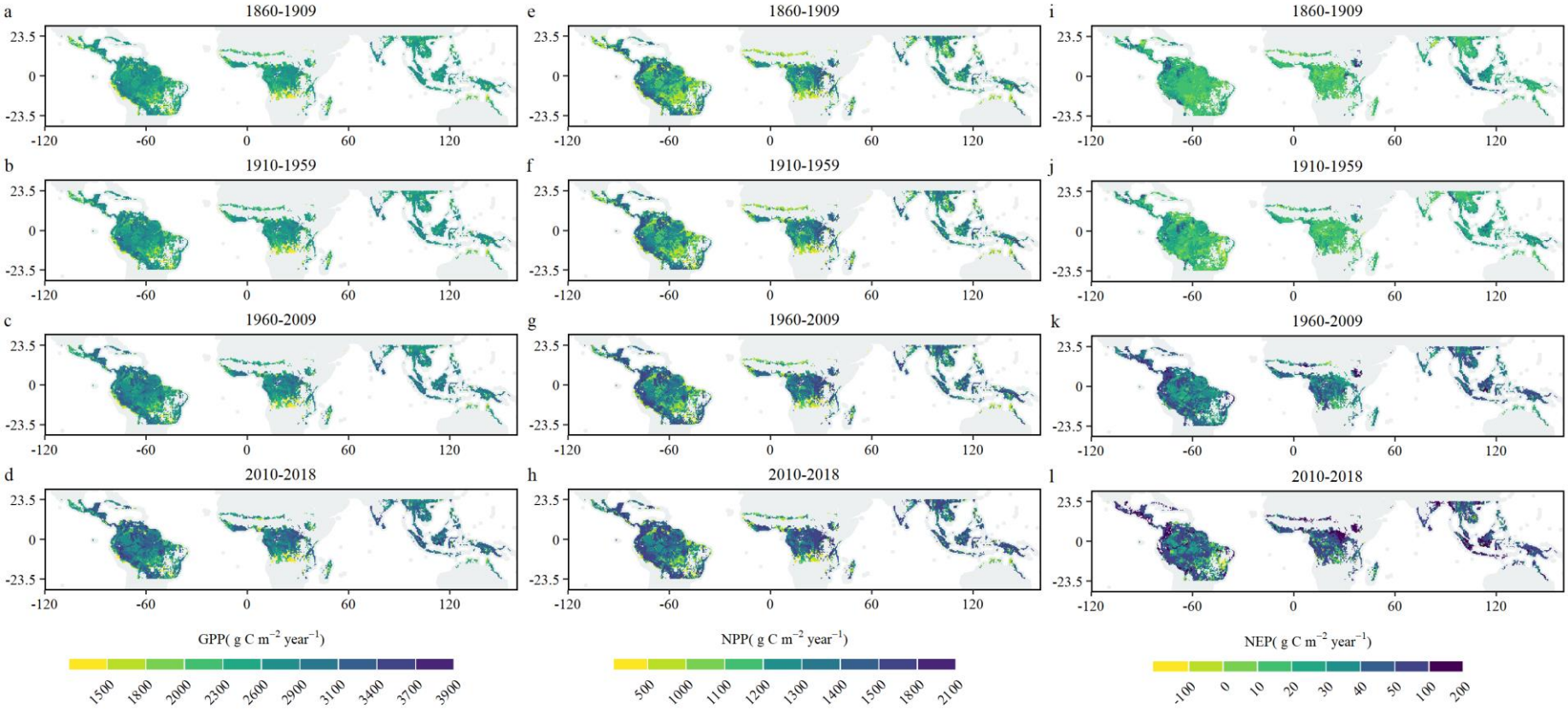

Figure S2- 4 Spatial distribution of the annual mean GPP (g C/m^2/yr), NPP (g C/m^2/yr), and NEP (g C/m^2/yr) in the tropical forests during 1860–1909, 1910-1959, 1960-2009, 2010-2018 simulated by the DLEM-CNP with historical environmental forcing.

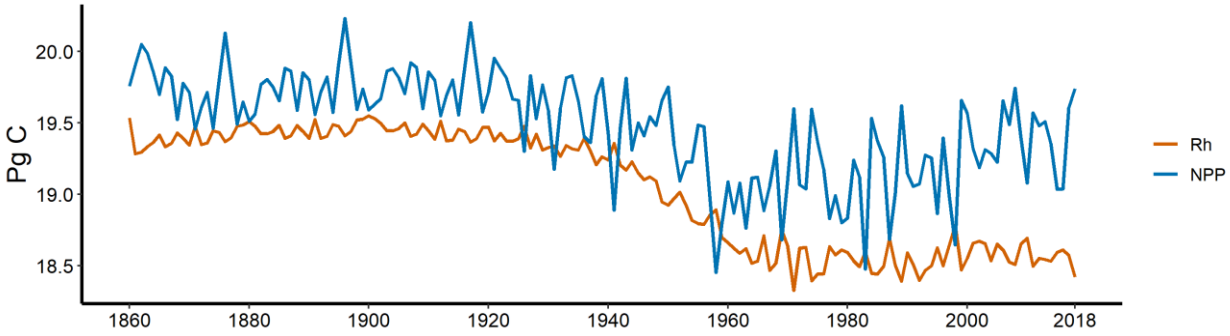

Figure S2- 5 Intact tropical rainforests net primary productivity (NPP) and heterotrophic respiration (Rh) under close to historical environmental conditions (climate, atmospheric CO_2 concentration, N deposition, CO_2 concentration, land-cover, and land-use change, S1 simulation) during 1860-2018.